Dissertation

submitted to the

Combined Faculty of Natural Sciences and Mathematics

of the Ruperto Carola University Heidelberg, Germany

for the degree of

Doctor of Natural Sciences

Presented by

Master of Science **Kaiqing Zhang**

Born in: Anshan, China

Oral examination: …….

The role of WNT/STOP signaling during neurogenesis and ciliogenesis

Referees: Prof. Dr. Christof Niehrs
Prof. Dr. Ana Martin-Villalba

Contents

1. ABSTRACT

WNT signaling is an evolutionarily conserved pathway that plays essential roles in development and disease. A recently described branch of WNT signaling, known as WNT/STOP (stabilization of proteins), promotes cell growth and division by stabilizing target proteins from glycogen synthase 3 (GSK3)-mediated degradation. Key regulators of WNT/STOP are Cyclin Y (CCNY) and Cyclin Y like 1 (CCNYL1), conserved cyclins that, together with their associated cyclin dependent kinase 14 (CDK14) and 16 (CDK16), phosphorylate and prime the WNT co-receptor LRP6, thereby inhibiting GSK3. Most of the biological functions of WNT/STOP signaling have been described in vitro, or in post-transcriptional germ cells. However, whether or not WNT/STOP signaling plays essential roles in dividing somatic cells is incompletely understood.

In order to study the *in vivo* functions of WNT/STOP signaling in somatic cells, Ccny/Ccnyl1 double knockout (DKO) mice were generated and analyzed. Strikingly, mutant embryos displayed severe defects in the neocortex characterized by a thinner lateral cortex and reduced basal progenitors and post mitotic neurons. Mechanistically, WNT/STOP is shown to promote asymmetric cell division by regulating the levels of apical-basal astral microtubules, and the differentiation of neural progenitors by stabilizing Sox4 and Sox11, two neurogenic transcription factors that are characterized as direct GSK3 substrates in this thesis.

Apart from the neurogenesis defects, Ccny/l1 deficiency also led to defects in primary cilia formation in apical progenitors. Primary cilia are microtubule-based organelles involved in transducing cell signaling pathways and defects in cilia formation are associated with human disease. A detailed phenotypic analysis of DKO embryos and cell lines deficient or mutant for Ccny/l1 revealed that the regulation of ciliogenesis by WNT/STOP signaling was also extended to developing kidneys, 293T cells and adult mouse preadipocytes. Mechanistically, CCNY and LRP6 concentrate in primary cilia and LRP6 becomes phosphorylated following WNT stimulation, suggesting that cilia act as WNT-responsive organelles. WNT/STOP signaling activates the Protein

phosphatase 1 regulatory subunit PPP1R2 in the cilia, which then inhibits the negative ciliary regulator protein phosphatase 1 (PP1). In summary, the findings in this thesis unveil crucial *in vivo* roles for WNT/STOP signaling in neocortex development and primary cilia formation, with important implications for embryonic development and disease.

2. ZUSAMMENFASSUNG

Der Wnt Signalweg ist evolutionär konserviert und spielt eine wesentliche Rolle in der Entwicklungsbiologie sowie in diversen Krankheitsbildern. Ein Subtyp, der sogenannte Wnt/STOP Signalweg, fördert das Zellwachstum und die Zellteilung indem Zielproteine vor dem Abbau durch GSK-3 geschützt werden. Die konservierten Cycline Cyclin Y (CCNY) und Cyclin Y like 1 (CCNYL1) phosphorylieren gemeinsam mit den assoziierten Cyclin-abhängigen Kinasen 14 (CDK14) und 16 (CDK16) den Wnt Co-Rezeptor LRP6 und inhibieren somit GSK-3. Die Rolle des WNT/STOP Signalweges wurde bisher hauptsächlich in vitro oder in post-transkriptionellen Keimzellen beschrieben. Es ist nicht vollständig aufgeklärt, ob der WNT/STOP Signalweg ebenso in sich teilenden, somatischen Zellen relevant ist.

Um WNT/STOP *in vivo* zu wurden Ccny/Ccnyl1 double-knockout (DKO) Mäuse generiert. Erstaunlicherweise zeigten die Embryonen Fehlbildungen im Neocortex, welche sich durch einen dünneren lateralen Cortex und reduzierte Neurogenese äußerten. WNT/STOP fördert die asymmetrische Zellteilung durch die Regulierung der apikal-basalen astralen Mikrotubuli und die Differenzierung von neuronalen Vorläuferzellen durch die Stabilisierung von Sox4 und Sox11, zwei neurogene Transkriptionsfaktoren, welche in dieser Arbeit als direkte Substrate für GSK3 charakterisiert wurden.

Zusäztlich, hat die Unterversorgung mit Ccny/l1 auch zu Fehlern in der Entstehung von primären Zilien in apikalen Voräuferzellen geführt. Primäre Zilien sind Mikrotubuli-basierte Organellen, die für die Weiterleitung von Zellsignalen und Signalwegen benötigt werden und fehlerhalte Ziliogenese wird häufig mit menschlichen Krankheiten assoziert. Eine genaue Analyse der DKO Phänotypen sowie von Ccny/l1 defizienten- oder mutierten Zelllinien hat ergeben, dass die Regulierung der Ziliogenese durch WNT/STOP auch in der Nierenentwicklung, in 293T Zellen und in Pre-Adipozyten von ausgewachsenen Mäusen eine wichtige Rolle spielt. Mechanistisch konnten wir zeigen, dass CCNY und LRP6 in primären Zilien angereichert sind und die Phosphorylierung von LRP6 nach Wnt-Stimulierung lässt darauf schließen, dass Zilien WNT-reaktive Zellorganellen sind. WNT/STOP

aktiviert dabei PPP1R2, was wiederum eine Inhibierung von PP1, einem Inhibitor der Ziliogenese, zur Folge hat. Die Erkenntnisse in dieser Arbeit enthüllen die wesentliche Rolle von WNT/STOP in der Entwicklung des Neocortex und der Ziliogenese von primären Zilien, mit wichtigen Anwendungen in der Embryonalentwicklung und in unterschiedlichen Krankheitsbildern.

3. INTRODUCTION

3.1 Canonical WNT signaling pathway

WNT signaling plays important roles in development and disease. Depending on which ligands and receptors are engaged, WNT signaling is generally sub-divided into either canonical or non-canonical pathways[1]. The well-characterized canonical WNT pathway, also referred to as the WNT/β–catenin pathway, regulates target gene transcription through a complex signaling transduction cascade that begins at the plasma membrane and ends in the nucleus. In the absence of WNT ligands, cytoplasmic β-catenin is bound by the so-called 'destruction complex' made up of the scaffold proteins Axin and adenomatous polyposis coli (APC), and the kinases glycogen synthase kinase 3 (GSK3), and casein kinase 1α (CK1α) (Ikeda et al., 1998; Pronobis et al., 2015), the latter of which sequentially phosphorylate β-catenin at the amino-terminus (Liu et al., 2002). Phosphorylated β-catenin is ubiquitinated by β-transducin repeat containing protein (β-Trcp) and degraded via the ubiquitin-proteasome pathway (Aberle et al., 1997). In the absence of β-catenin, Tcf/Lef transcription factors bind to target gene promoters and repress transcription (Niehrs and Shen, 2010).

Upon WNT ligand binding to both the Frizzled (FZD) and low-density lipoprotein receptor-related protein 5/6 (LRP5/6) receptors, dishevelled (DVL), an essential scaffold protein, is recruited to the cell membrane to provide a platform for receptor clustering. LRP6 is then phosphorylated by CK1γ and GSK3 on the intracellular domain (ICD). Phosphorylated LRP6 interacts with Axin, which sequesters the destruction complex, resulting in further amplification of the LRP6/Axin interaction via increased GSK3 and CK1-mediated LRP6 phosphorylation (Niehrs and Shen, 2010). The clustering of the above mentioned proteins leads to what are known as 'LRP6 signalosomes', which are first endocytosed into early endosomes, and later, mature into multivesicular bodies (Bilic et al., 2007).The sequestering of the destruction complex via endocytosis leads to the stabilization of cytoplasmic β-catenin, which then translocates to the nucleus where it binds Tcf/Lef and activates target gene transcription.

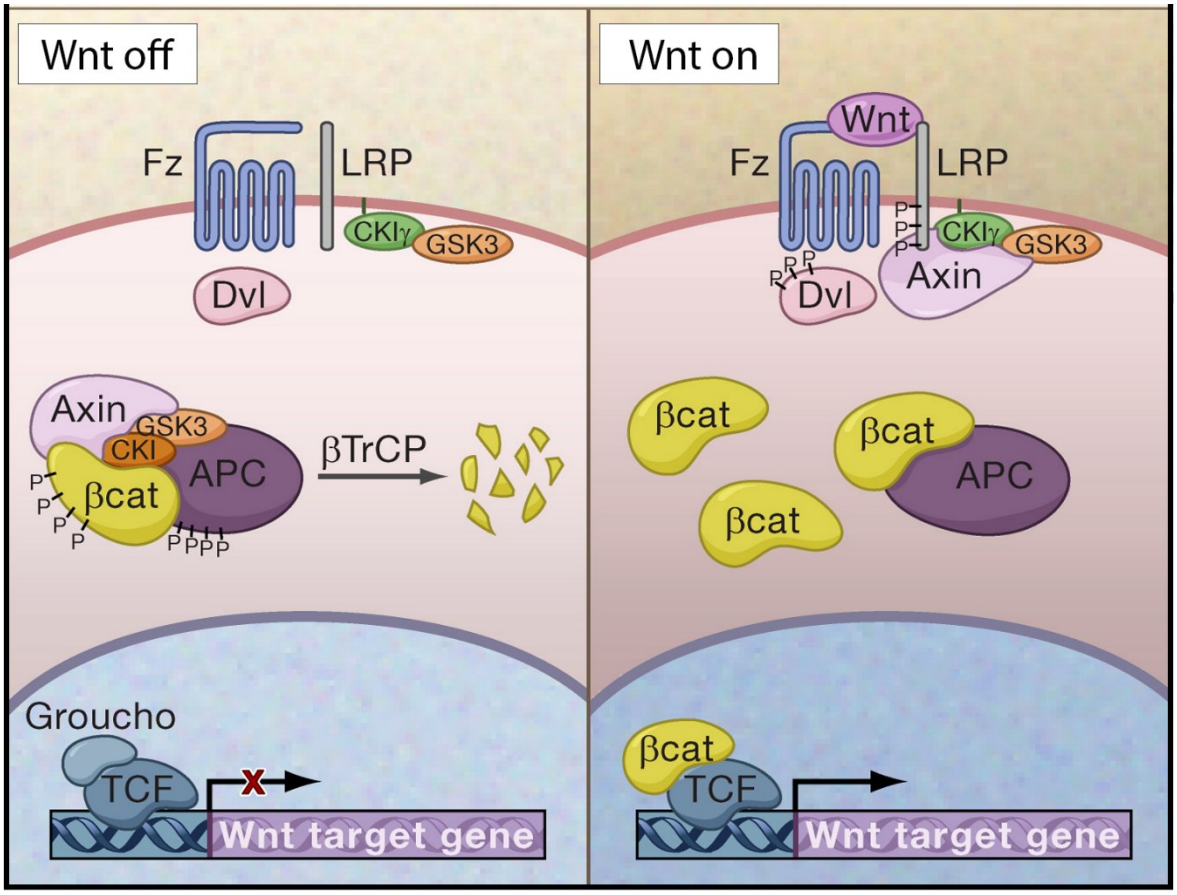

Figure 1.1 Canonical WNT signaling.

In the absence of Wnt (left panel), cytosolic β-catenin is targeted for proteasomal degradation by the destruction complex consisting of Axin, APC, CKI and GSK3. In the presence of Wnt (right panel), the destruction complex is disrupted by the WNT-receptor complex, which further promotes β-catenin translocation to the nucleus and WNT target gene expression. Figure modified from(Clevers, 2006).

3.2 Non-canonical WNT signaling pathway

Non-canonical WNT signaling is is independent of β-catenin-mediated transcription. Two of the best characterized non canonical pathways are the WNT/planar cell polarity (PCP) and WNT/Ca^{2+} pathways(Kikuchi et al., 2009). WNT/PCP signaling is triggered via the binding of non-canonical WNT ligands such as Wnt5a or Wnt11 to FZD, the binding then recruits DVL to the plasma membrane and activates the small GTPases

RHOA and RAC1. RHOA and RAC1 then further activate Rho-associated coiled-coil containing protein kinase (ROCK) and JUN-N-terminal kinase (JNK), resulting in cytoskeletal reorganization and regulation of cell polarity(Bengoa-Vergniory and Kypta, 2015; Semenov et al., 2007) WNT/PCP signaling is involved in several morphogenetic processes such as gastrulation, neural tube closure, and stereocilia orientation in the inner ear(Gomez-Orte et al., 2013).

In the WNT/Ca^{2+} pathway, Wnt binds to FZD receptors and then recruits DVL, resulting in activation of phospholipase C (PLC), which then produces 1,2 diacyglycerol (DAG). DAG activates protein kinase C (PKC) and inositol 1,4,5-tri-phosphate (IP_3), leading to an increase in Ca^{2+} concentration in the cell. Increased Ca^{2+} can activate Protein kinase C (PKC), which is an activator of Cdc42 to promote cell adhesion and tissue separation. Ca^{2+} can also activate Ca^{2+}/calmodulin-dependent protein kinase II (CaMKII) and phosphatase CAN, which together activate the transcription factor-Nuclear factor of activated T cells (NFAT). NFAT is a well-known regulator of ventral patterning during development(Semenov et al., 2007).

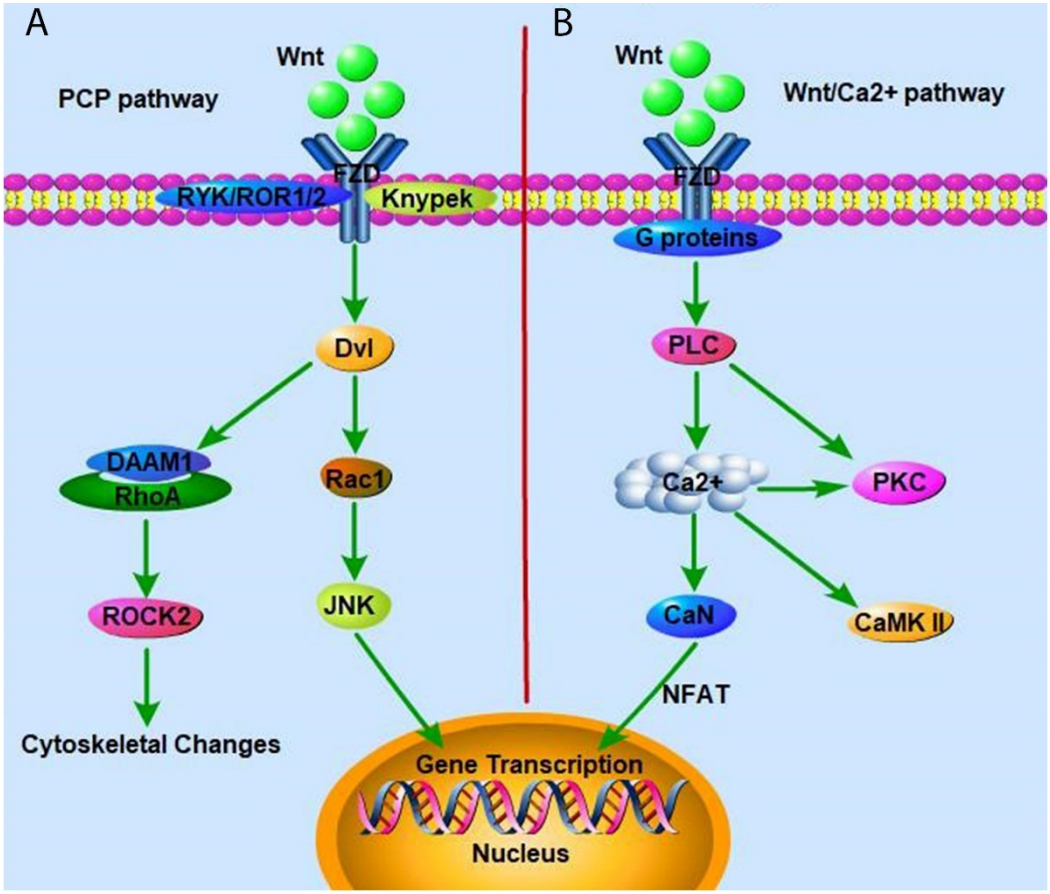

Figure 1.2 Non-canonical WNT signaling.

A) WNT/PCP signaling activates RHOA and RAC1, which further activate, respectively, ROCK and JNK to regulate cell polarity and cell migration.
B) WNT/Ca2+ signaling functions by activating PLC, which induces intracellular Ca2+ release and activation of CaN and CaMKII. Figure modified from(Han et al., 2020)

3.3 WNT/STOP signaling pathway

WNT/STOP (stabilization of proteins) signaling is a newly discovered WNT branch that functions on the post-transcriptional level and is independent of β-catenin (Bilic et al., 2007). Key players in WNT/STOP are cyclin Y (CCNY) and cyclin Y-like 1 (CCNYL1), conserved cyclins that together with their associated cyclin-dependent protein kinases CDK14 and CDK16 phosphorylate LRP6 at the ICD and thereby prime it for WNT dependent phosphorylation by CK1γ (Davidson and Niehrs, 2010; Koch et al., 2015). CCNY/L1 are concentrated at the inner surface of the plasma membrane and their

protein levels oscillate with the cell cycle, peaking at G2M (Acebron et al., 2014). Hence, WNT/STOP signaling is most active during mitosis, when cells are transcriptionally inactive. The main purpose of WNT/STOP signaling is to inhibit GSK3 activity, since GSK3 can, aside from β–catenin, phosphorylate numerous other target proteins. Indeed proteomics analyses have revealed that up to 20% of the human proteome contains putative GSK phosphorylation sites (Bilic et al., 2007). Upon phosphorylated, these GSK3 substrates are recognized by E3 ubiquitin ligases such as F box/WD repeat-containing protein 7 (FBW7), β-TrCP and Neural precursor cell expressed, developmentally downregulated 4-like (NEDD4L), which anchor them for proteasomal degradation (Huang et al., 2015). The activation of WNT/STOP signaling during mitosis thus protects essential proteins from degradation, ensuring that critical biological processes such as cell growth and cell cycle progression are carried out in a timely and effective manner (Acebron et al., 2014).

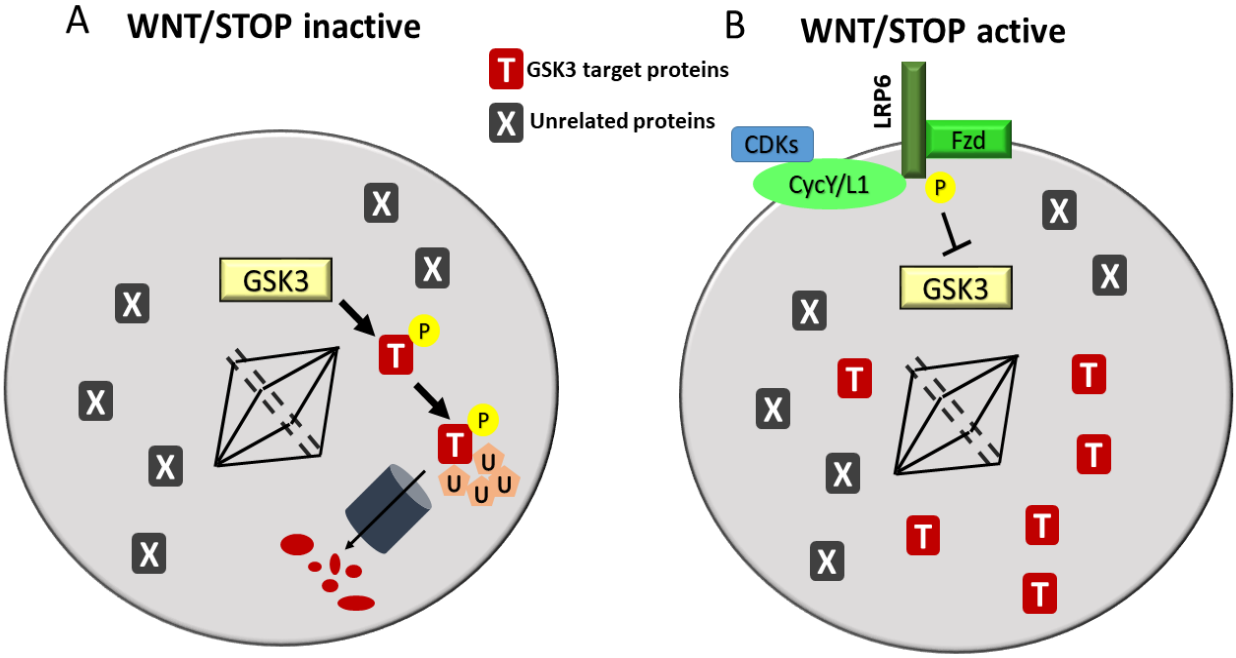

Figure 1.3 WNT/STOP signaling pathway

A) In the absence of WNT/STOP signaling in mitotic cells, GSK3 phosphorylates target proteins, leading to their ubiquitination and proteasomal degradation.
B) WNT/STOP signaling is activated by Cyclin Y/L1 and their associated CDKs, which phosphorylate LRP6 during mitosis. Phosphorylated LRP6 inhibits GSK3 activity, resulting in protein stabilization. Figure modified from(Acebron et al., 2014).

3.4 *In vivo* roles for WNT/STOP signaling

In vivo evidence for WNT/STOP signaling was first discovered in germ cells and, later, in cancer cells. In *Xenopus*, WNT/STOP signaling is upregulated in oocytes after their entry into meiotic metaphase II, when transcription is silenced. Inhibition of maternal WNT/STOP signaling by Ccny morpholino treatment gives rise to early cleavage arrest after fertilization due to enhanced protein degradation (Huang et al., 2015). Further evidence for WNT/STOP can be found in *Ccnyl1* mutant mice, which display sperm structural and motility defects and are infertile as a result. Interestingly, despite being transcriptionally silent, spermatozoa respond to WNT signals from the epididymis. The main role of WNT/STOP signaling in spermatozoa is to promote sperm maturation by maintaining the protein diffusion barrier and regulating sperm motility(Koch et al., 2015). In regards to cancer, WNT/STOP has been reported to induce asparaginase sensitization in drug-resistant leukemia cells and to regulate ribosome biogenesis in pancreatic cancer cells(Hinze et al., 2019).

3.5 Cerebral cortex development

3.5.1 Cerebral cortex

The cerebral cortex, also regarded as the cerebral mantle, is a central region in the mammalian brain that coordinates complex cognitive behaviors [19]. The cerebral cortex consists mainly of the six-layered neocortex and, occupying a much smaller percentage, the allocortex. It is divided into two cortices by the longitudinal fissure that distinguishes the cerebrum into the left and right hemispheres. In most mammals, the

cerebral cortex is folded, resulting in a larger surface within the confined volume of the cranium. Cortical folding is crucial for the functional organization of the brain(Fernandez et al., 2016). Based on the presence or absence of cortical folding, mammals are classified as lissencephalic species (e.g. mice), which display smooth-surfaced cortices, and gyrencephalic species (e.g. ferrets and most primates), which display convolutions in the cerebral cortex. Regardless of the structural differences among species, the growth of the cerebral cortex depends heavily on the coordination of cellular and molecular networks. On one hand, it counts on the expansion of neural stem cells (NSCs) and neural progenitors (NPs), as well as the subsequent maturation and migration of post-mitotic neurons. On the other hand, it also requires the expression of key components from different signaling pathways such as WNT, NOTCH, and FGF signaling, among others.

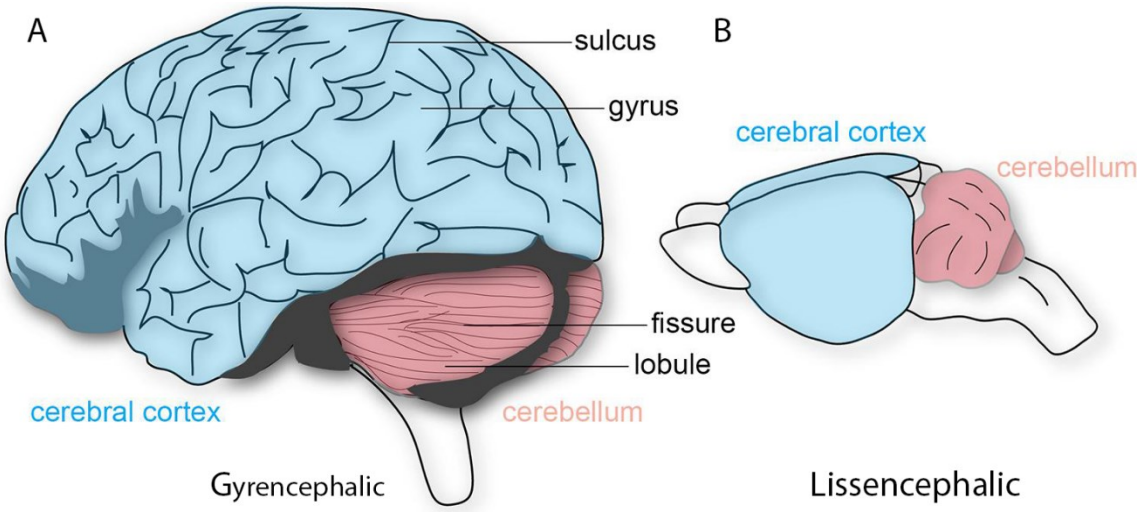

Figure 1.4 Structure of cerebral cortex.

A) The cerebral cortex from gyrencephalic species displays a typical folding pattern, consisting of gyri (peaks) that are interrupted by sulci (valleys).
B) The cerebral cortex from lissencephalic species is not folded and displays a smooth surface. Figure modified from(Miterko et al., 2018).

3.5.2 Development of the cerebral cortex

Right before the onset of neurogenesis, the neuroepithelial stem cells undergo several rounds of symmetric cell division to expand and generate neurogenic ventricular radial glia (vRG) cells,. At this early stage, morphogen gradients, such as fibroblast growth factor (FGF), WNT and bone morphogenetic protein (BMP) signaling by the roof plate area, and transforming growth factor α (TGF-α) from the ventral pallium, trigger the expression of a variety of transcription factors in the epithelium(Bayatti et al., 2008; Britanova et al., 2006). These factors subsequently induce regional-specific programs and control the cell fate of different lineages of neuronal cells in different brain regions. In the neocortex, these transcription factors include EMX1, EMX2, PAX6 and COUP-TF1. Most of these factors are expressed basaically in radial glia (RG) cells, and their loss of function results in changes in the cortical area map, demonstrating their critical function in corticogenesis. Right after the onset of neurogenesis, dividing intermediate progenitor (IP) cells are generated at the basal border of the VZ(1970). Accumulation of these progenitor cells leads to the formation of a distinct new compartment above the VZ, named the subventricular zone (SVZ). These progenitor cells arise from asymmetrically dividing RGs, and they afterwards migrate into the SVZ(Haubensak et al., 2004). Once generated, the majority of these SVZ progenitors are thought to undergo terminal symmetric division, giving rise to two neurons(Noctor et al., 2004). Unlike radial glia cells that mainly express PAX6 and GLAST, intermediate progenitors express the transcription factors TBR2, neurogenin 2 (NGN2), cut-like homebox 1 (CUX1) and CUX2(Gotz and Barde, 2005).

3.5.3 WNT signaling and early cerebral cortex development

WNT signaling plays essential roles during brain development and is indispensable for initial patterning of the cortex(Agirman et al., 2017). Several WNT ligands (e.g. Wnt (2b, 3a, 5a, 7b,8b)) are secreted by the cortical hem, a transient structure in the dorsalmedial telencephalon. Through interaction with receptors in VZ progenitors, WNT ligands orchestrate dorsal-ventral patterning of the cerebral cortex(Caronia-Brown et al., 2014; Grove et al., 1998). Studies utilizing a WNT reporter mouse model indicate that WNT activity is originally scattered in the developing cerebral cortex at E8.5, however, from E10.5 onwards WNT activity becomes distributed along a dorsally

restricted medial-to-lateral gradient(Machon et al., 2007). This gradient is consistent with the formation of an opposing anteroposterior and lateromedial neurogenesis gradient, indicating the pivotal role of WNT signalling in the specification of the dorsoventral and mediolateral telencephala(Machon et al., 2007).

3.5.4 Mouse cerebral cortex development

The mouse cerebral cortex originates from the rostral part of the neural tube during embryonic development (Agirman et al., 2017). During early stages of development, the rostral part of the neural tube expands and gives rise to two telencephalic vesicles. The dorsal half of these vesicles constitute the primordium of the cerebral cortex(Mukhtar and Taylor, 2018). At this stage the cortex only consists of a single population of cells known as neuroepithelial cells (NECs)(Gotz and Barde, 2005). The NECs are highly polarized NSCs that attach to each other by adherent and tight junctions. During the initial stages of neocortical development, NECs undergo several rounds of symmetric self-amplifying divisions in order to generate more daughter NECs for later neurogenesis stages. Immediately prior to neurogenesis, NECs begin to lose their polarity and, by asymmetric cell division, are transformed into apical radial glia cells (aRGs), also referred to as primary neural progenitor cells (NPCs)(Gotz and Barde, 2005). The aRGs display radial glia fibers that support the migration of new born cortical neurons to the outer layers of the neocortex. These aRG cells reside at the apical surface of the cortex, forming the ventricular zone (VZ). During neurogenesis, aRG cells undergo asymmetric cell division, giving rise to one aRG and either one intermediate progenitor (IP) (the most common pathway and mammals) or one post-mitotic neuron. Intermediate progenitors (IPs) do not display apical-basal polarity and reside in the region located basally to the VZ, termed the subventricular zone (SVZ)(Sun and Hevner, 2014). Afterwards, the IP cells usually undergo symmetric consumptive divisions to generate two post-mitotic neurons. These new-born neurons, which are primarily cortical excitatory neurons, travel from their layer of birth (mostly the SVZ) to the vicinity of the cortical surface, being guided by the radial glia fibers that perpendicularly span the apical and pial surfaces of the cortex(Arai and Taverna, 2017). Once the neurons finish radial migration and detach from the radial fibers, they undergo terminal differentiation(Arai and Taverna, 2017). Overall, the

process of neuron generation from their progenitor precursors is critical for determining the final size of the cerebral cortex.

Several signaling cascades are involved in the early stages of cortical development(Grasby et al., 2020). One of the most prominent pathways is the canonical WNT pathway, which has been repeatedly shown to promote NEC self-amplification(Chenn, 2008). On the other hand, the FGF signaling pathway is reported to promote the transition of NEC cells to aRG cells(Iwata and Hevner, 2009). This transition is also benefited by Notch signaling(Hashimoto-Torii et al., 2008). Later on, by modulating the cell cycle of NPCs, FGF signaling can inhibit neurogenesis and promote NPC proliferation. Specifically, FGF2 upregulates cyclin D1 and downregulates p21, a cyclin-dependent kinase inhibitor, thereby shortening the G1 phase of the cell cycle and promoting self-renewal(Iwata and Hevner, 2009; Matsumoto et al., 2017). Similarly, activation of the Notch signaling pathway at later stages also inhibits the generation of IPs from aRGs. However, the expression of the Notch ligand Dll1 is closely regulated by Ngn2 and Ascl1, two major regulators of neurogenesis. Importantly, NOTCH signaling is also important for the proliferation of human neural progenitor cells(Martynoga et al., 2012).

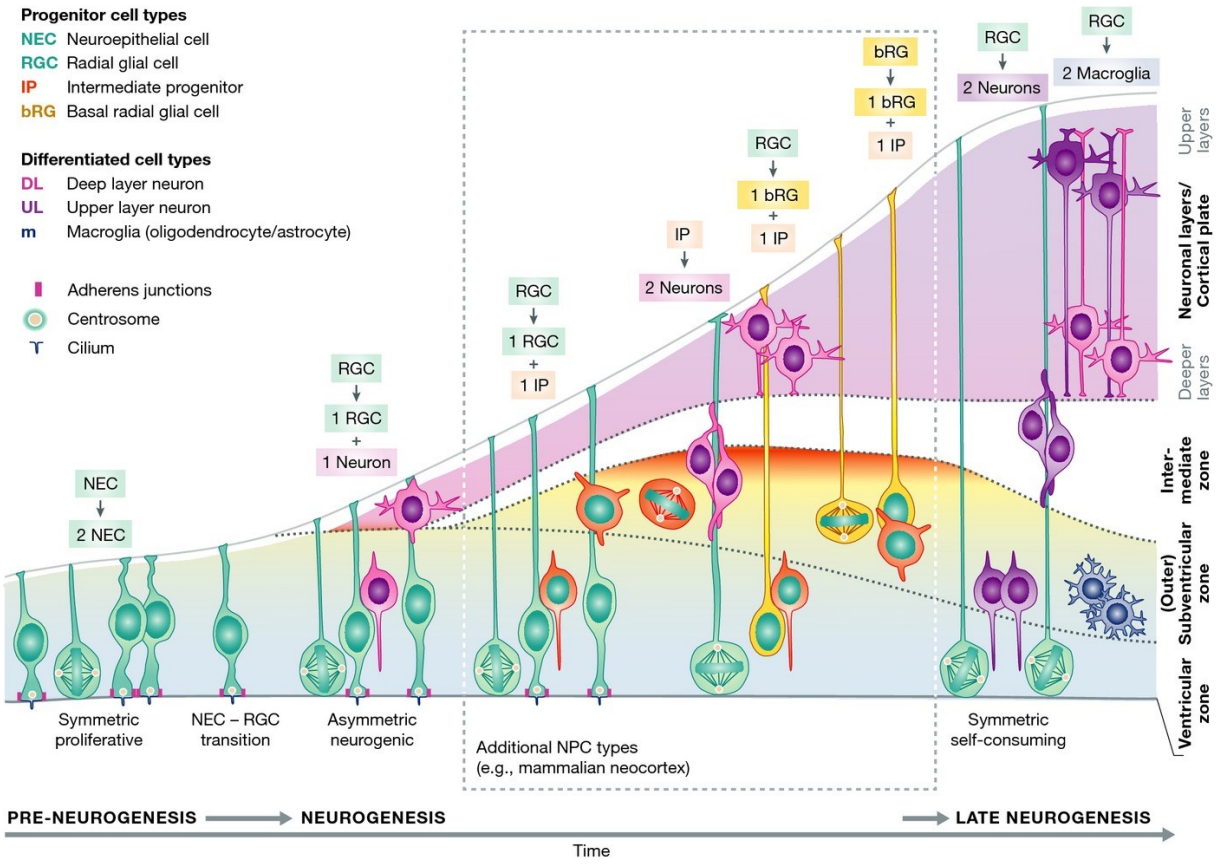

Figure 1.5 Schematic overview of mammalian cerebral cortex development .

The cellular and laminar organization in developing cortex. The principle types of neural progenitor cells and the progeny they produce are indicated by different colors. Additional neural cells types that are typically found in neocortex are indicated in the box. Figure modified from(Aberle et al., 1997).

3.5.5 Sox4/11 and Cerebral Cortex Development

The Sry-related high mobility group (HMG) box (SOX) family of transcription factors is defined by the highly conserved HMG motif. SOX transcription factors bind to the minor groove of DNA and, together with numerous co-factors, they regulate a multitude of biological processes during embryonic development(Lefebvre et al., 2007). According to their sequence similarity both in the HMG box domain and in the C-terminal region, Sox4 and Sox11 belong to the SoxC subgroup (Bowles et al., 2000; Dy et al., 2008). These two proteins share similar expression patterns and display redundant functions during development and disease, especially in the central nervous system (Dy et al., 2008; Liu et al., 2006; Pramoonjago et al., 2006; Weigle et al., 2005). In the neocortex,

Sox4 is highly expressed by BPs whereas Sox11 is detected in both BPs and newly formed neurons. Conditional loss of function of Sox4 in the neuroepithelium leads to a drastic reduction of Tbr2+ cells while ablation of Sox11 reduces the number of deep layer post-mitotic neurons, with minimal effects on BPs(Aberle et al., 1997).

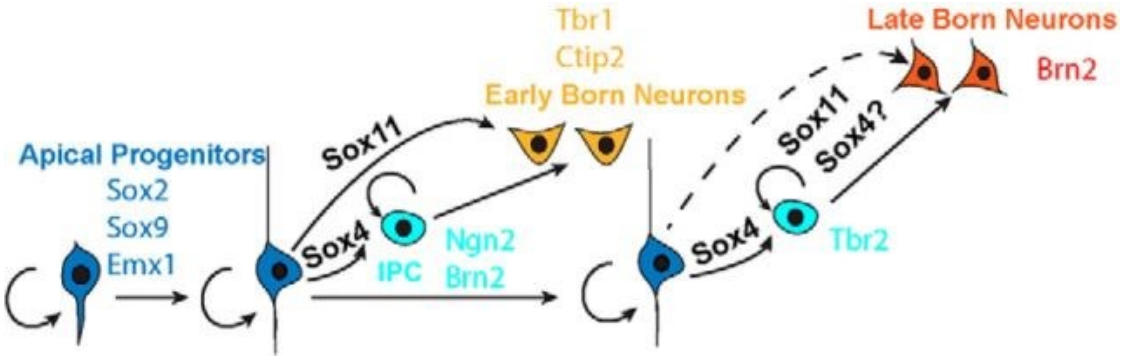

Figure 1.6 Sox4/11 roles during corticogenesis.

Sox4 is mainly expressed in intermediate progenitor (IP) cells, whereas Sox11 displays broader expression, being detected in both IPs and early born neurons. During cortical neurogenesis, Sox4 promotes the transition of apical progenitors in the VZ to IPs within the SVZ, and Sox11 (and perhaps Sox4) promotes the transition of IPs in the SVZ to early and late-born neurons of the SP and deep CP. Figure modified from(Chen et al., 2015).

3.5.6 The role of WNT Signaling in neocortex development

The role of WNT signaling in the cerebral cortex is complex and highly dependent on the models used as well as the epistatic level at which the pathway is manipulated (Harrison-Uy and Pleasure, 2012). During early patterning stages of the telencephalon, WNT signaling is crucial to generate dorsal telencephalic cells in chick explanted cultures (Gunhaga et al., 2003). In the mouse brain, conditional loss of function of β-catenin in the telencephalon before the onset of neurogenesis induces ventralization, with upregulation of the ventral markers Gsh2, Mash1 and Dlx2 (Backman et al., 2005). After the onset of neurogenesis, focal genetic ablation of β-catenin causes cells to prematurely exit the ventricular zone and migrate to the developing cortical plate. This is consistent with additional studies in which overexpression of dominant negative TCF4 or ICAT, specific inhibitors of the WNT/β-catenin pathway, led to premature

differentiation of APs into neurons and increased cell cycle exit(Woodhead et al., 2006). Conversely, overexpression of stabilized β-catenin or deletion of GSK3, a negative regulator of β-catenin, caused massive expansion of the cerebral cortex, owing to cell cycle re-entry and over production of apical progenitors at the expense of basal progenitors(Chenn and Walsh, 2002; Kim et al., 2009; Machon et al., 2007). These gain and loss of function studies indicate that the essential function of canonical WNT/β-catenin signaling is to promote self-renewal in apical progenitors (APs) instead of differentiation. However, *in vitro* studies reveal a different story. Through transcriptional regulation of *N-myc* and the neurogenic transcription factor *Ngn1/2*, WNT/β-catenin signaling has been shown to promote neural progenitor differentiation(Hirabayashi et al., 2004; Li et al., 2016). An interesting observation is that if the manipulation of WNT is on the ligand, receptor or intracellular level, the outputs differ. For instance, Wnt7a/b overexpression in cortical explants display more $PCNA^{+}$ cells, indicating that WNT can promote neural progenitor proliferation(Qu et al., 2013; Viti et al., 2003). Meanwhile, electroporation of Wnt3a into the ventricles of developing embryos leads to both AP self-renewal and neuronal differentiation(Munji et al., 2011). In contrast, mice mutant for LRP6, the core component for both canonical WNT and WNT/STOP, display only neuronal differentiation defects, and no major differences in self-renewal(Zhou et al., 2006)

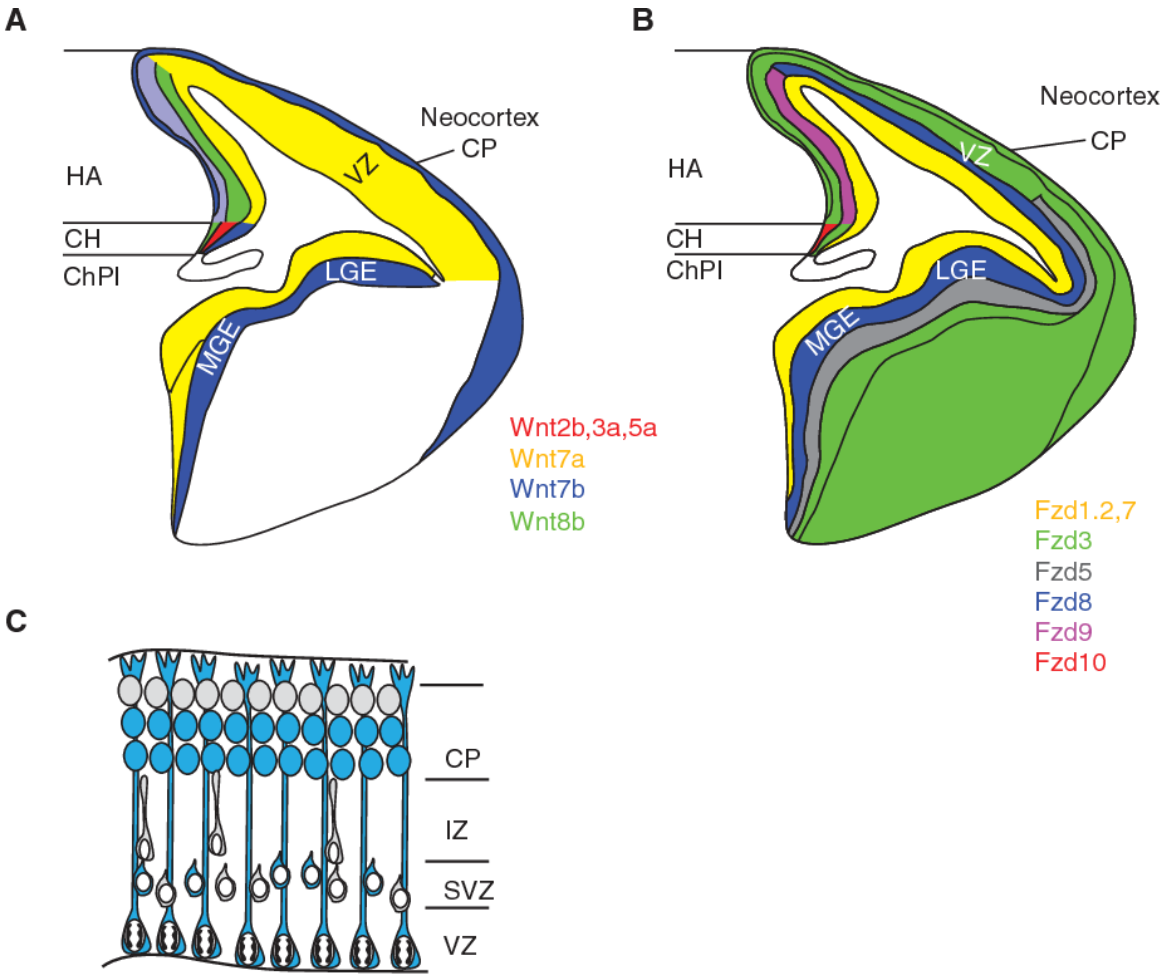

Figure 1.7 WNT Signaling in the neocortex.

A) and **B)** Expression of WNT ligands and receptors in the neocortex at E12.5 and E14.5.
C) At E14.5, WNT signaling is activated (blue) in radial glia cells in the VZ, a subpopulation of IPCs in the SVZ, and is decreased in migrating neurons in the IZ. One day after cells achieve the CP, they shift to WNT responsive. Abbreviations: ChPl, choroid plexus; CH, cortical hem; HA, hippocampal anlage; VZ, ventricular zone; CP, cortical plate; LGE, lateral ganglionic eminence; MGE, medial ganglionic eminence; VZ, ventricular zone; SVZ, subventricular zone; IZ, intermediate zone. Figure modified from(Harrison-Uy and Pleasure, 2012)

3.6 Primary cilia and WNT signaling

3.6.1 Cilia structure

Cilia are highly conserved microtubule-based organelles protruding from the cell surface(Malicki and Johnson, 2017). These complex and dynamic structures are broadly divided into motile or primary subtypes, based on thr structures and functions. Motile cilia are found in specialized cells such as sperm and multiciliated epithelial cells. These cilia display distinctly regulated and organized beating dynamics(Mitchison and Valente, 2017). Primary cilia are existing as a single copy on most sensory cells, and they can recognize extracellular chemicals and transduce crucial signaling pathways(Malicki and Johnson, 2017). Regarding the structure, the cilium is made up of a microtubule-based core compartment called the axoneme, which is enveloped by the ciliary membrane that is continuous with the plasma membrane. The axoneme is initiated from nine parallel doublet microtubules that protrude from the centriole-derived basal body. The doublet microtubules consist of one complete microtubule (the A tubule) and a second incomplete microtubule (the B tubule). In order to promote bending motions, motile cilia have an extra pair of microtubules in the center of the axoneme, termed the central pair, to which radial spokes and dynein arms are attached. The tubulin of the outer doublets is subject to numerous post-translational modifications such as acetylation (Gaertig and Wloga, 2008), glutamylation and glycylation, all of which appear to be important for ciliary assembly and motility(Kubo et al., 2010; Pathak et al., 2007; Thazhath et al., 2004). The region where the axonemal outer doublets start to establish is referred to as the transition zone, a conserved ciliary subdomain characterized by Y-shaped fibers that links the doublet microtubule to the ciliary membrane(Reiter et al., 2012). Mutations in proteins that traffic to and regulate the function of the transition zone are closely associated with cilia-related diseases, generally regarded as ciliopathies (Garcia-Gonzalo et al., 2011). The transition zone itself serves as a gatekeeper controlling the movement of proteins into the cilium, thereby maintaining the unique composition of proteins present in cilia(Goncalves and Pelletier, 2017). The ciliary pocket, a recessed part of the plasma membrane in which the primary cilium is based, emerges in most but not all of the mammalian ciliated cells, although its function and ultrastructure are not well-known(Ghossoub et al., 2011).

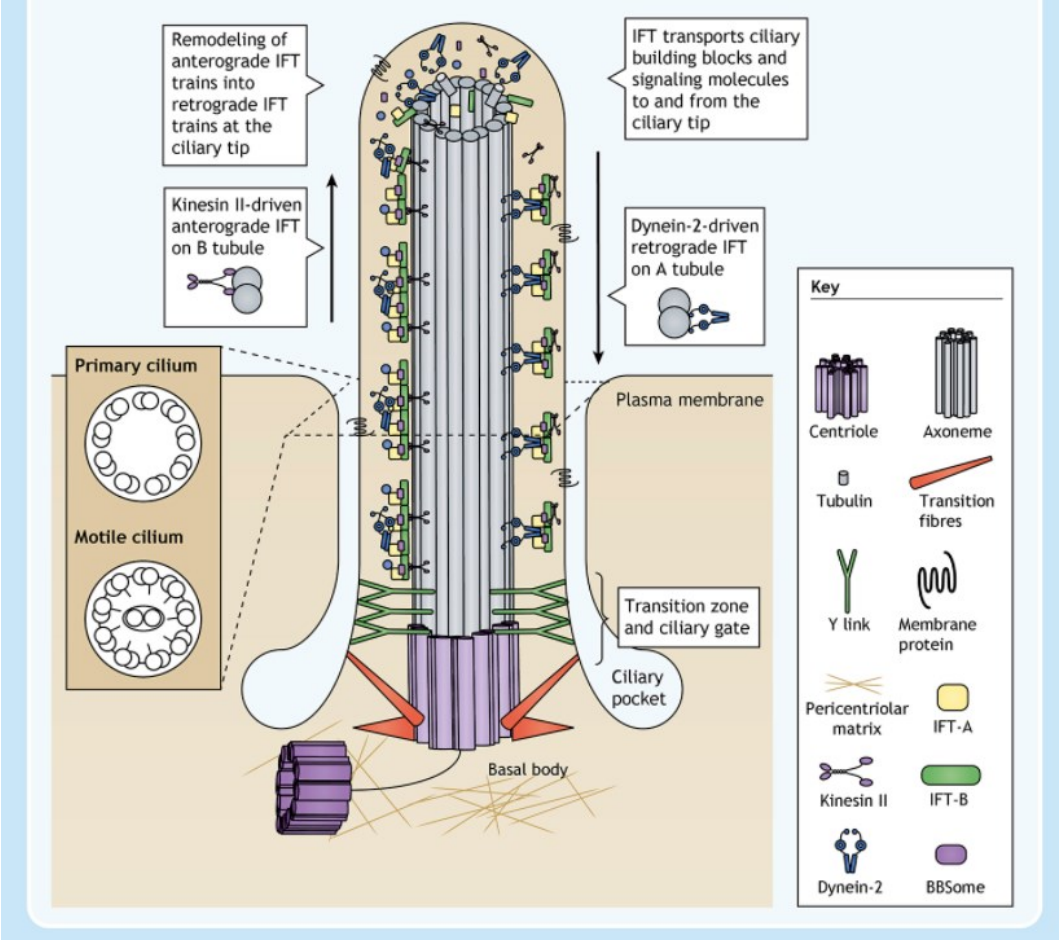

Figure 1.8 Structure of primary cilia and motile cilia.

The structure of cilia contains a bunches of subdomains that are each marked by a specific collection of proteins. The cilium elongatess from the basal body, initiated by the mother centriole, along with subdistal and distal appendage proteins. Transition fibres anchor the basal body to the plasma membrane. Distal to the basal body is the transition zone, characterised by membrane-associated Y-shaped links. Transition fibres and the transition zone compartment shape a permeability barrier named the ‘ciliary gate’ that regulates the composition of ciliary proteins. Figure modified from (Vuolo et al., 2020)

3.6.2 Cilia assembly

The assembly of cilia takes place through a series of delicate and highly coordinated steps and events. Primary cilia typically shape during the G1 or G0 phase of the cell cycle and disassemble prior to mitosis. This ciliary cycle does not apply to multiciliated cells, which are terminally differentiated and do not go through cell division(Ishikawa and Marshall, 2011). At the onset of ciliogenesis, the mother and daughter centrioles migrate to the cell surface and the mother centriole anchors at the bed of the ciliary membrane by transition fibers, becoming what is regarded as the basal body (Sorokin, 1968). The positioning and orientation of the basal body is crucial for proper ciliary alignment and is strictly regulated(Anvarian et al., 2019). After anchoring, the basal body nucleates the outgrowth of the axonemal microtubules that elongate beneath an extension of the membrane, giving rise to cilium generation. Since cilia cannot produce proteins on their own, they rely on the selective protein import and transport from the cytoplasm to the ciliary tip. This is achieved by intraflagellar transport (IFT,) a bidirectional transport system in cilia that moves ciliary components from the cell body to the tip of cilia by anterograde transport and moves back turnover products to the cell body via retrograde transport(Rosenbaum and Witman, 2002). IFT is mainly made up of two large complexes: IFT complex A and complex B (Cole et al., 1998; Piperno and Mead, 1997). IFTA and IFTB complexes function in retrograde and anterograde IFT, respectively(Pedersen and Rosenbaum, 2008). Two types of microtubule motors protein drive IFT: the canonical anterograde IFT motor is a heterotrimeric kinesin-2 with two heterodimerized kinesin-2 motor subunits and is essential for assembly and maintenance for cilia(Cole et al., 1993), whereas dynein 2 is a classical retrograde IFT motor protein and is critical for ciliary disassembly(Pazour et al., 1998).

3.6.3 Cilia function and ciliopathy

The main function of primary cilia is to act as sensory organelles. For instance, during olfaction, the ciliary membrane G protein-coupled receptor (GPCR) transduces the signal from an odorant by producing the secondary messenger cyclic adenosine monophosphate (cAMP), which then activates downstream cascades(Buck and Axel, 1991). A similar process takes place during photoreception. In this case, the opsin GPCRs, which are concentrated at the tip of cilia from vertebrate retinal cells, respond

to light photons by increasing hydrolysis of cyclic guanosine monophosphate (cGMP) to drive light sensation(Elias et al., 2004; Strissel et al., 2005). Recent studies in mice also suggest that primary cilia from preadipocytes play important roles in adipogenesis and fat homeostasis(Hilgendorf et al., 2019). In addition to sensing environmental inputs, primary cilia are also involved in transducing intercellular signals, especially for the Hedgehog (Hh) signaling pathway (Huangfu et al., 2003). Further studies also imply there are some links between cilia and Wnt, Bmp, and platelet derived growth factor (PDGF) signaling (Singla and Reiter, 2006). The dysfunction of primary cilia is associated with a wide range of diseases know as ciliopathies, which stresses the importance of cilia during development, homeostasis and disease(Reiter and Leroux, 2017).

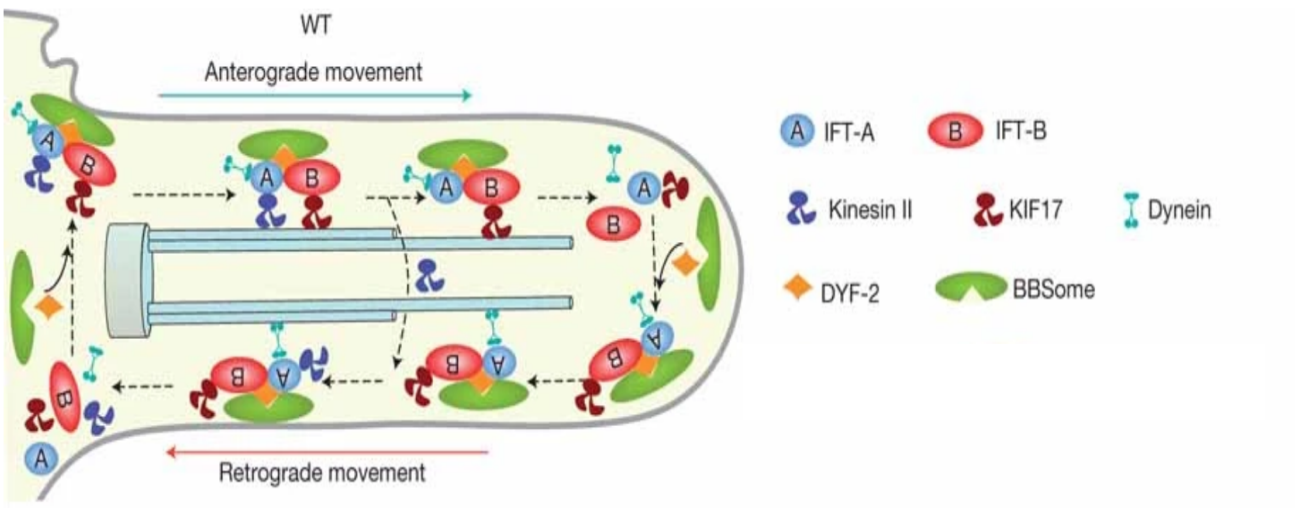

Figure 1.9 Mode for primary cilia IFT assembly and turnover.

At the cilia bed the BBsome organizes IFT-A, IFT-B and kinesin motors into a functional complex. The IFT particles dissociate after arriving at the ciliary tip. The BBSome then starts to reorganize the entire IFT complex to get ready for retrograde transport. Figure modified from(Vuolo et al., 2020; Wei et al., 2012).

3.6.4 WNT signaling and ciliogenesis

A direct relationship between primary cilia and WNT signaling exists through Inversin, a left-right determinant protein located at the basal body of cilia that promotes the transition of canonical Wnt to Wnt/PCP signaling by degrading cytoplasmic Dvl. Mutation of Inversin can cause misoriented hair patterning, a developmental defect similar to that observed in mice lacking the PCP regulator Frizzled-6, and to the wing bristle misorientation displayed by Drosophila PCP mutants.(Lienkamp et al., 2012; Simons et al., 2005). Further studies suggest that removal of cilia by deleting ciliary genes such as Kif3a and Ift88 induces hyper-activation of canonical WNT signaling (Corbit et al., 2008). However, phenotypes of mouse mutants lacking cilia do not overlap with the phenotypes of WNT pathway mutants and many of these mutants have normal canonical WNT signaling(Scholey and Anderson, 2006). Importantly, a systematic analysis of canonical WNT signaling in embryos and cells that are mutant for four different IFT proteins showed no impairment in canonical WNT signaling (Ocbina et al., 2009). Likewise, zebrafish without cilia show dampened hedgehog signaling but normal canonical WNT signaling (Huang and Schier, 2009). Therefore, the restraint of canonical WNT signaling by cilia is cell type and context dependent.

In regards to the effects of WNT signaling on ciliogenesis, there remains much to be learned. On the one hand, there is good evidence that canonical WNT signaling can promote cilia formation through transcriptional activation of phospholipase C (Zhang et al., 2020)or Foxj1a(Caron et al., 2012; Walentek et al., 2012), a master regulator of ciliogenesis in zebrafish. The WNT pathway scaffold protein Dvl is required for basal body anchoring and planar polarization in Xenopus multiciliated and mouse ependymal layer cells(Ohata et al., 2014; Park et al., 2008). Moreover, stimulation with Wnt3a promotes ciliogenesis in human telomerase reverse transcriptase-immortalized retinal pigment epithelial (hTERT-RPE) cells and MCF7/ADR cells by triggering phosphorylation of β-catenin at serine 47 by CK1δ at the subdistal appendage of the mother centriole(Kyun et al., 2020). Conversely, WNT/PCP signaling, which generally antagonizes canonical WNT signaling, is implicated in ciliary disassembly (Lee et al., 2012). On the other hand, β-catenin upregulation in APC mutant mice does not promote- but rather disrupts ciliogenesis in cortical progenitors (Nakagawa et al., 2017) and deleting various WNT pathway components fails to affect cilia in various human

cell lines altogether. Hence, whether WNT signaling promotes or inhibits ciliogenesis is still not clear.

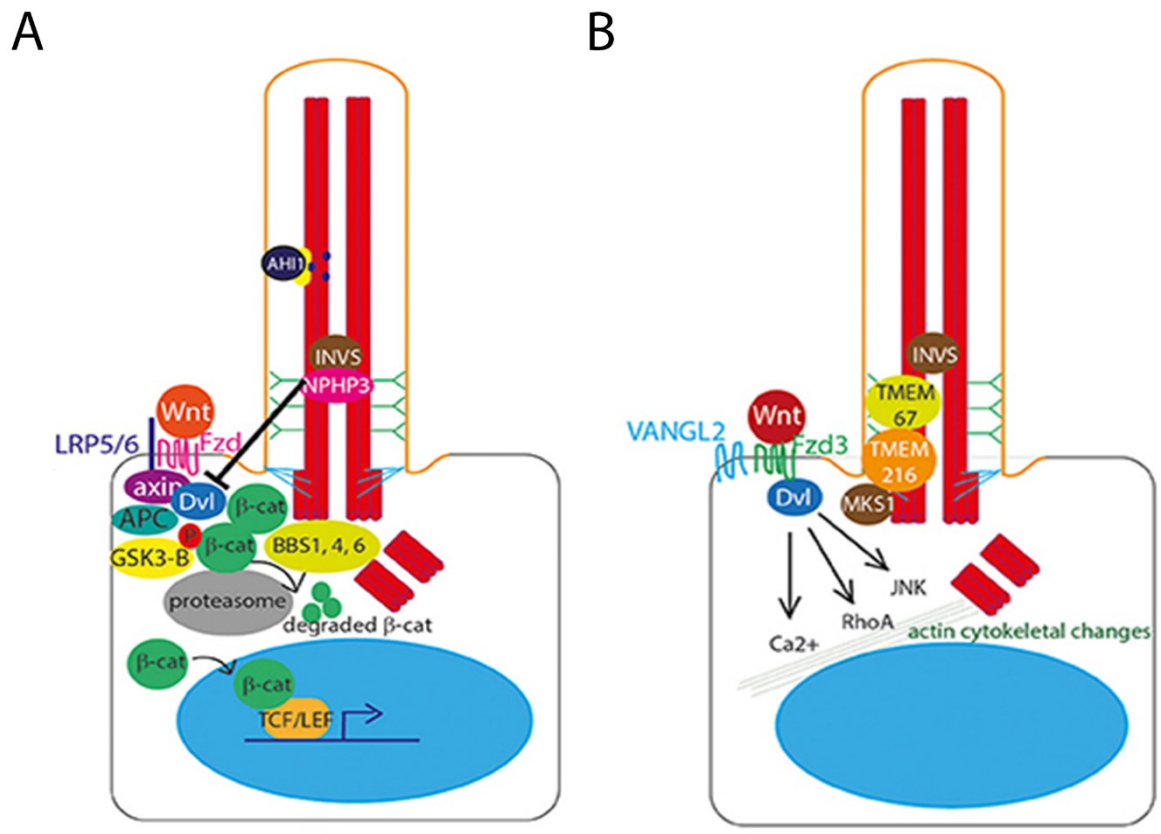

Figure 1.10 Canonical and non-canonical WNT signaling in primary cilia.

A) The primary cilium controls WNT target gene transcription via regulating degradation of Dvl through the ciliary proteins Inversin and NPHP3, and by sequestering AHI1 at the cilium so it cannot assist β-catenin translocation to the nucleus.

B) Non-canonical WNT signaling functions via Dvl to activate RhoA and JNK pathways to stimulate Ca^{2+} release, and actin cytoskeleton remodeling. This is required for accuratet organization of cell polarity by basal body migration to the apical cell surface. The migration is regulated by Dvl and the transition zone proteins meckelin (TMEM67) and TMEM216, together with the basal body protein MKS1.Inversin also plays a critical role in this process. Figure modified from(Wheway et al., 2018).

3.6.5 Protein phosphatase1 (PP1)

The serine/threonine protein phosphatase1 (PP1) is an important enzyme which regulates a variety of cellular processes in eukaryotic cells (Bollen et al., 2010). It is made up of a catalytic subunit, which is conncected to a variety interacting proteins, and solvent-exposed loops that regulate the shape and surface charge as along with the affinity for ligands(Peti et al., 2013). Mammals contain three PP1 encoding genes that translate into four distinct catalytic subunits: PP1α, PP1β, PP1γ1 and PP1γ2. The PP1 isoforms share a similar spectrum of substrate specificity(Ceulemans and Bollen, 2004) and they are ubiquitously expressed in different organs and species(Bollen et al., 2010). PP1 itself can form a stable complex with numerous proteins named PP1 interacting proteins (PIPs), and a large proportion of PIPs are PP1 substrates(Eto, 2009; Margolis et al., 2006). Interestingly, the catalytic activity of PP1 is depending on for its interaction with corresponding PIPs(Fardilha et al., 2011). This interaction is crucial for a dozen of biological functions. For example, in the liver, PP1 regulates glycogen metabolism by verifying the opposite regulation of glycogen breakdown and glycogen synthesis via its interaction with phosphorylase(Berg et al., 2012). In terms of HIV development, PP1 interacting protein Tat anchors PP1 to the nucleus and the then interaction is important to HIV-1 transcription(Nekhai et al., 2007). In Alzheimer's disease, PP1 is anchored by another PIP Tau to microtubules to regulate their stability, indicating its importance in neurodegenerative diseases(Virshup and Shenolikar, 2009).

3.6.6 Protein phosphatase1 (PP1) and Protein phosphatase inhibitor (PPP1R2) and ciliogenesis

One of the PP1 interacting proteins that inhibits its catalytic activity is Protein phosphatase inhibitor (PPP1R2). PPP1R2 interacts with the catalytic subunit of PP1 to form the ATP-Mg^{2+}-dependent protein phosphatase, whose activity is regulated by the phosphorylation of PPP1R2(Yang et al., 2000). PPP1R2 inhibits PP1 activity in two ways: it inhibits the free catalytic subunit, and it controls the cyclic inactivation of the catalytic subunit in the ATP-Mg^{2+}-dependent phosphatase complex. The inhibition of PP1 by PPP1R2 occurs rapidly and leaves the catalytic subunit in its "active"

conformation, even though its activity is blocked. However, inactivation is slower and involves the conversion of the catalytic subunits to an inactive conformation(Yang et al., 2000). The inactive PP1-PPP1R2 complex can be overcome by phosphorylation of PPP1R2 at Thr^{72} by GSK3 or other extracellular kinases(DePaoli-Roach, 1984; Hemmings et al., 1982). PPP1R2 can also be phosphorylated by casein kinase II on Ser^{86}, which serves as a priming phosphorylation for GSK3 (Park et al., 1994).

The PP1-PPP1R2 protein complex regulates a variety of biological processes. In mouse sperm, PPP1R2 promotes the motility of sperm progenitor cells by inhibiting PP1, and this can be inhibited by phosphorylation of PPP1R2 by GSK3 at Thr^{72}. This PP1-PP1R2 axis in mice sperm is orchestrated by WNT/STOP signaling(Koch et al., 2015). In cultured cells, the PP1-PPP1R2 complex plays an important role during ciliogenesis. PP1 and PPP1R2 were found to be concentrated in cilia of human retinal epithelial cells, and knockdown of PPP1R2 significantly reduced microtubule stability in cilia via microtubule acetylation(Wang and Brautigan, 2008).

3.6.7 Adipogenesis and ciliogenesis

White adipose tissue (WAT) saves energy and regulates homeostasis(Rosen and Spiegelman, 2014). WAT can regenerate, expand and contract when tissue is damaged or the nutritional flux is altered(Sakaguchi et al., 2017). For instance, WAT can expand by either generating more adipocytes (hyperplasia) or by storing more fat and lipid in individual adipocytes (hypertrophy)(Haczeyni et al., 2018). The balance between hypertrophic and hyperplastic WAT growth is affected by the potential of WAT precursors, known as preadipocytes, as well as by age, sex, WAT depot distribution, and nutritional intake(Arner et al., 2013; Karastergiou and Fried, 2017; Palmer and Kirkland, 2016).

Adipogenesis is regulated by a variety of signaling pathways, notably insulin and cyclic AMP (cAMP) signaling. Upon stimulation by adipogenic signals, the preadipocytes, which are normally quiescent, re-enter the cell cycle and give rise to daughter cells that eventually differentiate into adipocytes(Jeffery et al., 2015; Wang et al., 2013). The molecular mechanisms of adipogenesis have been further studied in an immortalized murine cell line, namely 3T3-L1 cells. In response to the differentiation factors insulin and glucocorticoid dexamethasone (Dex), as well as the cAMP elevating drug IBMX,

3T3-L1 cells re-enter the cell cycle and activate an adipogenic transcriptional cascade involving PPARγ and CEBPα(Rosen et al., 2000).

Recent studies have indicated a possible role for primary cilia in regulating the differentiation of preadipocytes into adipocytes (Forcioli-Conti et al., 2015; Marion et al., 2009; Zhu et al., 2009). Further work has identified an important role of primary cilia during adipogenesis in both *in vivo* and *in vitro* studies. In WAT, the preadipocytes along the blood vessels are ciliated and loss of preadipocyte cilia by conditionally deleting *Ift88* leads to white adipose tissue expansion defects. Consistently, knockdown of *Ift88* by siRNA transfection in 3T3-L1 cells impaired cililogenesis and adipogenesis(Hilgendorf et al., 2019). Hence, primary cilia appear to play critical roles during adipogenesis.

4. AIM OF THE THESIS

The discovery of WNT/STOP signaling opened the gate to study a novel WNT branch that regulates essential biological processes independently of target gene transcription.

The goal of this Ph.D. project was to further investigate the physiological roles of WNTSTOP signaling. Towards this goal, Ccny/Ccnyl1 (WNT/STOP specific regulators) double knockout mice were generated and characterized, where two striking brain phenotypes were observed: neocortical neurogenesis & ciliogenesis were perturbed at embryonic day E13.5. Multiple experimental strategies including histology, immunohistochemistry, biochemistry, as well as molecular biology techniques were applied to fully characterize these phenotypes. Finally, extensive rescue analyses were performed to comprehensively define the mechanisms and epistasis underlying the role of WNT/STOP signaling in neurogenesis & ciliogenesis.

5. Chapter 1: WNT/STOP SIGNALING REGULATES MOUSE EMBRYONIC NEUROGENESIS

5.1 Introduction and experimental design

WNT signaling is indispensable for neocortex development and understanding the mechanisms through which WNT regulates the various steps of neurogenesis holds great promise in the quest for developing novel regenerative therapies for neurodegenerative diseases. However, despite decades of research, a clear consensus on the precise function of canonical WNT signaling in neocortex development is lacking. Does WNT/β-catenin signaling promote symmetric, self-renewing divisions of neural progenitors or does it regulate asymmetric, neurogenic divisions? Or does it regulate both processes? Analysis of mice mutant for β-catenin suggests that WNT/β-catenin primarily promotes progenitor self-renewal at the expense of differentiation. However, *in vitro* studies suggest the opposite. Further complicating issues, are analyses of mice mutant for WNT regulators that function at different epistatic levels. For example, LRP6 deficient mice show primarily decreased neurogenesis while WNT ligand depletion leads to decreased proliferation. This is further complicated by WNT ligand overexpression in the neocortex, which leads to both self-renewal and neurogenesis. Hence, much remains to be learned about WNT signaling in neocortex development.

One of the difficulties with studying the WNT signaling pathway is that it consists of several sub branches that can have varied biological outputs depending on the cellular context. One of these sub branches is WNT/STOP signalling, a novel pathway with essential functions in germ cells and cancer, but whose functions in somatic dividing cells of the developing embryo are poorly described. In this chapter of my thesis I begin with the hypothesis that WNT/STOP plays an important role in the developing neocortex. Moreover, I predict that the functions of WNT/STOP in the neocortex, upon being characterized, could help clarify and resolve many of the longstanding issues surrounding WNT signaling and neocortical neurogenesis.

In order to study the *in vivo* roles of WNT/STOP signaling in neocortex development I have generated mice mutant for Ccny and Ccnyl1, which are considered the principle

regulators of the WNT/STOP pathway. Ccny/l1 prime LRP6 for incoming WNT ligands and thus activate WNT signaling during G2/M, when cells are transcriptionally inactive. Hence, depletion of Ccny/l1 allows us to study the WNT/STOP pathway without affecting β-catenin mediated transcription, thereby excluding possible confounding effects from canonical WNT signalling. Additionally, by collaborating with the Wieland Huttner lab in Dresden, Germany, I will perform *in utero* electroporation (IUE) of shRNA against *Ccny/l1* to acutely inhibit the WNT/STOP pathway. This will permit analysis of WNT/STOP signaling during later time-points in embryonic development (e.g. E15.5 and E17.5), when the cortical plate is further developed. Finally, to further dissect the mechanisms of WNT/STOP in neurogenesis I will isolate and culture neural progenitor cells from E13.5 control and mutant embryos and then induce their differentiation *in vitro*. This will allow for easy manipulation of the WNT pathway, and for the discovery and characterization of novel WNT/STOP target proteins involved in corticogenesis. The experimental schematic for Chapter 1 of my thesis is shown below:

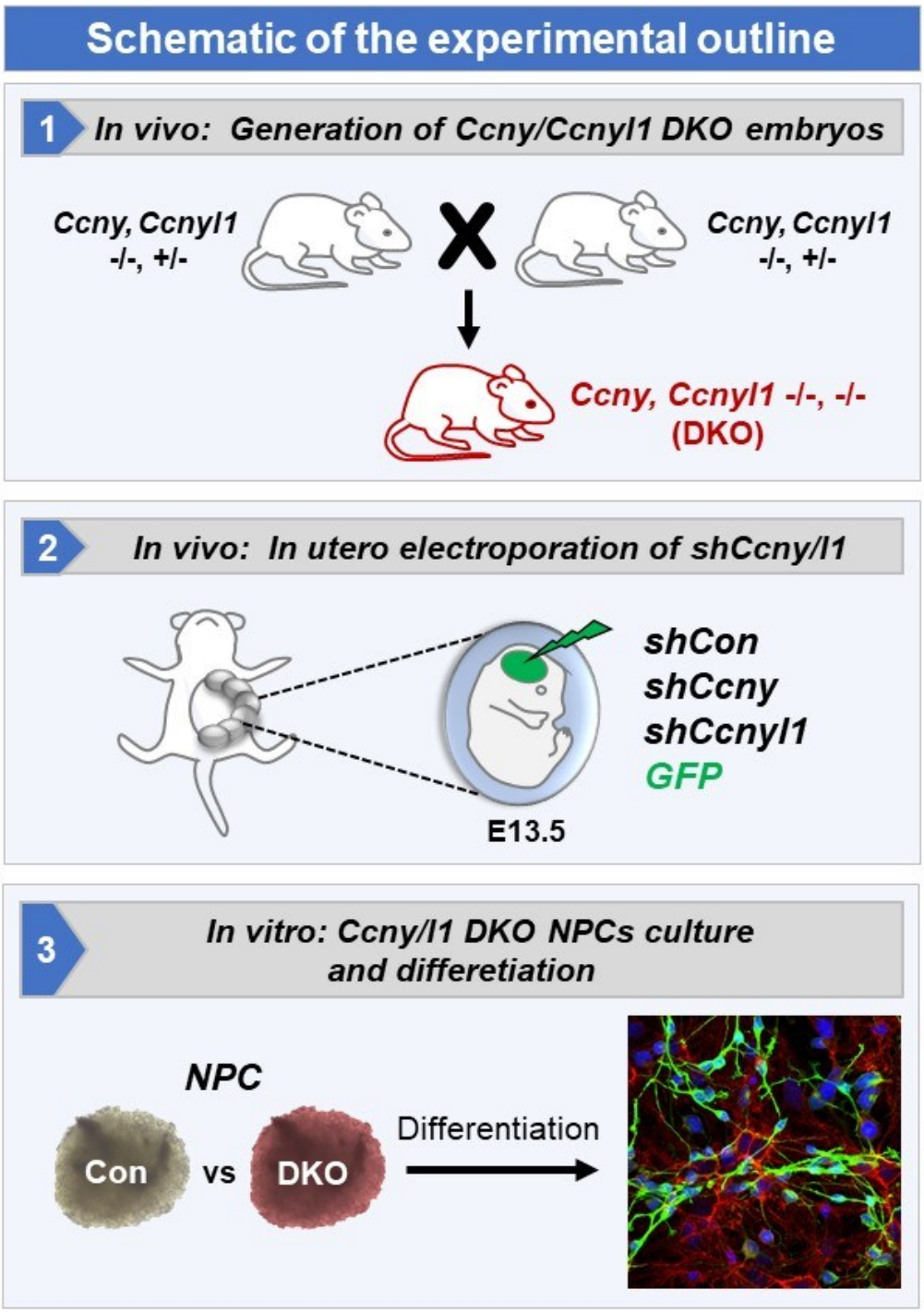
Schematic of the experimental outline
1
In vivo: Generation of Ccny/Ccnyl1 DKO embryos
Ccny, Ccnyl1
-/-, +/-
Ccny, Ccnyl1
-/-, +/-
Ccny, Ccnyl1 -/-, -/-
(DKO)
2
In vivo: In utero electroporation of shCcny/l1
shCon
shCcny
shCcnyl1
GFP
E13.5
3
In vitro: Ccny/l1 DKO NPCs culture
and differetiation
NPC
Con
vs
DKO
Differentiation

5.2 Results

5.2.1 WNT/STOP signaling is required for neurogenesis in the embryonic mouse neocortex

To investigate the function of WNT/STOP signaling, we generated mice mutant for *Ccny* and *Ccnyl1* (hereafter referred to as double knockout (DKO) mice). In comparison with *Ccny* or *Ccnyl1* single knock out mice, which are both viable(An et al., 2015; Koch et al., 2015), DKO embryos displayed embryonic lethality at embryonic day 14.5 (E14.5). Moreover, many DKO embryos displayed striking forebrain defects. To exclude possible non-specific effects resulting from early lethality, we analyzed brain phenotypes from DKO and littermate control embryos at E13.5. Haematoxylin-eosin (H&E) analysis displayed a significantly thinner neocortical wall (-32%, p=0.0004) compared with controls. Mediolateral neocortex length was comparable to control (Control 692±15μm; DKO 671±17μm, p=0.39) (Fig 2.1A). To further investigate the reduction in the thickness of the neocortical wall, we used immunofluorescence to measure VZ, SVZ and intermediate zone (IZ) plus cortical plate (CP) thickness via nuclear staining and T-box brain protein 2 (Tbr2), a BP marker to indicate the SVZ. It showed that the proportion of DKO neocortical wall thickness constituted by the VZ was increased by 12%, however that constituted by the SVZ and IZ+CP was decreased by 20% and 18%, respectively, (Fig 2.1B-C). To further dissect these observations, we measured the number of APs, BPs and post-mitotic deep-layer neurons with the respective markers Paired box protein 6 (Pax6), Tbr2, and T-box brain protein 1 (Tbr1). The proportion of Pax6+ cells in the DKO E13.5 neocortex was mildly increased (+11%, p=0.04) whereas the proportion of Tbr2+ and Tbr1+ cells were decreased (-38%, p=0.0006; -25%, p=0.01; respectively) (Fig 2.1D-I). Therefore, we conclude that DKO embryos display specific neurogenesis defects in the embryonic neocortex.

To analyze the localization WNT/STOP components in the embryonic neocortex, we first performed IF against Ccny and Ccnyl1. Interestingly, both Ccny and Ccnyl1 were enriched at the apical plasma membrane of the VZ (Figure 2.1J). In comparison, there was no Ccny or Ccnyl1 immunoreactivity detection in the neocortex of Ccny or Ccnyl1 KO embryos, confirming that the specificity of the two home-made polyclonal Ccny and

Ccnyl1 antibodies (Figure 2.7A-B) . Ccny and Ccnyl1expression were also found in BPs in the SVZ (Figure 2.1K). To further check the accurate cell type distribution of Ccny/l1 proteins we performed in utero electroporation (IUE) in E13.5 embryos by injecting agreen fluorescent protein (GFP) plasmid, and analyzed embryos at E15.5. Triple IF against Ccny/l1, the AP marker Sox2, and GFP showed Ccny/l1 expression at the apical membrane of electroporated APs, while IF for Ccny/l1, Tbr2 and GFP displayed Ccny/l1 expression pattern as single puncta in BPs (Figure 2.7C-D). In line with these observations, we next performed IF to check phosphorylation of LRP6 with an antibody specific for the casein kinase I gamma (CK1γ) phosphorylation site T1479,. Similar to the Ccny and Ccnyl1 expression pattern at the neocortex, phospho-T1479 LRP6 immunoreactivity was also found to be enriched at the apical cell membrane of the VZ of E13.5 control mouse neocortex (Figure 2.1J-K). To further confirm this staining pattern, we used another phospho-LRP6 antibody that detects the CDK14 priming phosphorylation site S1490(Davidson et al., 2009). Similarly, phospho-S1490 LRP6 was enriched in E13.5 mitotic APs (90%) and BPs (88%) (Figure 2.7E). Ccny (30%) and Ccnyl1 (29%) were also found in mitotic APs.(Figure 2.7F). In addition, LRP6, CDK14 and GSK3β were also found enriched at the apical plasma membrane of the VZ of E13.5 control mouse neocortex (Figure 2.7G). In summary, these data suggest that WNT/STOP signaling core components are expressed in the embryonic mouse neocortex, and that WNT/LRP6 signaling peak during mitosis in APs and BPs.

To check WNT signaling in DKO forebrains, we quantified the LRP6 phosphorylation level (T1479) in mitotic APs and BPs of E13.5 neocortex, and detected a decrease (-15%, p=0.01) (Figure 2.1L). The decrease of phosphorylation of LRP6 at S1490 was even more significantly reduced (-45%, p=0.001) when analyzed protein lysates extracted from E13.5 DKO and control forebrains (Figure 2.1N). To investigate transcriptional WNT signaling, we performed *RNA*Scope on E13.5 neocortex sections with a WNT target gene *Axin2* probe. The general *Axin2* transcriptional level was not changed in the DKO neocortex (Figure 2.1O-P). This result was further confirmed by analyzing *Axin2* as well as *N-myc*, another WNT target gene in the neocortex(Kuwahara et al., 2010) from the total RNA from E13.5 dorsal forebrains (Figure 2.1Q). In addition, by analyzing the proteins level of dephosphorylated β-catenin, which is the active form of β-catenin during WNT signaling transduction, we

found no significant change in E13.5 DKO embryos (Figure 2.7I). Therefore we conclude that *Ccny/l1* loss of function in the embryonic mouse neocortex results in decreased WNT activity at the receptor level not the transcriptional level

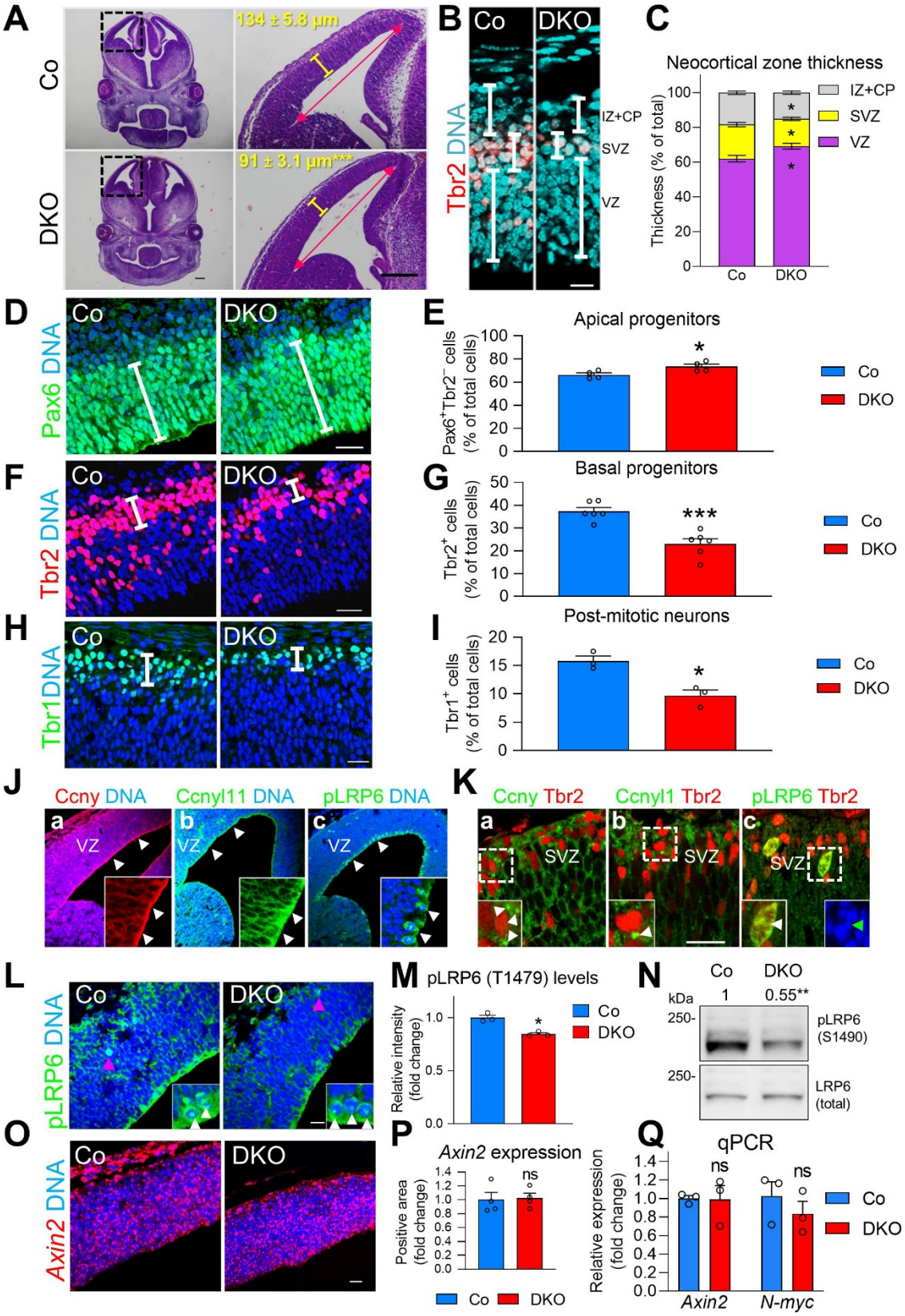
A
Co
DKO
134 ± 5.8 µm
91 ± 3.1 µm***
B
Co
DKO
Tbr2 DNA
IZ+CP
SVZ
VZ
C
Neocortical zone thickness
Thickness (% of total)
IZ+CP
SVZ
VZ
Co
DKO
D
Pax6 DNA
E
Apical progenitors
Pax6+Tbr2− cells (% of total cells)
F
Tbr2 DNA
G
Basal progenitors
Tbr2+ cells (% of total cells)
H
Tbr1 DNA
I
Post-mitotic neurons
Tbr1+ cells (% of total cells)
J
Ccny DNA
Ccnyl11 DNA
pLRP6 DNA
VZ
K
Ccny Tbr2
Ccnyl1 Tbr2
pLRP6 Tbr2
SVZ
L
pLRP6 DNA
M
pLRP6 (T1479) levels
Relative intensity (fold change)
N
kDa
1
0.55**
pLRP6 (S1490)
LRP6 (total)
O
Axin2 DNA
P
Axin2 expression
Positive area (fold change)
ns
Q
qPCR
Relative expression (fold change)
Axin2
N-myc

Figure 2.1 WNT/STOP signaling is required for neurogenesis in the embryonic mouse neocortex.

A) H&E staining and quantification on neocortex sections from control (Co) and Cyclin Y (*Ccny*) and Cyclin Y like 1 (Ccnyl1) double knockout (DKO) embryos at E13.5.. Numbers show average thickness ± SEM and asterisk indicate statistical significance. Pick arrows indicate mediolateral neocortex length,. Scale bars 100 µm.

B) IF against Tbr2 and DNA of the VZ, SVZ and intermediate zone + cortical plate (IZ+CP) in control and DKO E13.5 neocortices. Scale bar 10 µm.

C) Quantification of VZ, SVZ and IZ+CP thickness in control and DKO E13.5 neocortex. Columns are means ± SEM (n=6 embryos, 4 litters).

D) IF against Pax6 and Tbr2 in control and DKO E13.5 neocortex. White bars indicate thickness of $Pax6^+$ zone. Scale bar 20 µm.

E) Quantification of the number of APs ($Pax6^+Tbr2^-$) from (D). $Pax6^+Tbr2^+$ cells were excluded from final counts. AP numbers are expressed as percentage of total cell number (sum of D,F and H). Columns are means ± SEM (n=4 embryos, 3 litters).

F) IF against Tbr2 in control and DKO E13.5 neocortex. White bars show thickness of $Tbr2^+$ zone. Scale bar 20 µm.

G) Quantification of the number of BPs from (F). Columns are means ± SEM (n=6 embryos, 3 litters).

H) IF for Tbr1 in control and DKO E13.5 neocortex. White bars show thickness of $Tbr1^+$ zone. Scale bar 15 µm.

I) Quantification of the number of deep-layer post-mitotic neurons from (H). Columns are means ± SEM (n=3 embryos, 3 litters).

J) IF agianst Ccny, Ccnyl1 and LRP6 phosphorylated at T1479 (pLRP6) in the E13.5 control neocortex.

K) IF against Ccny, Ccnyl1 and pLRP6 with IF for Tbr2 in the E12.5 control embryos respectively. White arrowheads in the insets depict Ccny/l1 puncta in the Tbr2+ BPs. High level of LRP6 phosophorylation is detected in mitotic BPs (H-c, inset, white arrowhead). DNA staining for mitotic pLRP6+ BP shown in bottom right inset (c, green arrowhead).

L) IF against pLRP6 (T1479) in the neocortex of E13.5 control and DKO embryos.

M) Quantification of relative pLRP6 staining intensity in mitotic APs (white arrow head insets) and BPs (purple arrowheads) from

L). Data are expressed as fold change vs. controls and are means ± SEM (n=3 embryos, 3 litters). Scale bar 20µm.

N) Immunoblot analysis of LRP6 phosphorylated at S1490 (pLRP6) from E13.5 control and DKO forebrains. (n=6 embryos, 3 litters).

O) Expression analysis of the β-catenin target gene *Axin2* by RNAScope *in situ* hybridization on neocortex sectins from E13.5 control and DKO embryos.
P) Quantification of (O). Axin2$^+$ area was calculated and normalized to total neocortex area. Data are expressed as fold change vs. controls and are means ± SEM (n=4 embryos, 3 litters). Scale bar 20 μm.
Q) *Axin2* and *N-myc* qPCR expression analysis on RNA extracted from E13.5 dorsal forebrains Unpaired two tailed *t*-test for all statistical analyses: ns, not significant; *p<0.05, **p<0.01, ***p<0.001.
Panel A-I and **N-Q** are provided by Dr.*Fabio da Silva*.

5.2.2 DKO embryos show delayed cell cycle progression and increased mitosis length in BPs

In consideration of the decreased number of BPs and neurons in the DKO neocortex, we further measured cell cycle procession of APs and BPs, as the alteration in cell cycle progression have been shown to influence NPC fate and cortical neurogenesis(Borrell and Calegari, 2014; Dehay and Kennedy, 2007; Gotz and Barde, 2005). To label S-phase NPCs, the thymidine analog bromo-deoxyuridine (BrdU) was injected at E11.5, E12.5 and E13.5 and the mice were sacrificed one hour later. Co-IF against Pax6 and Tbr2 and BrdU did not display any major difference between control and DKO neocortex in the percentage of APs (Pax6$^+$ Tbr2$^-$) that were in S-phase (i.e. BrdU$^+$) at E11.5 and E12.5, despite that a slight increase was detected for DKO neocortex at E13.5 (Figure 2.2A-F).

We next measured the length of S-phase of APs and BPs in E13.5 control and DKO neocortex. To achieve this, we performed time-point injections of the thymidine analogs iododeoxyuridine (IdU) and BrdU. In short, IdU was injected at T=0 to mark APs and BPs in S-phase, and BrdU was injected at T=1.5 hrs to mark those APs and BPs that were still in S-phase at this time point vs. those that were out of S-phase. The mouse brain tissues were collected 30 minutes after BrdU injection. Then the percentage of APs (Tbr2$^-$) and BPs (Tbr2$^+$) of control and DKO neocortex that were IdU$^+$ but BrdU$^-$ were extrapolated, and the time when all control and DKO APs and BPs would have left S-phase, which gave us the length of S-phase for control and DKO APs and BPs was calculated. This showed a mild increase in S-phase length of E13.5 DKO APs as compared to control APs, and around 50% increase in S-phase length of

E13.5 DKO BPs as compared to control BPs (Figure 2.2G-H). Therefore, the information of the percentage value of E13.5 control and DKO APs and BPs in S-phase (Figure 2.2G-H), and the length of S-phase of these types of NPCs (Figure 2.2I), allowed us to further calculate the total length of the cell cycle of E13.5 control and DKO APs and BPs by dividing the S-phase length values (Figure 2.2J) by the percentage values for these NPCs in S-phase and then multiplying the resulting numbers with 100 (Figure 2.2J). This displayed no major difference between E13.5 control and DKO APs, but almost a doubling of total cell cycle length in DKO BPs (Figure 2.2J).

Regarding the length of mitosis, we first performed co-IF against pHH3, Ki67 and Tbr2 to measure the percentage of cycling (Ki67+) E13.5 control and DKO APs (Tbr2-) and BPs (Tbr2+) that were in mitosis (pHH3+) (Figure 2.2K-L). This displayed no differences between control and DKO APs, nor between control and DKO BPs (Figure 2.2L). We then multiplied the total cell cycle length values for each of these NPCs with the percentage values for the respective NPC in mitosis to determine the length of mitosis of E13.5 control and DKO APs and BPs (Figure 2.2L), and divided the resulting numbers by 100, to get the length of mitosis (Figure 2.2M). However, there was no significant difference in mitosis length between control and DKO APs. Nevertheless, mitosis length of DKO BPs was found to be increased more than doubled fold when compared to controls (Figure 2.2M). Data consistent with these observation were obtained when percentage of APs and BPs in mitosis, deduced from ventricular and abventricular pHH3+ cells, respectively, were compared between E11.5-E13.5 control and DKO neocortex.

Mitotic delay can result in cell cycle arrest and increased apoptosis(Pilaz et al., 2016). To check apoptosis levels in DKO vs. control forebrains, we performed IF with an antibody against cleaved caspase 3 (Figure 2.2N-O). In spite of a minor, however statistically not significant, increase at E11.5, apoptosis levels in the E12.5 and E13.5 neocortex of DKO embryos were comparable to controls (Figure 2.2N-O). Therefore, apoptosis is not likely to account for reduced thickness of the cortical plate in DKO embryos. We conclude that reduction in DKO embryos of cortical plate thickness involves delayed cell cycle progression and increased mitosis length in BPs.

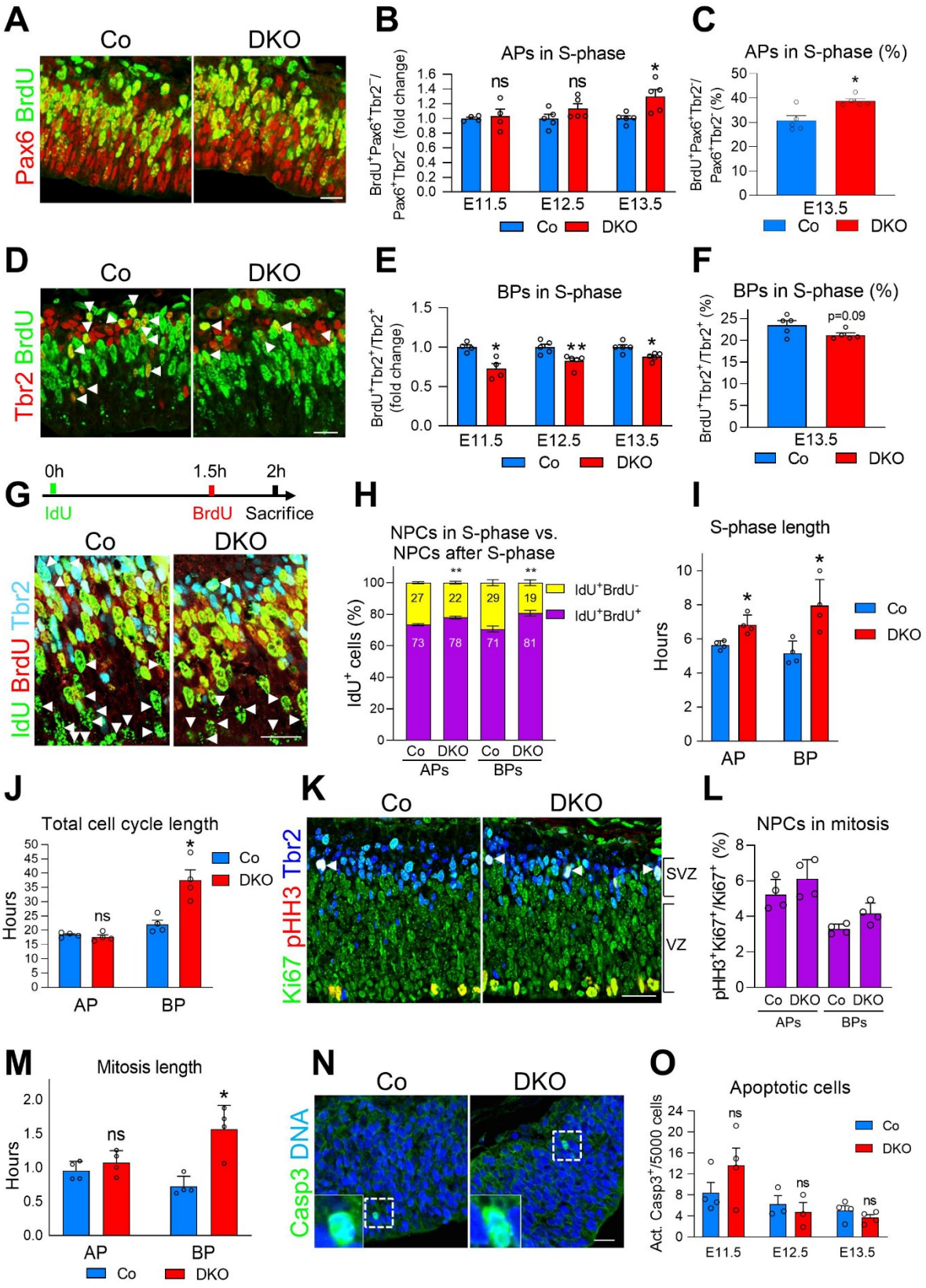
A
Co
DKO
Pax6 BrdU
B
APs in S-phase
BrdU+Pax6+Tbr2− / Pax6+Tbr2− (fold change)
ns
ns
*
E11.5
E12.5
E13.5
Co
DKO
C
APs in S-phase (%)
BrdU+Pax6+Tbr2− / Pax6+Tbr2− (%)
*
E13.5
Co
DKO
D
Co
DKO
Tbr2 BrdU
E
BPs in S-phase
BrdU+Tbr2+/Tbr2+ (fold change)
*
**
*
E11.5
E12.5
E13.5
Co
DKO
F
BPs in S-phase (%)
BrdU+Tbr2+/Tbr2+ (%)
p=0.09
E13.5
Co
DKO
G
0h
1.5h
2h
IdU
BrdU
Sacrifice
Co
DKO
IdU BrdU Tbr2
H
NPCs in S-phase vs. NPCs after S-phase
IdU+ cells (%)
27
22
29
19
73
78
71
81
IdU+BrdU−
IdU+BrdU+
Co
DKO
Co
DKO
APs
BPs
I
S-phase length
Hours
*
*
Co
DKO
AP
BP
J
Total cell cycle length
Hours
ns
*
Co
DKO
AP
BP
K
Co
DKO
Ki67 pHH3 Tbr2
SVZ
VZ
L
NPCs in mitosis
pHH3+Ki67+/Ki67+ (%)
Co
DKO
Co
DKO
APs
BPs
M
Mitosis length
Hours
ns
*
AP
BP
Co
DKO
N
Co
DKO
Casp3 DNA
O
Apoptotic cells
Act. Casp3+/5000 cells
ns
ns
ns
Co
DKO
E11.5
E12.5
E13.5

Figure 2.2 DKO embryos display delayed cell cycle progression and increased mitosis in BPs.

A) IF against BrdU, Pax6 and Tbr2 (not shown) in E12.5 control and DKO neocortices.
B) Quantification of the proportion of $Pax6^{+}Tbr2^{-}$ cells that are $BrdU^{+}$, in control and DKO neocortices at E11.5, E12.5 and E13.5. (E11.5, n=4 embryos, 3 litters; E12.5 n=5 embryos, 5 liiters and E13.5 n=5 embryos, 4 litters).
C) Quantification of APs ($Pax6^{+}Tbr2^{-}$)(from B) that are $BrdU^{+}$, in E13.5 control and DKO neocortices. Data are means ± SEM.
D) IF against Tbr2 and BrdU (double positive cells depicted by white arrowheads) in E12.5 control and DKO neocortices. BrdU was injected into pregnant dams one hour before sacrifice.
E) Quantification of proportion of $Tbr2^{+}$ cells that are $BrdU^{+}$, in control and DKO neocortices at E11.5, E12.5 and E13.5. (E11.5 n=4 embryos, 3 litters; E12.5 n=5 embryos, 5 litters and E13.5 n=5 embryos, 4 litters).
F) Average percentage of BPs ($Tbr2^{+}$) (from E) that are $BrdU^{+}$, in E13.5 control and DKO neocortices. Data are means ± SEM.
G) Double IdU/BrdU injection strategy used to calculate S-phase length. Top, scheme. Bottom, IF against IdU/BrdU/Tbr2 to detect APs ($Tbr2^{-}$) and BPs ($Tbr2^{+}$) that have exited S-phase(IdU^{+}/BrdU, white arrowheads) in control and DKO E13.5 neocortices.
H) Quantification (number in bar graphs) of IdU^{+} cells that are either $BrdU^{+}$ or $BrdU^{-}$, socred as in (G), for control and DKO APs and BPs. Data are means ± SEM (n=4 embryos, 3 litters).
I) Calculation of S-phase length of E13.5 control and DKO APs and BPs,. Data are means ± SEM (n=4 embryos, 3 litters).
J) Quantification of total cell cycle length of E13.5 control and DKO APs and BPs, calculated from the data of panels (C), (F) and (I) as described in Methods Data are means ± SEM (n=4 embryos, 3 litters).
K) IF against the proliferation marker Ki67, the mitotic marker phosphor-histone H3 (pHH3), and Tbr2 to identify mitotic APs (division at apical surface) and BPs (division in basal VZ or SVZ) in control and DKO E13.5 neocortices. Arrowheads depic $pHH3^{+}Tbr2^{+}$ cells.
L) Quantification of $Ki67^{+}$ APs and BPs that are $pHH3^{+}$ in control and DKO E13.5 neocortices. Data are means ± SEM (n=4 embryos, 3 litters).
M) Calculation of mitosis length of E13.5 control and DKO APs and BPs from the data of panels (J) and (L) as described in Methods. Data are means ± SEM (n=4 embryos, 3 litters).
N) IF against cleaved caspase 3 (Casp3) in E13.5 control and DKO neocortices.
O) Quantification of apoptotic cells in control and DKO neocorices at E11.5, E12.5 and E13.5. Data are represented as number of $Casp3^{+}$ cells per 5000 cells. Data are means ± SEM (E11.5 n=4 embryos, 3 litters; E12.5 n=3 embryos, 3 litters, and E13.5 n=4 embryos, 3 litters). All scale bars 20

μm. Unpaired two-tailed *t*-test for all statistical analyses: ns, not significant; *p<0.05, **p<0.01, ***p<0.001. The panel **A-O** are provided by Dr.*Fabio da Silva*.

5.2.3 Loss of Ccny/l1 function reduces asymmetric AP division and neurogenesis in neocortex

The increase in VZ thickness and reduced levels of BPs in DKO embryos raised the possibility that the thinner neocortex was not only to the result of a delayed cell cycle progression of BPs. Conversely, the results indicated that *Ccny/l1* may influence the generation of BPs from APs, and as a consequence, of post-mitotic neurons. In the mammalian neocortex, the transition of APs from symmetric, proliferative divisions to asymmetric, BP-genic divisions is often associated with changes in apical membrane distribution, whereby unequal inheritance of the apical plasma membrane by daughter cells suggests an asymmetric mode of AP division(Delaunay et al., 2017; Kosodo et al., 2004). We then measured the number of symmetrically vs. asymmetrically dividing APs by IF with the “cadherin hole” method allowing us to determine the plane of division in mitotic APs (Figure 2.3A). Interestingly, E13.5 DKO neocortex displayed a 36% reduction in asymmetric AP division (from 47% to 30% of all AP division, Figure 2.3B), consistent with decreased generation of BPs in the absence of *Ccny/l1*.

Mitotic spindle orientation is crucial for NPCs division mode in the developing neocortex(Asami et al., 2011; Konno et al., 2008; LaMonica et al., 2013; Lizarraga et al., 2010), with astral microtubules (aMTs) playing a key role. A specific subpopulation of aMTs, which attain the apical or basal cell cortex and are regarded as apical-basal aMTs, are more abundant in symmetrically dividing APs than in asymmetrically dividing APs. These apical-basal aMTs aid a mitotic spindle orientation perpendicular to the apical-basal axis of APs and minimize mitotic spindle movement, which then promotes symmetric AP division. Alterations specifically of these apical-basal aMTs promotes asymmetric BP-genic APs divisions and neurogenesis. To check aMT frequency, we performed IF against α-tubulin, obtained Z-stack images of dividing APs, and measured the number of apical-basal aMTs vs the aMTs reaching the central cell cortex (central aMTs) (Figure 2.3C). Interestingly, E13.5 DKO APs displayed an increase specifically in apical-basal, but not central, aMTs (Figure 2.3C-D), which

indicated a possible mechanistic explanation for the increase in symmetric AP division (Figure 2.3A-B). We conclude that in dividing APs, the absence of *Ccny/l1* leads to an increase in the number of apical-basal aMTs, which reduces asymmetric, BP-genic cell division and hence neurogenesis in the embryonic neocortex.

DKO embryos died early *in utero* at E14.5, limiting our analysis of neurogenesis to early stages of development in which the cortical plate is less developed. To analyze the effect of *Ccny/1* loss of function in NPCs at later time-points, we performed IUE of mouse embryos at E13.5 by injection of a control shRNA (*Co*), or shRNAs against *Ccny* and *Ccnyl1* (sh*Ccny/l1*), together with a GFP plasmid. At E15.5, knockdown of *Ccny/l1* dramatically decreased the proportion of the GFP+ progeny of the electroporated cells that were Tbr2, i.e. BPs (Figure 2.3E and G). Consistently, at E17.5, the proportion of the GFP+ progeny of the electroporated cells expressing the deep-layer neuron marker Ctip2 was depleted (Figure 2.3F and H). Altogether, these data support that loss of function of *Ccny/l1* reduces neurogenesis in the embryonic mouse neocortex, and show that this effect is consistent throughout embryonic development. The IUE results also rule out the possibility that the neurogenesis defect in DKO embryos is because of an overall delay in embryonic development, or results from indirect effects related to global deletion of *Ccny/l1*.

We next asked whether NPCs mutant for *Ccny/l1* also showed decreased neurogenesis *in vitro*. To achieve this, we obtained NPCs from *Ccny*+/-; *Ccnyl1*-/- neocortex and infected with a lentivirus expressing shRNA against *Ccny* (hereafter referred to as mutant NPCs) to knockdown *Ccny/l1* . NPCs were then induced to differentiate *in vitro*. IF against Tuj1 showed a dramatic decrease in the proportion of Tuj1+ cells as well as a significant reduction in neurite length (control 47.4+/-1.4µm vs. mutant 23.8+/-1.8µm) (Figure 2.3I). The defect was further confirmed by qPCR, which indicated a major decrease of the neuronal markers Tuj1 and doublecortin in mutant NPCs-derived neurons.However, the neural stem cell marker Sox2 displayed a mild but not significant increase in mutant cells (Figure 2.8A-C). The levels of phospho-LRP6 (S1490) , a hallmark of primed WNT signaling, were greatly decreased, whereas *Axin2* expression was not significantly altered in mutant cells, confirming that the function of *Ccny/l1* during neurogenesis *in vitro* are independent of transcriptional WNT signaling (Figure 2.8D-E). In addition, analysis of total protein lysates from mutant

NPCs displayed overall strongly increased lysine-48 ubiquitination (Figure 2.3J), which indicated globally enhanced protein degradation, a feature of impaired WNT/STOP signaling. These results further support that *Ccny/l1* and WNT/STOP signaling promote asymmetric AP division and neurogenesis.

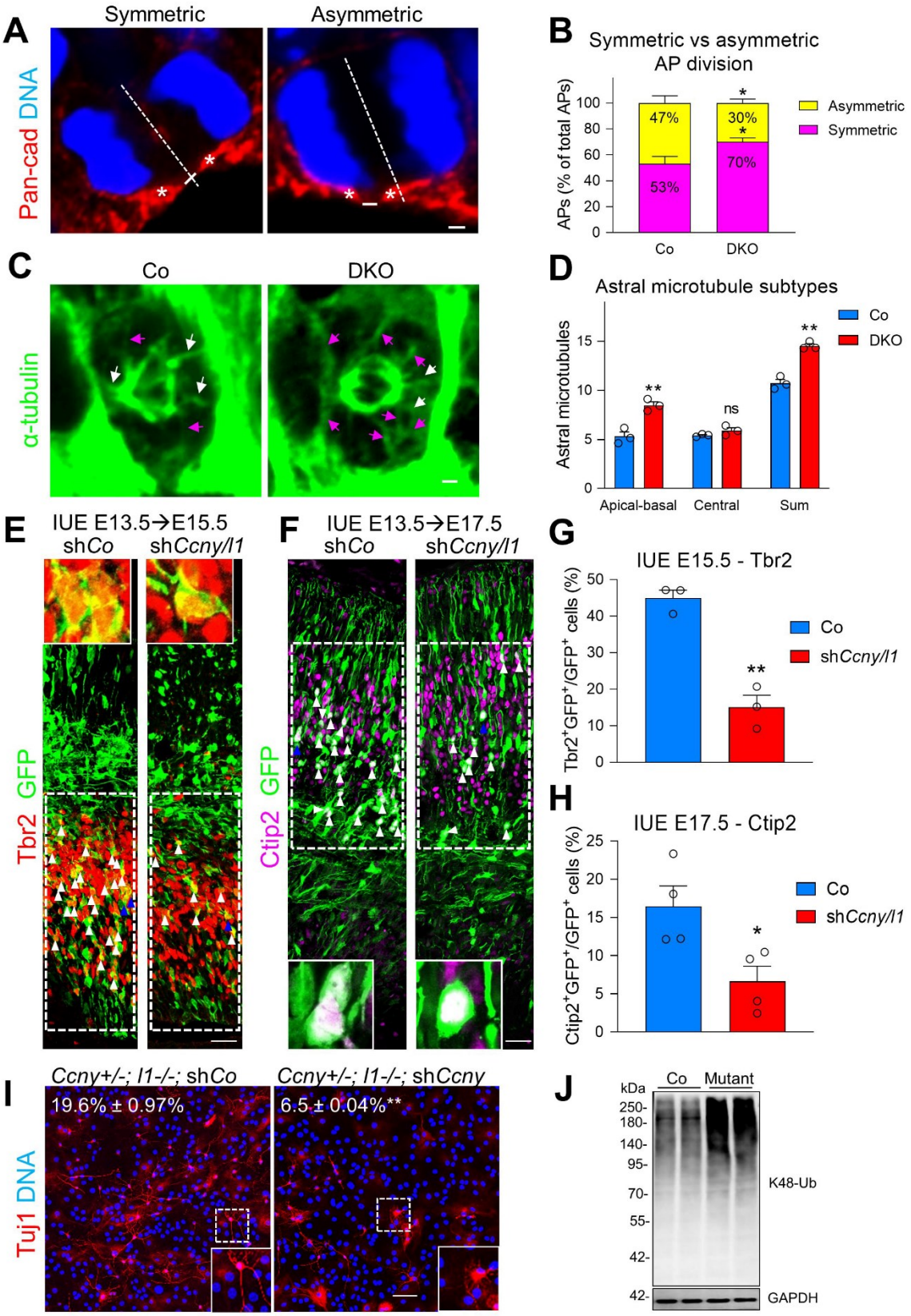
A
Symmetric
Asymmetric
Pan-cad DNA
B
Symmetric vs asymmetric AP division
APs (% of total APs)
47%
53%
30%
70%
Asymmetric
Symmetric
Co
DKO
C
Co
DKO
α-tubulin
D
Astral microtubule subtypes
Astral microtubules
Co
DKO
ns
Apical-basal
Central
Sum
E
IUE E13.5→E15.5
shCo
shCcny/l1
Tbr2 GFP
F
IUE E13.5→E17.5
shCo
shCcny/l1
Ctip2 GFP
G
IUE E15.5 - Tbr2
Tbr2+GFP+/GFP+ cells (%)
Co
shCcny/l1
H
IUE E17.5 - Ctip2
Ctip2+GFP+/GFP+ cells (%)
Co
shCcny/l1
I
Ccny+/-; l1-/-; shCo
Ccny+/-; l1-/-; shCcny
19.6% ± 0.97%
6.5 ± 0.04%**
Tuj1 DNA
J
kDa
Co
Mutant
250-
180-
140-
95-
70-
55-
42-
42-
K48-Ub
GAPDH

Figure 2.3 Lack of *Ccny/l1* expression reduces asymmetric AP division and neurogenesis in the embryonic neocortex.

A) IF against pan-cadherin, to quantify asymmetric vs. symmetric division in VZ APs. Cell divisions were scored as symmetric or asymmetric when the cleavage plane bisects (left) or bypass (right) the cadherin hole, respectively. Scale bar 2µm.

B) Quantification of symmetric vs. asymmetric AP division in E13.5 control and DKO neocortices, expressed as percentage of total AP divisions. Data are means ± SEM.

C) IF against alpha-tubulin to visualize mitotic spindle and astral microtubules in E13.5 control and DKO neocortices. Central and apical-basal astral microtubules denoted by white and purple arrows, respectively. Scale bar 2µm.

D) Quantification of apical-basal, central and total (sum) number of astral microtubulues in mitotic APs of control and DKO E13.5 neocortices. Data are means of microtubules per cell ± SEM (at least 10 cells counted per embryo) (n=3 embryos, 3 litters).

E-F) *In utero* electroporation (IUE) of plasmids expressing GFP plus sh*Control* (Co) or sh*Ccny/l1* into the lateral ventricles of E13.5 wildtype embryos, followed by analysis at E15.5 or E17.5. **E**) IF against GFP and Tbr2 in the E15.5 neocortex. **F**) IF againstGFP and the deep-layer neuron marker CTIP2 in the E17.5 neocortex. **E-F**) White arrowheads denote double-positive cells. Insets of magnified cells (indicated by blue arrowheads) depict representative GFP+ Tbr2 (E) or GFP+Ctip2(F) co-staining. Scale bars 20µm.

G) Quantification of the percentage of GFP^+ cells that are $Tbr2^+$, in control and sh*Ccny/l1* neocortices at E15.5 upon IUE at E13.5. Data are means ± SEM (n=3 embryos).

H) Quantification of the percentage of GFP^+ cells that are $Ctip2^+$, in control and sh*Ccny/l1* neocortices at E17.5 upon IUER at E13.5. Data are means ± SEM (n=4 embryos).

I) IF against βIII-tubulin (Tuj1) of control (*Ccny*+/-; *Ccnyl1*-/-; shRNA *Co*) and mutant (*Ccny*+/-; *Ccnyl1*-/-; shRNA *Ccny*) differentiated neurons. Numbers depict quantification of the percentage of $Tuj1^+$ cells ± SEM (experiment performed twice in triplicates, representative experiment shown). Scale bar 20 µm.

J) Immunoblot analysis of protein lysates extracted from control and mutant NPCs to check polyubiquitinated proteins targeted for proteasomal degradation. GAPDH, loading control. Two representative samples per genotype are shown. Unpaired two-tailed *t*-test for all statistical analyses: ns, not significant; *p<0.05, **p<0.01, ***p<0.001. Panel **A-D** are provided by Dr.*Fabio da Silva*.

5.2.4 Sox4/11 are direct GSK3 substrates

WNT/STOP signaling functions by protecting proteins containing GSK3 phosphodegrons from proteasomal degradation. To pinpoint downstream targets of WNT/STOP signaling, we screened for poteintial target proteins which are required for neurogenesis and neuronal differentiation that harbor potential GSK3 phosphorylation sites. Among potential candidates, two SoxC subclass transcription factors, the SRY-related high-mobility-group box proteins Sox4 and Sox11 stood out. Sox4/11 are crucial for neurogenesis and neuronal differentiation(Bergsland et al., 2011). Sox4 is highly expressed by BPs, and Sox11 is expressed by both BPs and newly formed neurons(Chen et al., 2015). Conditional knockout of Sox4 in the neuroepithelium results in a robust reduction of BPs while Sox11 loss of function leads to decreased post-mitotic neurons(Chen et al., 2015). Combined phenotypes from loss of Sox4/11 thus phenocopy the neurogenesis defects observed in DKO embryos. Mouse Sox4 harbors a putative GSK3 phosphorylation site with three serines spaced by three amino acids (SxxSSxxSS(316)P) (Figure 2.4A), a classical signature of GSK3 motifs(Beurel et al., 2015). Mouse Sox11 has two putative GSK3 phosphorylation sites: (S(244)PxxS) and (S(289)PxxSxxxS) (Figure 2.4B). The Sox4/11 GSK3 sites are highly conserved in other species like chimps and humans. Furthermore, S315 and S316 of the Sox4 motif, and S244 and S289 of Sox11 motifs, are phosphorylated as shown in PhosphoSitePlus(Hornbeck et al., 2012). Finally, *in silico* analysis by NetPhos 3.1(Blom et al., 1999) suggested GSK3 to be a topmost candidate for S316 of the Sox4 motif, and both S244 and S289 of the Sox11 motifs phosphorylation (Figure 2.4A-B).

To further check if Sox4/11 are phosphorylated, we expressed N-terminally Flag-tagged Sox4/11 in HEK293T (293T) cells and treated protein lysates with γ-phosphatase. Immunoblot analysis displayed a downshift of Sox4 band from 70kDa to 65kDa (Figure 2.8F). Interestingly, endogenous Sox4 was also downshifted in 293T cells after γ-phosphotase treatment (Figure 2.4C). Next, we checked the potential GSK phospho-motifs of Sox4/11 by point mutation. For Sox4, we generated a mutant with S316 mutation to alanine and another one with all five serines mutation (S316all) (Figure 2.4A). For Sox11, we generated a mutant with S244 and S289 mutation (S244S289) and one with all serines of both motifs mutation (S244allS289all) (Figure

2.4B). Immunoblot analysis displayed a downshift in the Sox4 S316 mutant, with multiple bands showing up lower than expected size of wildtype Sox4. The S316all mutant displayed an even more dramatic downshift, similar to the effect of phosphatase treatment on wild type Sox4 (Figure 2.4E). For Sox11, a solight downshift of phosphorylated Sox11 was detected in the S244S289 mutant, while a larger shift was detected in S244allS289all mutants, with increase in the major Sox11 band, corresponding to unphosphorylated Sox11 (Figure 2.4F).

Next, we checked the effect of GSK3 on Flag-Sox4/11 by co-transfection in 293T cells. GSK3β overexpression resulted in a mild but significant decrease in total Sox4 protein levels, with a bigger decrease in non-phosphorylated Sox4 (65kDa band) (Figure 2.4G). Furthermore, this effect was inverted by treatment with the GSK3 inhibitor BIO (Figure 2.4G). GSK3β and BIO treatment had no effect on the Sox4 mutant S316all, validating this site is a GSK3β phospho-motif (Figure 2.4H). GSK3β also decreased Sox11 protein levels, chiefly in non-phosphorylated Sox11, and this effect was overturned by BIO treatment as well (Figure 2.4I). GSK3β and BIO treatment had no effect on the S244allS289all mutant form of Sox11 (Figure 2.4J).

To check if Sox4/11 are directly phosphorylated by GSK3, we immunopurified wildtype and mutant (S316all and S244allS289all) Sox4 and Sox11, applied λ-phosphatase to the proteins, and then carried out *in vitro* kinase assays by applying with recombinant GSK3β and gamma-^{32}P-labelled ATP. Wildtype Sox4/11 were both greatly phosphorylated by GSK3β, however, only modest phosphorylation of the mutants could be detected (Figure 2.4K-L). Because WNT/STOP signaling inhibits GSK3β to prevent target proteins from proteasomal degradation(Acebron et al., 2014; Taelman et al., 2010), we checked if Sox4/11 are ubiquitinated. We thereforeco-transfected HA-tagged ubiquitin with Flag-Sox4/11 and then briefly applied MG132 to block proteasomal degradation of ubiquitin-conjugated polypeptides. Pull-down of Sox proteins followed by immunoblot against HA-ubiquitin indicated a characteristic polyubiquitin-smear in both Sox4 and Sox11-transfected cells, suggesting that both Sox proteins are ubiquitin-conjugated (Figure 2.8G-H). We thereby conclude that Sox4/11 are (i) regulated by proteasomal , and (ii) directly phosphorylated by GSK3β.

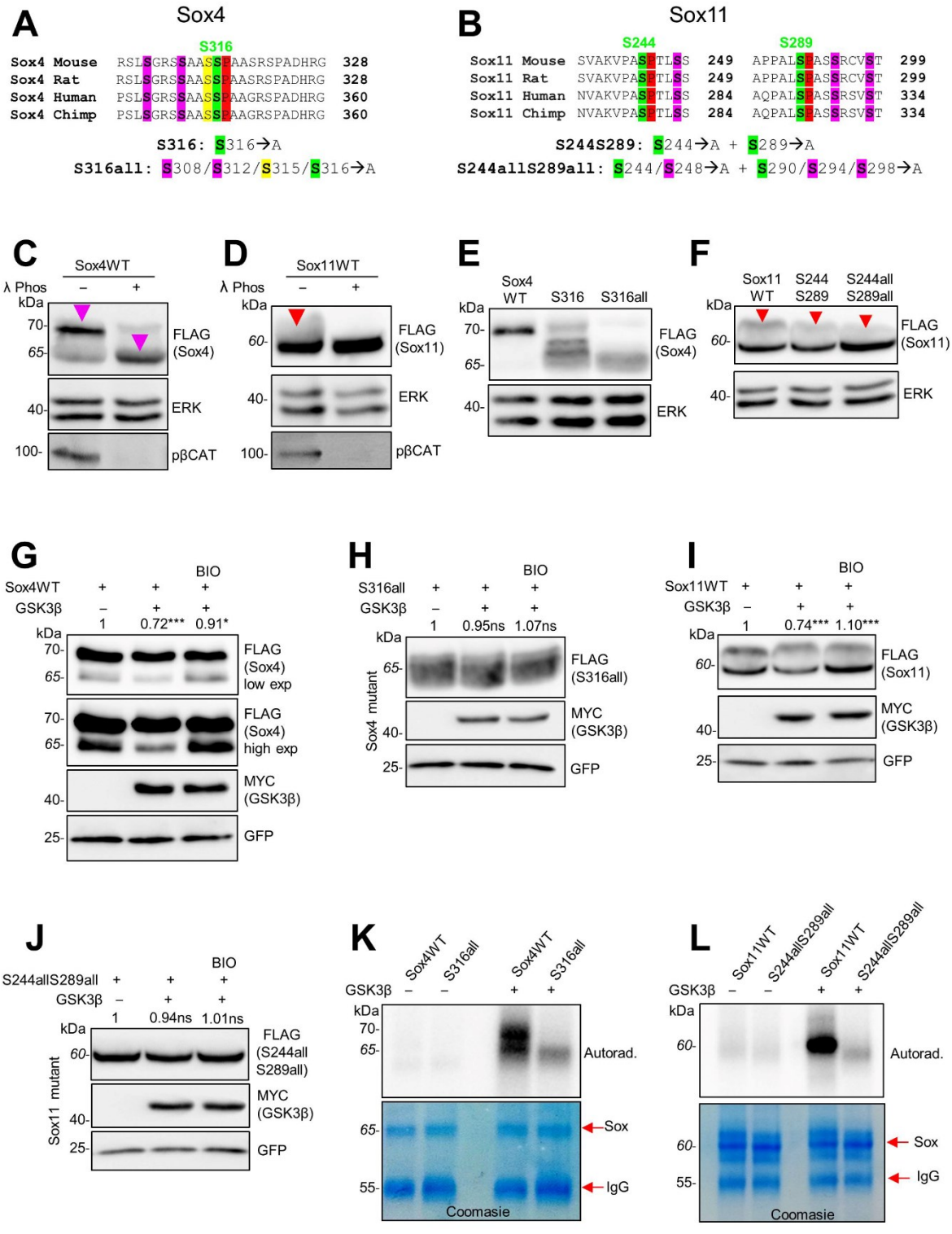
A
Sox4
S316
Sox4 Mouse RSLSGRSSAASSPAASRSPADHRG 328
Sox4 Rat RSLSGRSSAASSPAASRSPADHRG 328
Sox4 Human PSLSGRSSAASSPAAGRSPADHRG 360
Sox4 Chimp PSLSGRSSAASSPAAGRSPADHRG 360
S316: S316→A
S316all: S308/S312/S315/S316→A
B
Sox11
S244
S289
Sox11 Mouse SVAKVPASPTLSS 249 APPALSPASSRCVST 299
Sox11 Rat SVAKVPASPTLSS 249 APPALSPASSRCVST 299
Sox11 Human NVAKVPASPTLSS 284 AQPALSPASSRSVST 334
Sox11 Chimp NVAKVPASPTLSS 284 AQPALSPASSRSVST 334
S244S289: S244→A + S289→A
S244allS289all: S244/S248→A + S290/S294/S298→A
C
Sox4WT
λ Phos – +
kDa
70-
65-
FLAG (Sox4)
40-
ERK
100-
pβCAT
D
Sox11WT
λ Phos – +
kDa
60-
FLAG (Sox11)
40-
ERK
100-
pβCAT
E
Sox4 WT S316 S316all
kDa
70-
65-
FLAG (Sox4)
40-
ERK
F
Sox11 WT S244 S289 S244all S289all
kDa
60-
FLAG (Sox11)
40-
ERK
G
Sox4WT + + +
GSK3β – + +
BIO +
1 0.72*** 0.91*
kDa
70-
65-
FLAG (Sox4) low exp
70-
65-
FLAG (Sox4) high exp
40-
MYC (GSK3β)
25-
GFP
H
S316all + + +
GSK3β – + +
BIO +
1 0.95ns 1.07ns
kDa
65-
Sox4 mutant
FLAG (S316all)
40-
MYC (GSK3β)
25-
GFP
I
Sox11WT + + +
GSK3β – + +
BIO +
1 0.74*** 1.10***
kDa
60-
FLAG (Sox11)
40-
MYC (GSK3β)
25-
GFP
J
S244allS289all + + +
GSK3β – + +
BIO +
1 0.94ns 1.01ns
kDa
60-
Sox11 mutant
FLAG (S244all S289all)
40-
MYC (GSK3β)
25-
GFP
K
Sox4WT S316all Sox4WT S316all
GSK3β – – + +
kDa
70-
65-
Autorad.
65-
Sox
55-
IgG
Coomasie
L
Sox11WT S244allS289all Sox11WT S244allS289all
GSK3β – – + +
kDa
60-
Autorad.
60-
Sox
55-
IgG
Coomasie

Figure 2.4 Sox4/11 are direct GSK substrates.

A) Amino acid sequence alignment of Sox4 GSK3 phospho-motif from mouse, rat, human and chimp. Mouse serine 316 (S316) (highlighted in green) and S315 (highlighted in yellow) predicted by *PhosphoSitePlus* to be phosphorylated.
B) Amino acid sequence alignment of Sox11 GSK Amino acid sequence alignment of Sox11 GSK3 phospho-motifs from mouse, rat, human and chimp. Mouse S244 and S289 (highlighted in green) predicted by PhosphoSitePlus to be phosphorylated.
C) Analysis of Flag-tagged Sox4 wildtype (WT) protein overexpressed in HEK293T (293T) cells and detected with FLAG antibody.
D) Analysis of Flag-tagged Sox11 WT protein overexpressed in 293T cells and detected with FLAG antibody. Lysates treated with or without λ-Phos. Upper smear (red arrowhead) represents phosphorylated Sox11. Antibody for pβCAT was used to validate λ-Phos treatment.
E) Analysis comparing molecular masses of WT Sox4 to S316 and S316all mutants.
F) Analysis comparing molecular masses of WT Sox11 to S244S289 and S244allS289all mutants. Red arrowheads indicate downward shifts of phosphorylated Sox11.
G) Co-transfection of myc-tagged GSK3β and Flag-Sox4 in 293T cells. BIO treatment (0.5 μM) performed for 1 hour prior to harvest. Lower band (65kDa) represents non-phosphorylated Sox4. High and low exposure (exp) blots shown to better visualize non-phosphorylated Sox4. Numbers above blot are quantification of Sox4 protein levels 56 normalized to GFP and are expressed as fold change vs. controls. The sum of upper and lower bands was quantified (n=8).
H) *Myc-GSK3β* and S316all mutant co-transfection in 293T cells plus 0.5 μM BIO treatment one hour prior to harvest. Protein levels quantified as in (G) (n=4).
I) *Myc-GSK3β* and *Flag-Sox11* co-transfection in 293T cells. BIO treatment (0.5 μM) performed for 1 hour prior to harvest. Upper band represents phosphorylated Sox11. Numbers above blot are quantification of Sox11 protein levels normalized to GFP and are expressed as fold change vs. controls. The sum of lower and upper bands was quantified (n=14).
J) *Myc-GSK3β* and S244allS289all mutant co-transfection in 293T cells plus 0.5 μM BIO treatment one hour prior to harvest. Protein levels quantified as in (I) (n=6).
K) *In vitro* kinase assay on immuno-purified Sox4WT and S316all mutant using recombinant GSK3β protein and radiolabelled ATP. Samples were treated with λ-Phos prior to assay and run on Phos-tag gel. Coomasie Blue staining shows equal loading of WT and mutant proteins.
L) *In vitro* kinase assay of purified Sox11WT and S244allS289all mutant using recombinant GSK3β protein and radiolabelled ATP. Experiment performed as in (K). Protein ladder numbers in italics indicate estimated size. Unpaired two-tailed t-test for all statistical analyses: ns, not significant; * $p < 0.05$, *** $p < 0.001$. Panel **A-L** are provided by Dr,*Fabio da Silva*.

5.2.5 Sox4/11 protein levels are decreased in DKO NPCs, predominantly during mitosis

We next asked whether Sox4/11 are regulated by GSK3 in NPCs, starting first with Sox4. Mutant Ccnyl1 NPCs displayed significantly reduced Sox4 protein levels (Figure 2.5A), despite Sox4 mRNA levels being mildly elevated (Figure 2.8J). We further analyzed Sox4 protein levels in the E13.5 neocortex *in vivo*. Sox4 co-localized with Ccny and pLRP6 (S1490) in the SVZ (Figure 2.5B). In DKO embryos, Sox4 staining intensity in Tbr2+ cells is comparable to controls (Figure 2.5B). Similarly, immunoblot analysis of DKO forebrain lysates showed no decrease in total Sox4 protein levels (Figure 2.8K), and qPCR analysis of RNA extracted from dorsal forebrains displayed no significant changes in Sox4 expression (p=0.87) (Figure 2.8L). On the other hand, Sox4 protein levels were dramatically reduced in mitotic (pHH3+) BPs in DKO neocortex (-42%, p=0.0002; Figure 2.5B). To further check WNT/STOP regulation of Sox4 during mitosis, we applied NPCs with nocodazole to synchronize cells at G2/M. Strikingly, G2/M arrested mutant NPCs displayed a greater reduction of Sox4 compared to non-treated cells (-45%, p=0.02 vs -25%, p=0.001) (Figure 2.9A). G2/M arrest by nocodazole treatment was confirmed by FACs-analysis of NPCs.

To further explore Sox4 regulation in NPCs, we generated a phospho-specific antibody targeting the S316 site of Sox4 (pSox4) (Figure 2.5D). Immunoblot analysis of Flag-Sox4 overexpression in 293T cell lysates treated with λ-phosphotase showed a specific band at 70kDa in the non-treated samples alone, indicating specificity of the antibody (Figure 2.9B). Consistently, the pSox4 antibody could not detect the S316 mutant (Figure 2.9B). Treatment of Flag-Sox4-transfected 293T cells with BIO leaded to decreased Sox4 phosphorylation, and this effect was more dramatic in G2/M synchronized cells (Figure 2.5E). In addition, analysis of forebrains protein lysate displayed a specific band at 70kDa which was increased in DKO embryos (Figure 2.5F), corresponding to elevated phosphorylation by GSK3.

For Sox11, Ccny/l1 mutant NPCs displayed greatly decreased protein levels and increased (but not significantly) mRNA levels, comparable to Sox4 (Figure 2.5G). Moreover, IF analysis on E13.5 neocortex sections displayed significantly reduced Sox11 protein levels in mitotic cells within the SVZ (-23%, p=0.04) (Figure 2.5H).

Sox11 protein levels were also reduced in newborn neurons and non-mitotic BPs, according to immunoblot analysis and co-IF with Tbr2 (-10%, p=0.01), respectively (Figure 2.5I-J, 2.5K-L). Sox11 expression was not significantly changed in DKO dorsal forebrains (p=0.46) corroborating that regulation of Sox11 by Ccny/l1 is post-transcriptional. Together, Ccny/l1 deficiency results in decreased Sox4/11 protein levels in NPCs and predominatly in mitotic cells, consistent with Sox4/11 being new WNT/STOP targets in the developing neocortex.

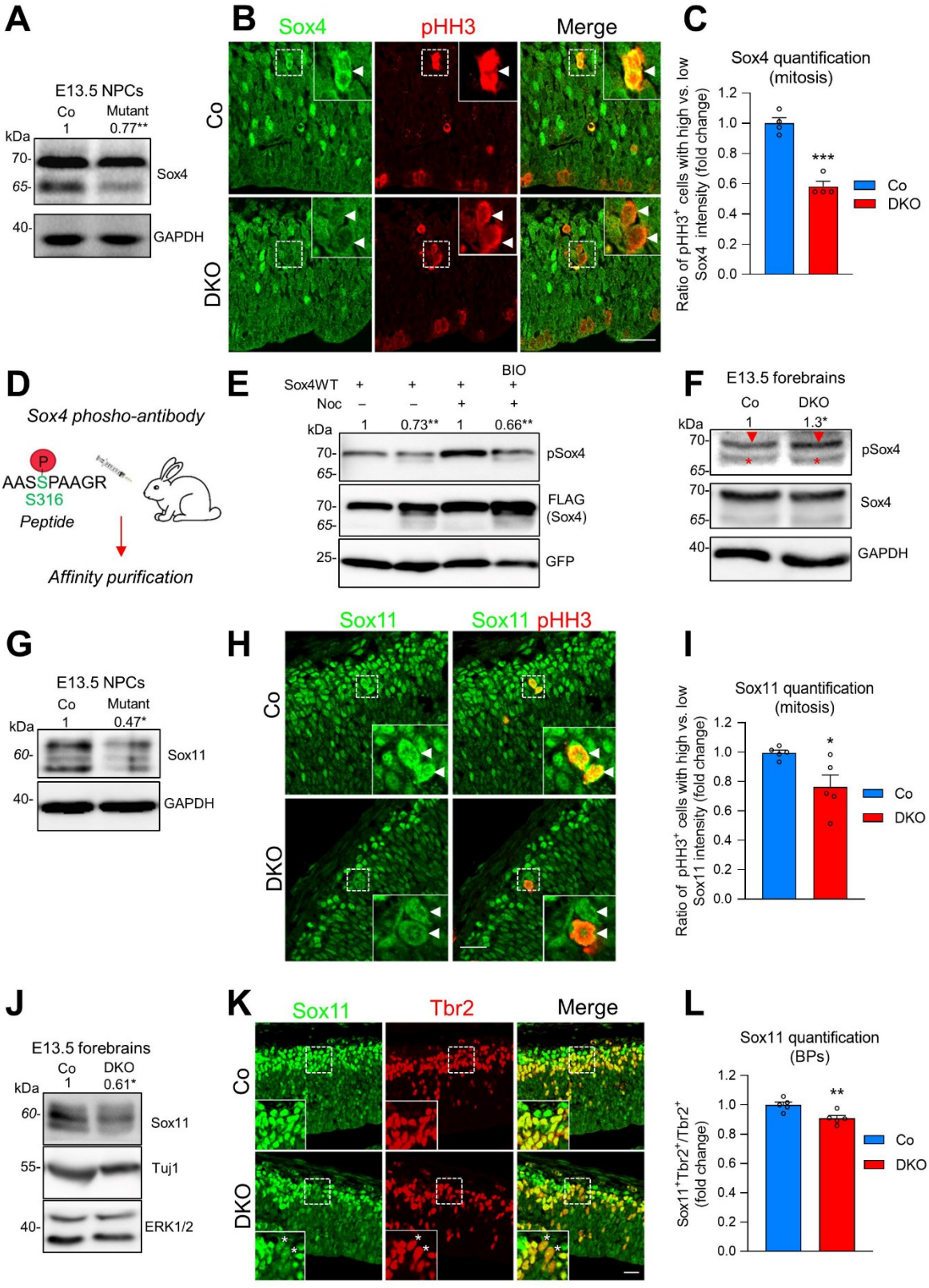
A
E13.5 NPCs
Co
Mutant
1
0.77**
kDa
70-
65-
Sox4
40-
GAPDH
B
Sox4
pHH3
Merge
Co
DKO
C
Sox4 quantification
(mitosis)
Ratio of pHH3+ cells with high vs. low Sox4 intensity (fold change)
1.2
1.0
0.8
0.6
0.4
0.2
0.0
***
Co
DKO
D
Sox4 phosho-antibody
P
AASSPAAGR
S316
Peptide
Affinity purification
E
BIO
Sox4WT + + + +
Noc – – + +
kDa
1
0.73**
1
0.66**
70-
65-
pSox4
FLAG
(Sox4)
25-
GFP
F
E13.5 forebrains
Co
DKO
1
1.3*
pSox4
Sox4
GAPDH
G
E13.5 NPCs
Co
Mutant
1
0.47*
60-
Sox11
GAPDH
H
Sox11
Sox11 pHH3
Co
DKO
I
Sox11 quantification
(mitosis)
Ratio of pHH3+ cells with high vs. low Sox11 intensity (fold change)
*
Co
DKO
J
E13.5 forebrains
Co
DKO
1
0.61*
60-
Sox11
55-
Tuj1
40-
ERK1/2
K
Sox11
Tbr2
Merge
Co
DKO
L
Sox11 quantification
(BPs)
Sox11+Tbr2+/Tbr2+
(fold change)
**
Co
DKO

Figure 2.5 Sox4/11 protein levels are decreased in DKO NPCs, predominantly during mitosis.

A) Immunoblot analysis with Sox4 antibody of protein lysates extracted from control (Co) (Ccny+/-; Ccnyl1-/-; shRNA Co) and mutant (Ccny+/-; Ccnyl1-/-; shRNA Ccny) NPCs. Numbers are fold change vs. controls of Sox4 protein levels normalized to GAPDH (n=3).
B) IF for Sox4 and pHH3 on neocortex sections of E13.5 control and DKO embryos. The level of Sox4 immunoreactivity is reduced in pHH3+ cells (white arrowheads).
C) Quantification of Sox4 staining in SVZ mitotic cells from E13.5 control and DKO embryos. Mitotic Sox4 staining was defined as high if the pixel intensity was similar to, or higher than, non-mitotic cells, or low if the levels were below those observed in non-mitotic cells. Data are means ± SEM for ratios of cells with high vs. low Sox4, and are displayed as fold change vs. controls (n=4 embryos, 3 litters).
D) Strategy to generate Sox4 S316 phospho-antibody (pSox4) by phosphopeptide injection into rabbits.
E) *Flag-Sox4* transfection in 293T cells followed by 24-hour nocodazole (100 ng/ml) and BIO (1 μM) treatments. Samples analyzed by immunoblot using pSox4 antibody; numbers above blot are quantification of Sox4 phospho-band normalized to total Sox4 (FLAG) for nocodazole-treated and non-treated cells and are expressed as fold change vs. controls (n=6).
F) Immunoblot analysis with pSox4 antibody of cell lysates extracted from E13.5 control and DKO forebrains. Red arrowheads indicate Sox4 phosphorylation band; red asterisks are nonspecific bands. Numbers above blot are quantification of Sox4 phosphorylation levels normalized to total Sox4 and are expressed as fold change vs. controls (n=4 embryos, 3 litters).
G) Immunoblot analysis with a Sox11 antibody of protein lysates extracted from control and mutant E13.5 NPCs. Numbers are fold change vs. controls of Sox11 protein levels normalized to GAPDH (n=3).
H) IF for Sox11 and pHH3 in E13.5 control and DKO neocortices. Sox11 staining intensity is decreased in mitotic cells (white arrowheads, insets).
I) Quantification of Sox11 protein levels in SVZ mitotic cells from E13.5 control and DKO **I**) embryos. Quantification performed as in (B). Data are means ± SEM for ratios of high vs. low Sox11 and are displayed as fold change vs. controls (n=5 embryos, 3 litters).
J) Immunoblot analysis with a Sox11 antibody of protein lysates extracted from E13.5 control and DKO forebrains. Numbers are fold change vs. controls of Sox11 protein levels normalized to Tuj1 (n=5 embryos, 4 litters). ERK1/2 immunoblot shown to document equal loading.
K) Co-IF for Sox11 and Tbr2 in sections of neocortex of E13.5 control and DKO embryos. Sox11 immunoreactivity is reduced in some Tbr2 + cells (asterisks, insets).

L) Quantification of percentage of Tbr2+ cells that show with high Sox11 staining intensity, in control and DKO E13.5 neocortices. High or low staining intensity was judged based on visual inspection, taking background staining levels into account. Data are means ± SEM and are shown as fold change vs. controls (n=5 embryos, 3 litters). All scale bars 20 μm. Protein ladder numbers in italics indicate estimated size. Unpaired two-tailed t-test for all statistical analyses: ns, not significant; * $p < 0.05$, ** $p < 0.01$ *** $p < 0.001$. Panel **A-L** are provided by Dr.*Fabio da Silva*.

5.2.6 Sox4/11 overexpression and GSK3 inhibition both rescue differentiation defects Of DKO NPCs

To check if Sox4/11 dysregulation is responsible for the neurogenesis defects in DKO embryos, we tried to rescue the neurogenesis defect in mutant NPCs by introducing Sox4 and Sox11 using lentiviral transduction of Flag-Sox4 and Flag-Sox11 in the pLenti-CAG-IRES-EGFP vector (Figure 2.6A). To get rid of possible toxic effects resulting from excessive viral dosage, we obtained NPCs from DKO and control E13.5 neocortex . DKO NPCs displayed similar neurogenesis defects as sh*Ccny*-treated *Ccnyl1* mutants with decreased $Tuj1^{+}$ neurons (Figure 2.6E). To perform rescue experiments, we infected DKO and control NPCs with either Sox4 and Sox11-overexpressing lentiviruses, or empty pLenti-CAG-IRES-EGFP control vector, induced *in vitro* differentiation, and then traced neuronal output by IF against Tuj1 and Map2 (microtubule-associated protein 2, an additional neuron marker). IF for GFP or FLAG was used to quantify number of transfected cells. Interestingly, Sox4/11 introduction in DKO NPCs gave rise to a nearly complete rescue of the number of Tuj1+ and MAP2+ cells generated when compared to DKO NPCs transduced with empty vector (Figure 2.6B-C). However, many of the rescued Tuj1+/MAP2+ cells lacked mature neurites (Figure 2.6B-C), indicating that Sox4/11 introduction rescue initial stages of neurogenesis but not full neuronal differentiation in DKO NPCs.

Finally, to verify that the DKO differentiation phenotype in cultured NPCs is truely because of diminished WNT/LRP6 signaling, we performed a rescue experiment in DKO and control cells using the GSK3 inhibitor CHIR99021 (CHIR) (Figure 2.6E). 1μm CHIR treatment in DKO NPCs resulted in a dramatic increase in the number of immature neurons, while 3 μm CHIR treatment rescued the level of mature neurons to that of controls, thereby resulting in a complete rescue (Figure 2.6E-F). CHIR treatment

also increased neurogenesis in control NPCs, which is consistent with previous studies(Rosenbloom et al., 2020), however, the fold induction in neurogenesis observed was much lower to CHIR-treated DKO NPCs (Figure 2.6E-F). Therefore, we conclude that Ccny/l1 differentiation of cultured NPCs via the WNT signaling pathway.

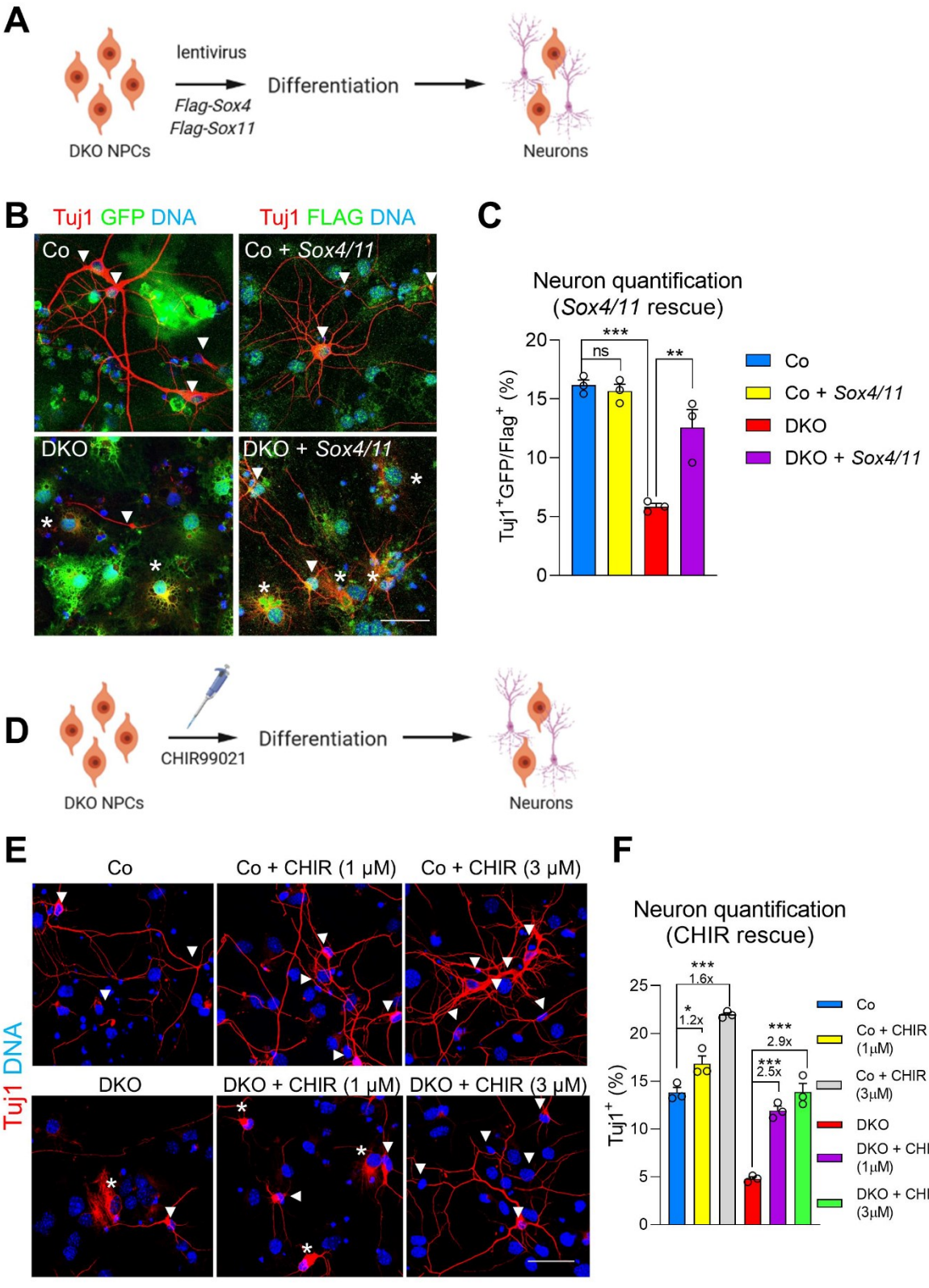
A
lentivirus
Flag-Sox4
Flag-Sox11
Differentiation
DKO NPCs
Neurons
B
Tuj1 GFP DNA
Tuj1 FLAG DNA
Co
Co + Sox4/11
DKO
DKO + Sox4/11
C
Neuron quantification
(Sox4/11 rescue)
Tuj1+GFP/Flag+ (%)
ns
***
**
Co
Co + Sox4/11
DKO
DKO + Sox4/11
D
CHIR99021
Differentiation
DKO NPCs
Neurons
E
Co
Co + CHIR (1 μM)
Co + CHIR (3 μM)
DKO
DKO + CHIR (1 μM)
DKO + CHIR (3 μM)
Tuj1 DNA
F
Neuron quantification
(CHIR rescue)
Tuj1+ (%)
1.2x
1.6x
2.5x
2.9x
Co
Co + CHIR (1μM)
Co + CHIR (3μM)
DKO
DKO + CHIR (1μM)
DKO + CHIR (3μM)

Figure 2.6 *Sox4/11* overexpression and GSK3 inhibition both rescue differentiation defects of DKO NPCs.

A) Schematic illustrating strategy to rescue DKO NPC differentiation defect by simultaneous lentiviral overexpression of Flag-Sox4 and Flag-Sox11 with two lentiviruses. Created with Biorender.com.
B) IF for Tuj1 and Map2 (not shown) to identify newly formed neurons in NPCs after seven-day culture in differentiation medium. Empty CAG-IRES-EGFP vector was used as control in cells not transduced with Sox4/11. Transduced cells were identified by IF for GFP (Co and DKO) or FLAG (Co + Sox4/11 and DKO + Sox4/11). Arrowheads indicate mature neurons and asterisks denote immature neurons lacking neurite extension. Scale bar 20 µm.
C) Quantification of transduced Tuj1 + cells from (B). Note the decrease in neuron number in DKO cultures compared to control, and the rescue in DKO cultures upon Sox4/11 expression (experiment performed twice in triplicates, representative experiment shown). Data are means ± SEM.
D) Schematic illustrating the rescue DKO NPC differentiation defect with the GSK3 inhibitor CHIR99021. Created with Biorender.com.
E) IF for Tuj1 to identify newly formed neurons in NPCs after seven-day culture in differentiation medium. Arrowheads indicate mature neurons and asterisks denote immature neurons lacking neurite extension. Scale bar 20 µm.
F) Quantification of Tuj1+ cells in control, control + CHIR (1 µM, 3 µM), DKO, and DKO + CHIR NPC cultures. Data are means ± SEM (experiment performed twice in triplicates, representative experiment is shown). Numbers below asterisks show fold change. One way ANOVA test for all statistical analyses: ns, not significant; * $p < 0.05$, ** $p < 0.01$ *** $p < 0.001$.

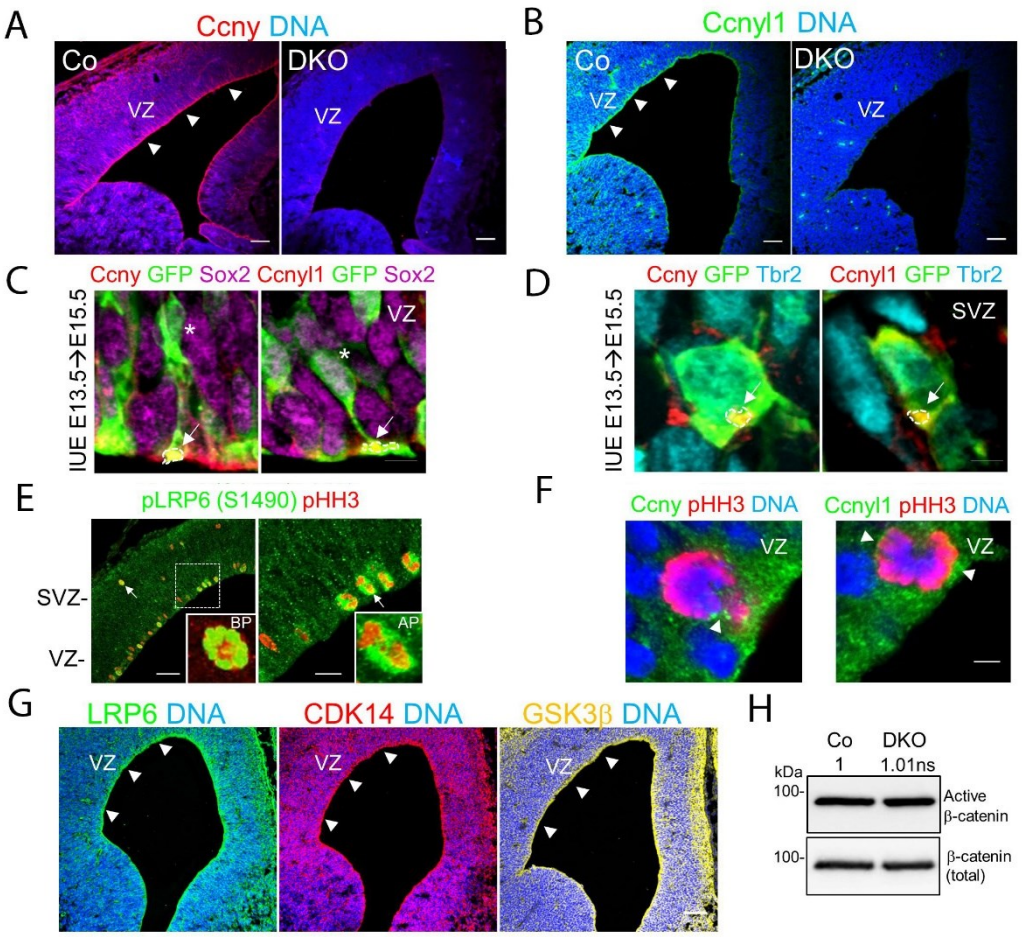

Figure 2.7 WNT/STOP component expression in the neocortex.

A-B) IF using homemade polyclonal antibodies against Ccny (A) and Ccnyl1 (B) in control and DKO E13.5 neocortices. All scale bars 50 µm.

C) Triple IF for Ccny or Ccnyl1 plus Sox2 and GFP in E15.5 embryos electroporated with GFP plasmid at E13.5. White arrows and dashed outlines depict Ccny/l1 immunoreactivity at the apical membrane of Aps in the VZ. Asterisks depict nuclei of cells. Scale bar 5µm.

D) Triple IF for Ccny or Ccnyl1 plus Tbr2 and GFP in E15.5 embryos electroporated with GFP plasmid at E13.5. White arrows and dashed outlines depict Ccny/l1 immunoreactivity as single puncta in BPs in the SVZ. Scale bar 2µm.

E) Co-IF for pLRP6(S1490) and pHH3 in E13.5 wildtype neocortex. Area in dashed box in left panel is shown at higher magnification in right panel. Mitotic BP(division in basal VZ/SVZ, left panel, arrow

and inset) and mitotic APs (division at apical membrane/cortex, right panel, arrow and inset) show high pLRP6 imuunoreactivity. Scale bar left panel 50 µm, right panel 20µm.

F) Ccny and Ccnyl1 co-IF with pHH3 shiwing mitotic Aps at the VZ surface of E13.5 wildtype neocortex. Scale bar 2µm.

G) Immunoblot analysis with a Sox11 antibody of protein lysates extracted from control and mutant E13.5 NPCs. Numbers are fold change vs. controls of Sox11 protein levels normalized to GAPDH (n=3).

H) IF for LRP6 (total levels), cyclin-dependent kinas14 (CDK14) and glycogen synthase kinase 3β (GSK3β) on the neocortex of control E13.5 embryos. Scale bar 40 µm.

I) Immunoblot analysis of control and DKO E13.5 forebrain lysates with an antibody against active (dephosphoryllated) β-catenin. Number above blot are quantification of active β-catenin levels normalized to total β-catenin and are expressed as fold change vs. Control (n=4 embryos, 2 litters). Unpaired two-tailed t-test for all statistical analyses: ns, not significant; * $p < 0.05$, ** $p < 0.01$ *** $p < 0.001$. Panels **C-F** are provided by Dr. *Fabio da Silva*

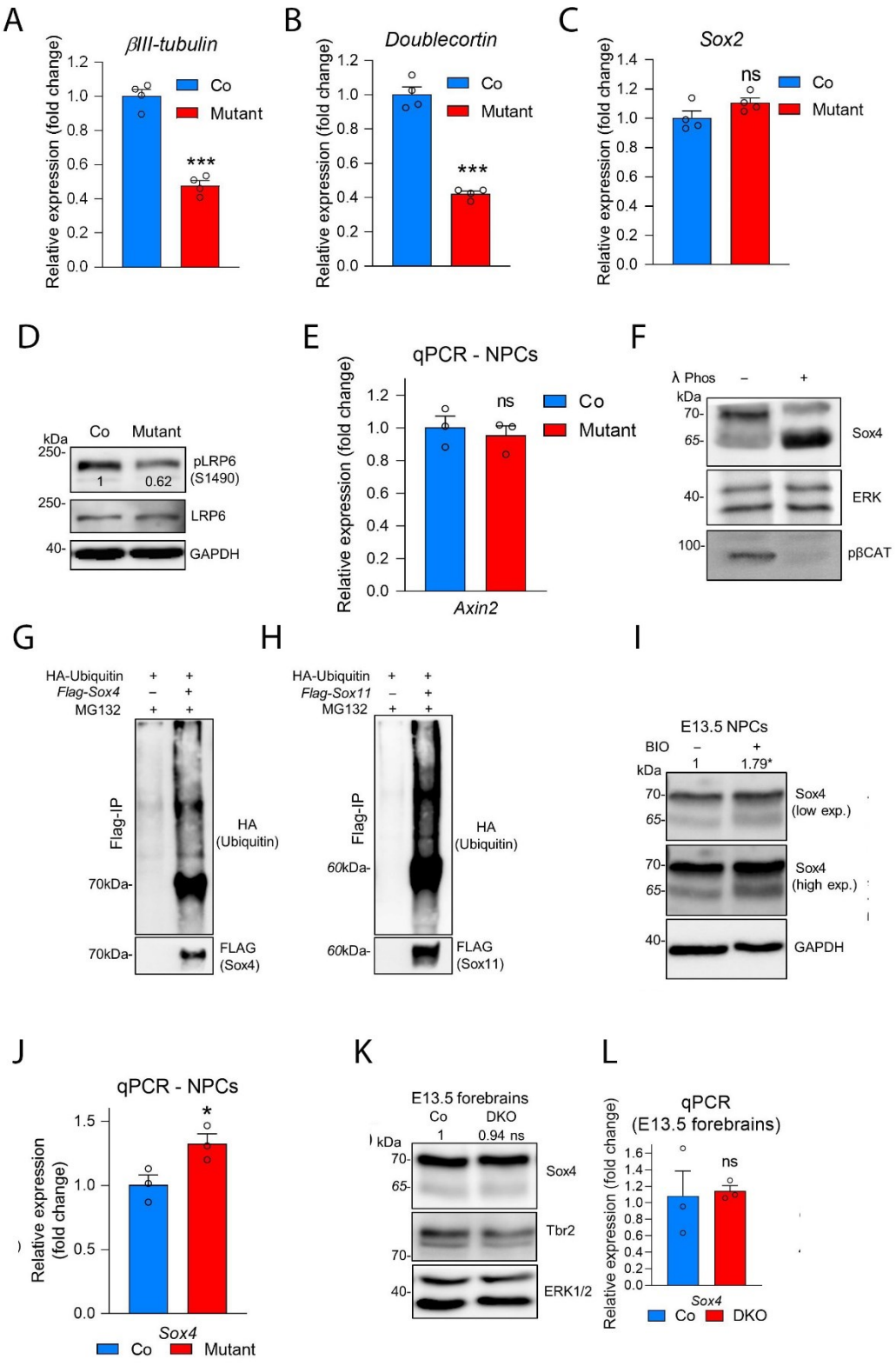
A
βIII-tubulin
Relative expression (fold change)
Co
Mutant
***
B
Doublecortin
Relative expression (fold change)
Co
Mutant
***
C
Sox2
Relative expression (fold change)
ns
Co
Mutant
D
kDa
Co
Mutant
250-
pLRP6 (S1490)
1
0.62
250-
LRP6
40-
GAPDH
E
qPCR - NPCs
Relative expression (fold change)
ns
Co
Mutant
Axin2
F
λ Phos
–
+
kDa
70-
65-
Sox4
40-
ERK
100-
pβCAT
G
HA-Ubiquitin
Flag-Sox4
MG132
Flag-IP
HA (Ubiquitin)
70kDa-
70kDa-
FLAG (Sox4)
H
HA-Ubiquitin
Flag-Sox11
MG132
Flag-IP
HA (Ubiquitin)
60kDa-
60kDa-
FLAG (Sox11)
I
E13.5 NPCs
BIO
–
+
1
1.79*
kDa
70-
65-
Sox4 (low exp.)
70-
65-
Sox4 (high exp.)
40-
GAPDH
J
qPCR - NPCs
Relative expression (fold change)
*
Sox4
Co
Mutant
K
E13.5 forebrains
Co
DKO
1
0.94 ns
kDa
70-
65-
Sox4
70-
Tbr2
40-
ERK1/2
L
qPCR (E13.5 forebrains)
Relative expression (fold change)
ns
Sox4
Co
DKO

Figure 2.8 WNT/STOP regulates neurogenesis in the neocortex.

A-C) qPCR expression analysis of the neuronal markers *βIII*-tubulin (A) and *doublecortin* (B) and of the stem cell marker Sox2 (C) using RNA extracted from control and mutant NPCs culture after 7-days differentiation. Data are expressed as fold change vs. Controls and are means ± SEM (experiment performed twice in quadruplicates, representative experiment shown.

D) Immunoblot analysis using an antibody against pLRP6 (S1490) of protein lysates extracted from control and mutant NPCs prior to culture prior to culture in differentiation medium. Numbers above blot represent pLRP6 levels (fold change) nromalized to total LRP6 (middle immunoblot). Experiment repeated three times and representative samples shown.

E) *Axin2* qPCR analysis using RNA extracted from control and mutant NPCs prior to culture in differentiation medium. Data are expressed as flod change vs. Controls and are means ± SEM (n=3).

F) Immunoblot analysis using a Sox4 antibody of 293T protein lysates treated without (-) or with (+) λ-Phosphatase (top). ERK (middle) and phospho-β-catenin immunoblots were used to validate equal loading and λ–Phosphatase treatment, respectively.

G-H) 293T cells were subjected to *Flag-Sox4* (G) or *Flag-Sox11* (H) overexpression as indicated, each other with HA-ubiquitin overexpression, followed by 4-hour MG132 (20μM) treatment to block proteasomal degradation and immunoprecipitation (IP) for Flag-tagged proteins. Immunoblot analysis using HA antibody was performed to detect ubiquitin conjugation. Experiment performed twice and representative results shown.

I) Sox4 immunoblot analysis of protein lysates from E13.5 wildtype NPCs treated without (-) or with (+) 1μM BIO for 24hrs. Low (top) and high (middle) exposures (exp) are shown. Numbers above blot represent the difference in the ratio of non-phospho Sox4 band (65kDa) to phospho-Sox4 band (70kDa), with this ration for control cells being set to 1.0 and the ration for BIO-treated cells being expressed relative to this (n=3). GAPDH immunoblot to document equal loading.

J) qPCR expression analysis of Sox4 expression using RNA extracted from control and mutant NPCs culture after 7-days differentiation. Data are expressed as fold change vs. Controls and are means ± SEM (experiment performed twice in quadruplicates, representative experiment shown.

K) Sox4 immunoblot analysis of protein lysates from E13.5 control and DKO forebrains (top). Numbers above blot represent fold change vs. control of Sox4 immunoreactivity upon normalization to Tbr2 immunoreactivity (middle) (n=5 embryosm 4 litters). ERK1/2 immunoblot (bottom) shows equal loading of samples.

L) Sox4 qPCR expression analysis of RNA extracted from E13.5 control and DKO dorsal forebrains. Sox4 mRNA levels were normalized tp Tbr2, also determined by qPCR expression analysis. Data are expressed as fold change vs. controls and are means ± SEM (n=3, 2litters). Unpaired two-tailed t-test

for all statistical analyses: ns, not significant; * p < 0.05, ** p < 0.01 *** p < 0.001. Panels **G-L** are provided by Dr.*Fabio da Silva*

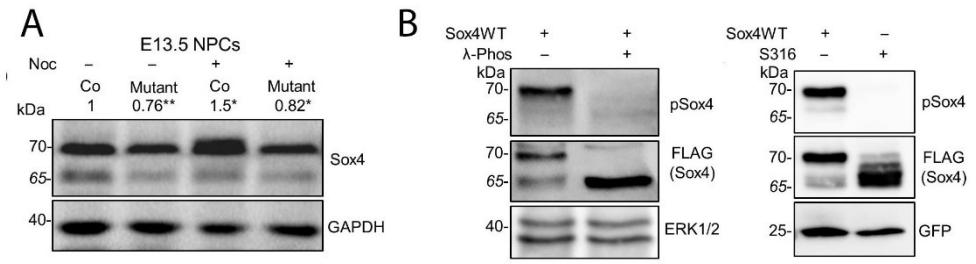

Figure 2.9 Sox4 is WNT/STOP target in the developing neocortex.

A) Sox4 immunoblot analysis of protein lysates from E13.5 control and mutant NPCs treated without (-) or with (+) 100ng/ml nocodazole overnight (Noc). Numbers above blot represent fold change vs. control (-Noc) of Sox4 protein levels normalized to GAPDH.

B) Immunoblot analysis (left) using the Sox4 phospho-antibody (pSox4) of protein lysates from 293T cells transfected with *Flag-Sox4* (top-left). Protein lysates were treated without (-) or with (+) λ-phosphotase for one hour prior immunoblot analysis. Anti-FLAG immunoblot to demonstrate the presence of dephosphorylated Sox4. ERK1/2 immunoblot shows equal loading of samples.using an antibody against pLRP6 (S1490) of protein lysates extracted from control and mutant NPCs prior to culture prior to culture in differentiation medium. Numbers above blot represent pLRP6 levels (fold change) nromalized to total LRP6 (middle immunoblot). Experiment repeated three times and representative samples shown. Immunoblot analysis (right) analysis using pSox4 antibody of protein lysates from 293T cells transfected with WT flag-Sox4 or S316 mutant plasmids as indicated (top-right). Anti-Flag immunoblot to demonstrate the presence of S316 mutant Sox4 (middle). GFP immunoblot (bottom-right) shows equal loading of samples. Unpaired two-tailed t-test for all statistical analyses: ns, not significant; * p < 0.05, ** p < 0.01 *** p < 0.001. Panel **B** is provided by *Fabio da silva*

5.3 Discussion

We were aiming to decipher the role of WNT/STOP signaling in neocortex development by analyzing Ccny/l1 double mutant mice. We discovered that WNT/STOP governs embryonic neurogenesis by (1) controling AP symmetric and asymmetric division mode; (2) modulating the length of the cell cycle, especially mitosis of BPs; (3) promoting neurogenesis via the SoxC transcription factors, Sox4 and Sox11, in BPs. The study provides an additional piece of *in vivo* evidence for WNT/STOP during embryonic neurogenesis. Our study also dissects the roles of different WNT branches during neocortex development, whereby WNT/STOP promotes a differentiative process, i.e. the generation of NPCs committed to neurogenesis, and canonical WNT promotes NPC self-renewal.

5.3.1 WNT/STOP vs canonical WNT signaling during neocortical neurogenesis

The precise biological output of WNT/β-catenin signaling in the mouse neocortex is controversial. According to β-catenin conditional knockout mice, which display increased AP cell cycle exit and premature neurogenesis(Draganova et al., 2015; Mutch et al., 2010), the major role of canonical WNT signaling is to promote self-renewal at the expense of differentiation. However, *in vitro* studies demonstrate that β-catenin can also promote NPC differentiation into neurons(Kuwahara et al., 2010)

More recently, WNT ligand overexpression by electroporation of a Wnt3a-expressing vector into the neocortex increased both, proliferation of APs and differentiation of BPs. However, this study depended on monitoring WNT signaling at the ligand level, which affects both canonical and WNT/STOP branches. By focussing on Ccny/l1, which are WNT/STOP specific regulators(Acebron and Niehrs, 2016) that are enriched during G2/M and hence function, for the most part, independently of β-catenin, we suggest a new model for WNT signaling during neurogenesis: WNT/STOP signaling promotes post-mitotic neuron generation from BPs through stabilization of Sox4/11, whereas canonical Wnt signaling promotes AP self-renewal. Our conclusions, based on the analysis of E13.5 DKO embryos, are further strengthened by the IUE results of *Ccny/l1* knockdown at later stages of neocortex development *in vivo* and by NPC culture *in vitro*. Together, these data indicate decreased generation of BPs, and consequently of

neurons, in the absence of Ccny/l1. We therefore conclude that DKO embryos exhibit reduced neurogenesis via decreased generation of BPs from APs, and of post-mitotic neurons from BPs.

LRP6 is a critical regulator in WNT/STOP and its phosphorylation at G2/M by the Ccny/CDK complex triggers GSK3 inhibition and WNT activation during mitosis, when transcription is minimal(Davidson et al., 2009). Analysis of *Lrp6* mutant mice displays a thinner neocortex, decreased neurogenesis, and only minor changes in proliferation(Zhou et al., 2006). Likewise, deficiency in *acting-binding protein filamin A* leads to mouse cerebral cortex neurogenesis defects with impaired LRP6/GSK3 signaling and asymmetric neural progenitors division(Lian et al., 2016; Lian et al., 2019). These phenocopied what we previously observed in Ccny/l1 DKO embryos, indicating that *Lrp6* mutants primarily present a WNT/STOP signaling defect.

5.3.2 WNT/STOP signaling promotes neurogenesis via Sox4 and Sox11 stabilization

Another crucial finding of this study is the discovery that the neurogenic transcription factors Sox4 and Sox11 are WNT/STOP target proteins. Previous links between SoxC transcription factors and WNT were previously known: Sox4 and Sox11 can interact with the β-catenin destruction complex(Bhattaram et al., 2014; Melnik et al., 2018), and Sox4 is a β-catenin target(Melnik et al., 2018). Our data strengthen and further develop these links by showing that Sox4/11 are directly phosphorylated by GSK3 and undergo proteasomal degradation afterwards. We also found that the Sox4 is mainly phosphorylated at a single GSK phospho-motif, while Sox11 is partially phosphorylated. GSK3 phosphorylation can generate phosphodegrons for recognition by E3 ubiquitin ligases undegoing proteasomal degradation(Taelman et al., 2010). In line with this, phosphorylation by GSK3β triggered ubiquitination and decreased Sox4 and Sox11 protein levels. It has been shown that in the neocortex, Sox11 protein stabilization and localization are regulated by ubiquitination and phosphorylation, respectively, indicating that post-transcriptional regulation of Sox11 is of great importance for its function *in vivo(Balta et al., 2018; Chiang et al., 2021)*.

WNT/STOP inhibits GSK3 predominantly at G2/M(Acebron et al., 2014). Similarly, we discover that the regulation of Sox4/11 by WNT/STOP is cell cycle-dependent, especially in mitotic cells. WNT/STOP signaling in G2/M of mother cells is believed to provide daughter cells with a survival and growth advantage, via stabilizing abundance of proteins. Defects of WNT/STOP signaling hinders G1 growth and delays cell cycle progression(Acebron et al., 2014; Huang et al., 2015). Likewise, WNT/STOP signaling in G2/M of NPCs most likely induces differentiation of daughter cells by increasing Sox4/11 levels during G1/S- phase. An intriguing hypothesis is that Sox4/11 are classic transcription factors, that stay bingding tochromosomes in mitosis to ensure target gene reactivation in a timely manner upon mitotic exit(Palozola et al., 2019).

The significance of reduced Sox4/11 protein levels for neurogenesis defect of DKO embryo is underscored by the fact that their re-introduction can rescue the differentiation defect. strikingly, the rescue is inadequate: Sox4/11 restore the number of $Tuj1^{+}$ DKO NPCs-derived neurons, but only partially rescue their morphology, giving rise to immature neurons. The incomplete rescue may be owing to unphysiologically high levels of *Sox4/11* from lentiviral transduction since *Sox11* overexpression inhibits dendrite morphogenesis(Hoshiba et al., 2016). On the other hand, WNT/STOP might have extra targets responsible for neuronal maturation and morphogenesis besides Sox proteins. Certainly, proteomic analysis indicates hundreds of potential WNT/STOP target proteins in cultured cells(Acebron et al., 2014).

5.4 Working model

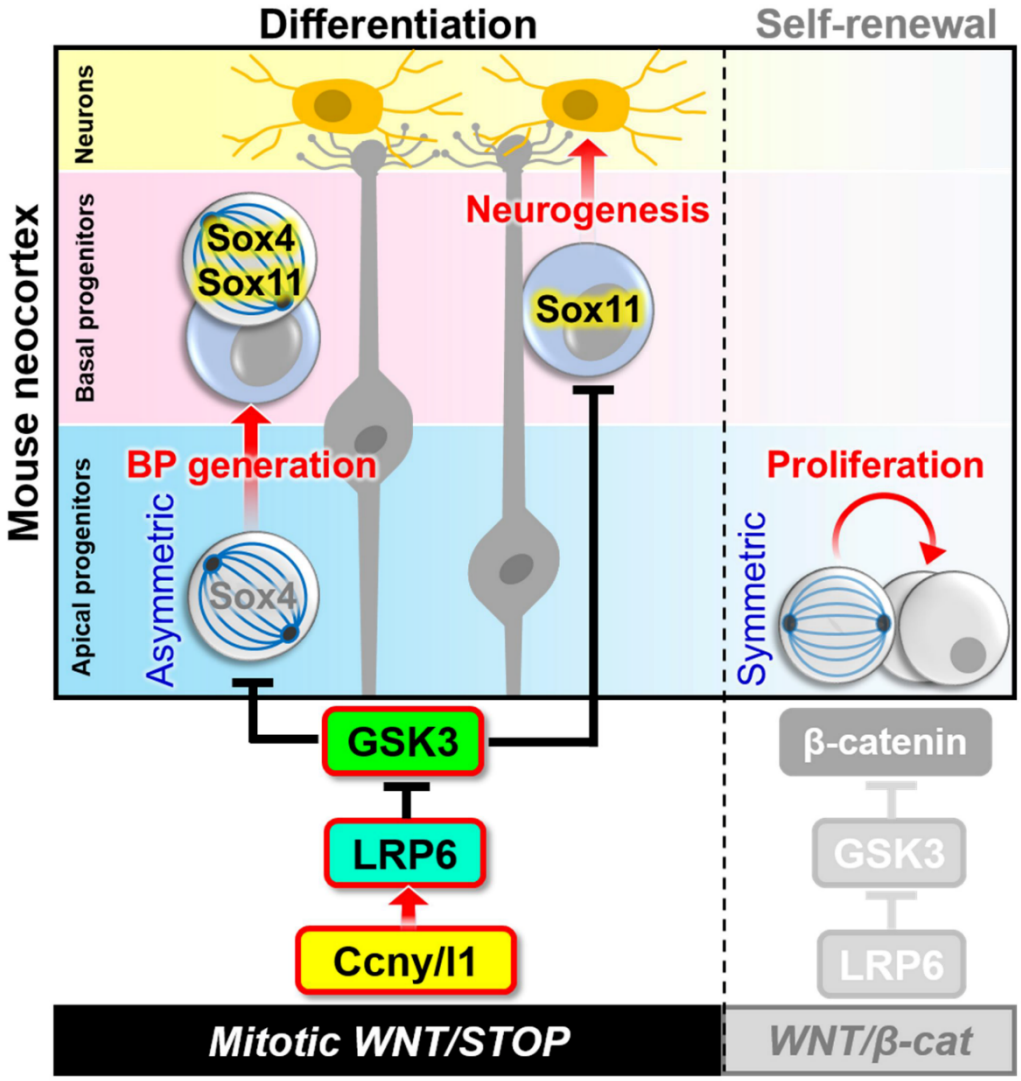

Figure 2.10 Division of labor model between WNT/STOP and WNT/β–catenin signalling during neocortical neurogenesis.

Ccny/l1 and cyclin-dependent kinases (CDK) 14 and 16 phosphorylate and activate LRP6, predominantly during G2/M (not shown). This WNT co-receptor activation leads to a peak of WNT/STOP signalling and GSK3 inhibition in mitosis. Mitotic WNT signalling has two consequences: First, it increases asymmetric AP division via unknown effectors, which leads 60 to more basal progenitors and hence post-mitotic neurons; Second, it protects Sox proteins from proteasomal degradation. Sox4 stabilization in mitotic APs leads to increased BP generation, and its stabilization in mitotic BPs may promote BP self-renewal and/or differentiation. Sox11 is stabilized in both mitotic and non-mitotic cells of the SVZ, which leads to increased post-mitotic neuron generation(Da Silva et al., 2021).

6. Chapter 2: Cilia ARE WNT SIGNALING ORGANELLES THAT INDUCE CILIOGENESIS VIA A CONSERVED WNT-PP1 AXIS

6.1 Introduction

Primary cilia are microtubule-based organelles that extend from most vertebrate cells (Anvarian et al., 2019). They concentrate signaling receptors and are prominent signaling hubs for many different growth factors including PDGF, EGFR, IGF, Notch and Hh(Goetz and Anderson, 2010). In regards to the WNT pathway, defining the relationship between cilia and WNT signaling has proven difficult. On the one hand, it has been shown that WNT signaling can promote cilia formation in zebrafish, frog, and mouse via transcriptional gene activation of ciliogenesis regulators such as of *Foxj1*(Song et al., 2014; Walentek et al., 2012; Walentek et al., 2015). However, these analyses have been limited to certain cell types and have not been explored on a universal level. On the other hand, many studies support an inhibitory function of primary cilia on canonical WNT signaling(Gerdes et al., 2007; Lancaster et al., 2011), but this finding is highly debated(Scholey and Anderson, 2006).

Despite the many known links between WNT and cilia, one basic question remains unanswered: Is canonical WNT signaling restricted to the plasma membrane or do cilia, as they do for Hh and other signaling pathways, accommodate WNT receptors that are engaged by WNT ligands? If so, what downstream events do WNT ligands trigger in cilia? What may be the cellular roles of such intra-ciliary WNT signaling, and what physiological significance does it have *in vivo*? A clue came from our previous report wherein WNT was shown to trigger a non-transcriptional WNT/GSK3 response in mouse sperm flagella to promote sperm maturation(Koch et al., 2015). First, this observation supports the emerging idea that the canonical WNT signaling cascade triggers a much richer response than just canonical WNT signaling. This is because GSK3 inhibition may lead to dephosphorylation of hundreds of other proteins apart from β-catenin(Taelman et al., 2010), and thereby directly affects a wide array of cellular functions besides transcription(Huang et al., 2015). Second, the link between flagella and WNT signaling raised the intriguing possibility that WNT/GSK3 signaling

may also operate directly in cilia in various cell types and not be limited to specialized spermatocytes.

To address the general role of WNT/GSK3 in cilia, I will first analyze primary cilia formation in Ccny/l1 DKO embryos, focusing on organs with ciliated cells and CCNY/L1 expression e.g. neocortex, kidney or fat tissue. To further dissect the mechanisms of WNT/GSK3 axis in ciliogenesis, I will next generate a CCNY/L1 DKO cell line that can form cilia and respond to WNT signaling e.g. 293T cells. This *in vitro* model will also permit me to test if cilia are WNT signaling hubs, since it will allow the spatial and temporal manipulation of WNT, as well as the analysis of the response using sophisticated microscopy techniques. The experimental schematic for Chapter 2 of my thesis is shown below:

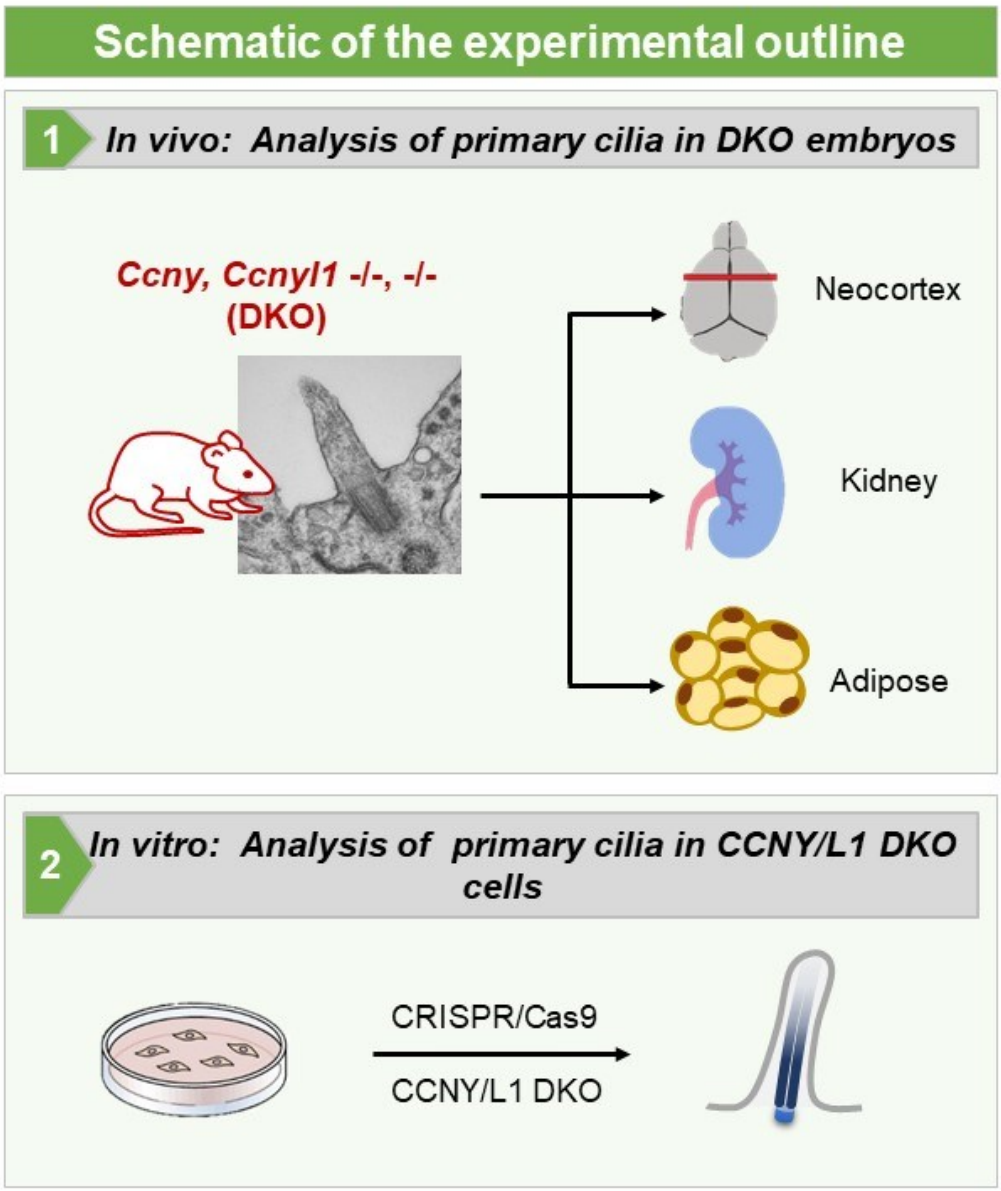
Schematic of the experimental outline
1
In vivo: Analysis of primary cilia in DKO embryos
Ccny, Ccnyl1 -/-, -/-
(DKO)
Neocortex
Kidney
Adipose
2
In vitro: Analysis of primary cilia in CCNY/L1 DKO cells
CRISPR/Cas9
CCNY/L1 DKO

6.2 Results

6.2.1 Ccny/l1 DKO embryos display cranial exencephaly and impaired primary cilia formation in the developing neocortex and kidney and adult preadipocytes

Previously we showed that DKO embryos were embryonic lethal at E14.5. To exclude possible non-specific phenotypes resulting from early lethality, we collected DKO embryos at E13.5. Strikingly, 16% of the DKO embryos (n=60) showed cranial exencephaly (Figure 3.1A), a severe defect also observed in humans. Excencephaly was also observed at earlier time points (E11.5 and E12.5) with a similar frequency, suggesting it was due to impaired neural tube closure, a process that is completed around E9.5 in mice. Interestingly, neural tube closure defects such as cranial exencephaly are closely associated with primary cilia defects(Vogel et al., 2012).

To analyze primary cilia formation in the neural tube of DKO embryos, we stained sections of the neocortex with ARL13B (ADP-ribosylation factor-like protein 13B), which is a ciliary membrane marker. To our surprise, DKO embryos displayed a 25% decrease (p=0.0001) in the number of cilia at the apical surface (Figure 3.1B-C). To confirm this phenotype, we perform IF with another axoneme marker IFT81 (Intraflagellar transport protein 81) and observed a similar decreased cilia number (-28%, p=0.02) (Figure 3.5A-B). To recapitulate the results *in vitro*, we isolated neural progenitor cells from Ccnyll1 KO embryos, transfected them with a lentivirus expressing shRNA against *Ccny* and performed IF against ARL13B. Consistently, Ccny/l1 deficient progenitors formed fewer cilia compared to shRNA controls (-36%, p-00.04) (Figure 3.1D).

We next tested if the cilia phenotype in the DKO neocortex could also be detected in other organs. The kidney is another organ in which primary cilia play essential roles. For example, polycystic kidney disease, a debilitating inherited disorder, is highly associated with mutations in genes required for primary cilia formation(Kathem et al., 2014). To see if *Ccny* and *Ccnyl1* are expressed in the developing kidney, we performed IF and detected enrichment of both WNT/STOP regulators in the apical membrane of glomeruli (Figure 3.5 C-D). More interestingly, DKO glomeruli displayed

reduced cilia formation (-26%, p=0.02) (Figure 3.1E-F). The effects of CCNY/L1 on ciliogenesis in the neocortex and kidney were related to cilia number but not their integrity, as no obvious defects in cilia length or morphology were detected by transmission electron microscopy (SEM) analysis (Figure 3.1G-H). These results indicate that CCNY/L1 promote primary cilia formation in the developing mouse brain and kidney, and that the defects may result in a well-known ciliopathy, excencephaly. Previously, it was reported that Ccny KO mice display defects in lipid metabolism and develop less adipose tissue owing to reduced differentiation of preadipocytes(An et al., 2015). Interestingly, preadipocytes represent the major ciliated cell type in white adipose tissue and removal of cilia in preadipocytes impairs their ability to differentiate *in vitro* and *in vivo*(Hilgendorf et al., 2019; Zhu et al., 2009). Hence, we asked the question that could adipogenesis defects in Ccny KO mice be due to impaired ciliogenesis?

To check this possibility, we first confirmed the adipogenesis defects in *Ccny KO* mice. Consistent with the previous data(An et al., 2015), Ccny KO mice were smaller in body size, lighter in body weight and exhibited decreased epididymal, inguinal and interscapular fat mass (Figure 3.5E-F) and reduced adipocyte size (Figure 3.1I-L). We next analyzed primary cilia in preadipocytes. We performed co-IF with the primary cilia marker ARL13B plus the preadipocyte marker PDGFα (Plate derived growth factor receptor alpha)(Berry and Rodeheffer, 2013). Strikingly, IF analysis of epididymal fat pads for ARL13B-positive preadipocytes in Ccny KO mice displayed a marked decrease in cilia number (-38%, p=0.01) (Figure 3.1M-N). Consistently, acute siRNA knockdown of Ccny in adipogenic 3T3-L1 cells also mildly decreased cilia number and length (Figure 3.1O-Q). Altogether, these results demonstrate that CCNY/L1 promote primary cilia formation in the developing mouse brain, kidney and preadipocytes, and that their deficiency can lead to ciliopathies, namely excencephaly and lipodystrophy.

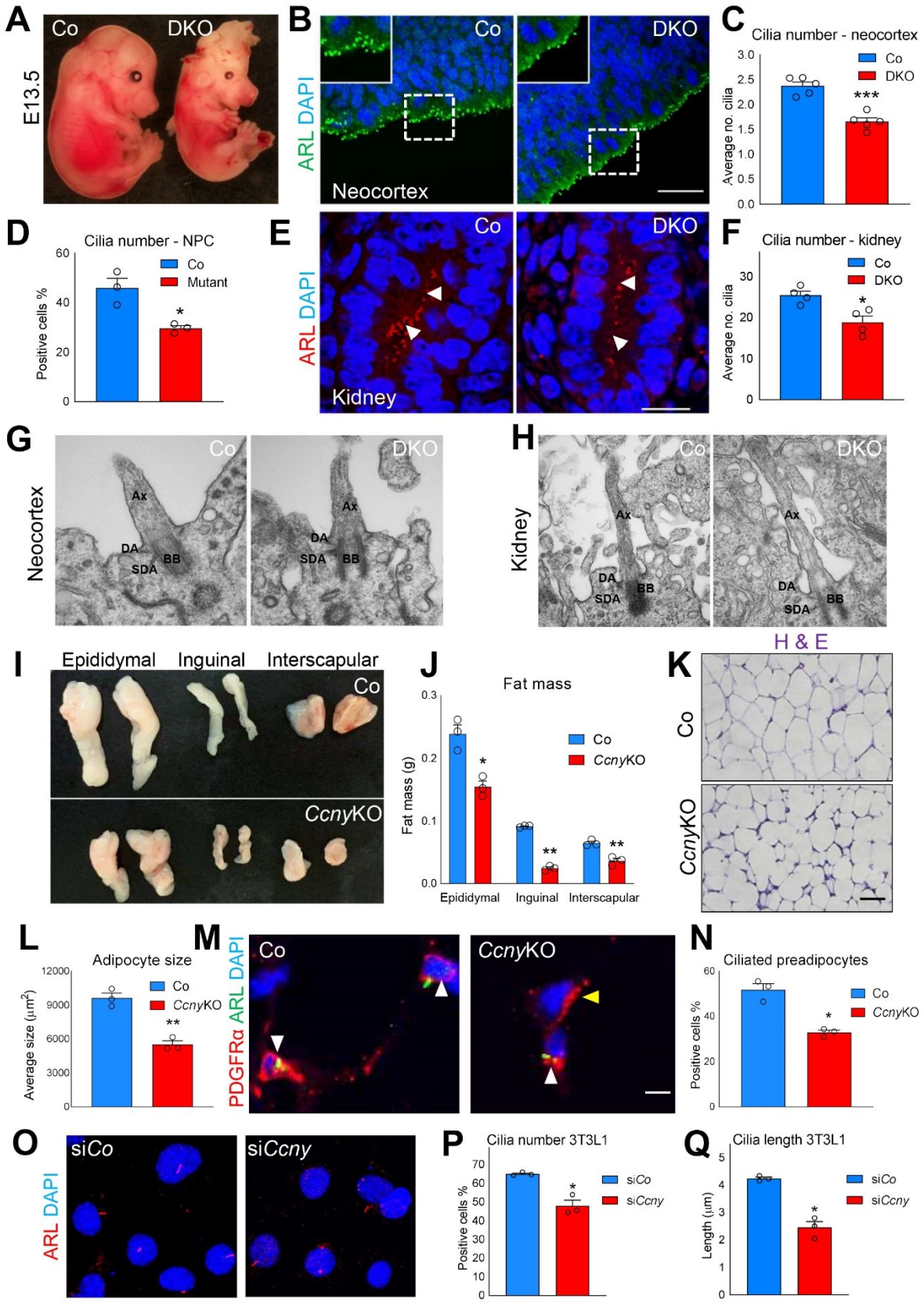
A
Co
DKO
E13.5
B
Co
DKO
ARL DAPI
Neocortex
C
Cilia number - neocortex
Co
DKO
***
Average no. cilia
D
Cilia number - NPC
Co
Mutant
*
Positive cells %
E
Co
DKO
ARL DAPI
Kidney
F
Cilia number - kidney
Co
DKO
*
Average no. cilia
G
Neocortex
Co
DKO
Ax
DA
SDA
BB
H
Kidney
Co
DKO
Ax
DA
SDA
BB
I
Epididymal
Inguinal
Interscapular
Co
CcnyKO
J
Fat mass
Co
CcnyKO
Fat mass (g)
Epididymal
Inguinal
Interscapular
K
H & E
Co
CcnyKO
L
Adipocyte size
Co
CcnyKO
**
Average size (μm²)
M
Co
CcnyKO
ARL DAPI
PDGFRα
N
Ciliated preadipocytes
Co
CcnyKO
*
Positive cells %
O
siCo
siCcny
ARL DAPI
P
Cilia number 3T3L1
siCo
siCcny
*
Positive cells %
Q
Cilia length 3T3L1
siCo
siCcny
*
Length (μm)

Figure 3.1 DKO embryos exhibit canial excencephaly and impaired cilia formation in the developing neocortex and kidney and adult preadipocytes.

A) Ccny/yl1 double knockout (DKO) mouse embryos exhibit cranial exencephaly. Exencephaly is observed at similar frequencies in Embryonic day 11.5 (E11.5) (9 embryos analyzed), E12.5 (10 embryos analyzed) and E13.5 (60 embryos analyzed).
B-C) IF against the ciliary membrane protein ARL13B (ARL) in the neocortex of E13.5 embryos. The average number of cilia were quantified in 5 independent control (Co) and DKO embryos obtained from 3 different litters. Columns are means ± SEM. Scale bar 20 µm.
D) ARL13B IF on control and mutant monolayer cultures of neural progenitor cells (NPC) isolated from E13.5 forebrains to quantify primary cilia (white arrowheads). Columns are means ± SEM (experiment performed twice in triplicates, representative experiment shown). Scale bar 5 µm.
E-F) ARL13B IF on E13.5 kidneys and quantification of cilia number in apical membrane (white arrowheads) of developing glomeruli. Columns are means ± SEM (n=4 embryos, 4 litters). Scale bar 10 µm.
G)Transmission electron microscopy (TEM) analysis of neocortical cilia in control and DKO embryos. No obvious differences in morphology observed. Ax = axoneme, DA = distal appendage, SDA = subdistal appendage, BB = basal body.
H) TEM analysis of control and DKO cilia in kidney glomeruli also reveals no major differences in morphology.
I-J) Comparison of fat mass between control and CcnyKO adult male mice. Weights for epididymal, inguinal and interscapular fat pads measured for 3 independent control and CcnyKO mice. Columns are means ± SEM.
K-L) Haematoxylin and Eosin staining on paraffin sections from control and CcnyKO epididymal fat pads. Average size of adipocytes was significantly decreased in CcnyKO mice. Columns are means ± SEM (n=3 mice).
M-N) Co-IF for ARL13B and the preadipocyte marker PDGFRα (platelet derived growth factor receptor alpha) on sections of epididymal fat pads. The average number of ciliated preadipocytes was quantified for control and CcnyKOs. Columns are means ± SEM (n=3 mice).
O) Acute siRNA knockdown of Ccny or Lrp5/Lrp6 (Lrp5/6) in mouse 3T3L1 preadipocyte cells followed by IF for ARL13B to identify primary cilia.
P-Q) Quantification of cilia number and length in 3T3L1 cells after Ccny and Lrp5/6 siRNA knockdown. Columns are means ± SEM (n=3) Unpaired two-tailed t-test for all statistical analyses: ns, not significant; * $p < 0.05$, *** $p < 0.001$. Panels **A-H** are provided by Dr.*Fabio da Silva.*

6.2.2 CCNY/L1 Promote Primary Cilia Formation through β-catenin-Independent WNT/GSK3 signaling

To dissect the molecular mechanisms underlying the role of CCNY/L1 in ciliogenesis, we used HEK293T cells, a model system to study primary cilia formation(Paridaen et al., 2013). Using CRISPR/Cas9 genome editing, we generated 293T cells deficient for CCNY and CCNYL1 (referred to as Y/L1 DKO cells) (Figure 3.5G-I). Western blot analysis confirmed that CCNY and CCNYL1 proteins were deleted in Y/L1 DKO cells, and SuperTOPFlash Wnt reporter assays displayed decreased luciferase activity upon Wnt3a stimulation in nocodazole-treated Y/L1 DKO mitotic cells, which is consistent with our previous discovery that CCNY/CCNYL1 are mitotic WNT signaling regulators(Davidson et al., 2009).

Ciliogenesis can be induced in 293T cells by serum starvation(Paridaen et al., 2013). Therefore we serum-starved 293T cells for 24hrs and performed IF against ARL13B. Strikingly, Y/L1 DKO cells revealed a drastic decrease in cilia number (-74%, p=0.0002) and length (-67%, p=0.007) (Figure 3.2A-B). To confirm that CCNY/L1 regulation of primary cilia in 293T cells was related to WNT signaling, we also analyzed a previously established LRP5/LRP6 double knockout 293T cell line(Kirsch et al., 2017). In LRP5/6 DKO cells, there was a similar reduction in cilia number (-65%, p=0.0006) and length (-65%, p=0.03) (Figure 3.2A-B).

Reduced ciliogenesis was not due to general cell cycle defects (e.g. mitotic arrest) since DKO cells exited the cell cycle (Ki67 negative) at comparable rates to controls in response to serum starvation. To support that cilia defects were not due to off-target effects from CRISPR/Cas9, we performed acute knockdown of CCNY/L1 and LRP5/6 using siRNA, which phenocopied reduced cilia number and cilia length (Figure 3.2C-D). In contrast, siRNA knockdown β-catenin did not lead to cilia defects (Figure 3.2C-D) We next performed rescue experiments in Y/L1 DKO cells according to different modes of WNT stimulation. Interestingly, treatment with GSK3 inhibitor lithium chloride or BIO significantly rescue the cilia defects whereas overexpression of active β-catenin had no effect (Figure 3.2E-F). In summary, these data suggest that CCNY/L1 promote ciliogenesis via WNT/GSK3 signaling, independently of β-catenin.

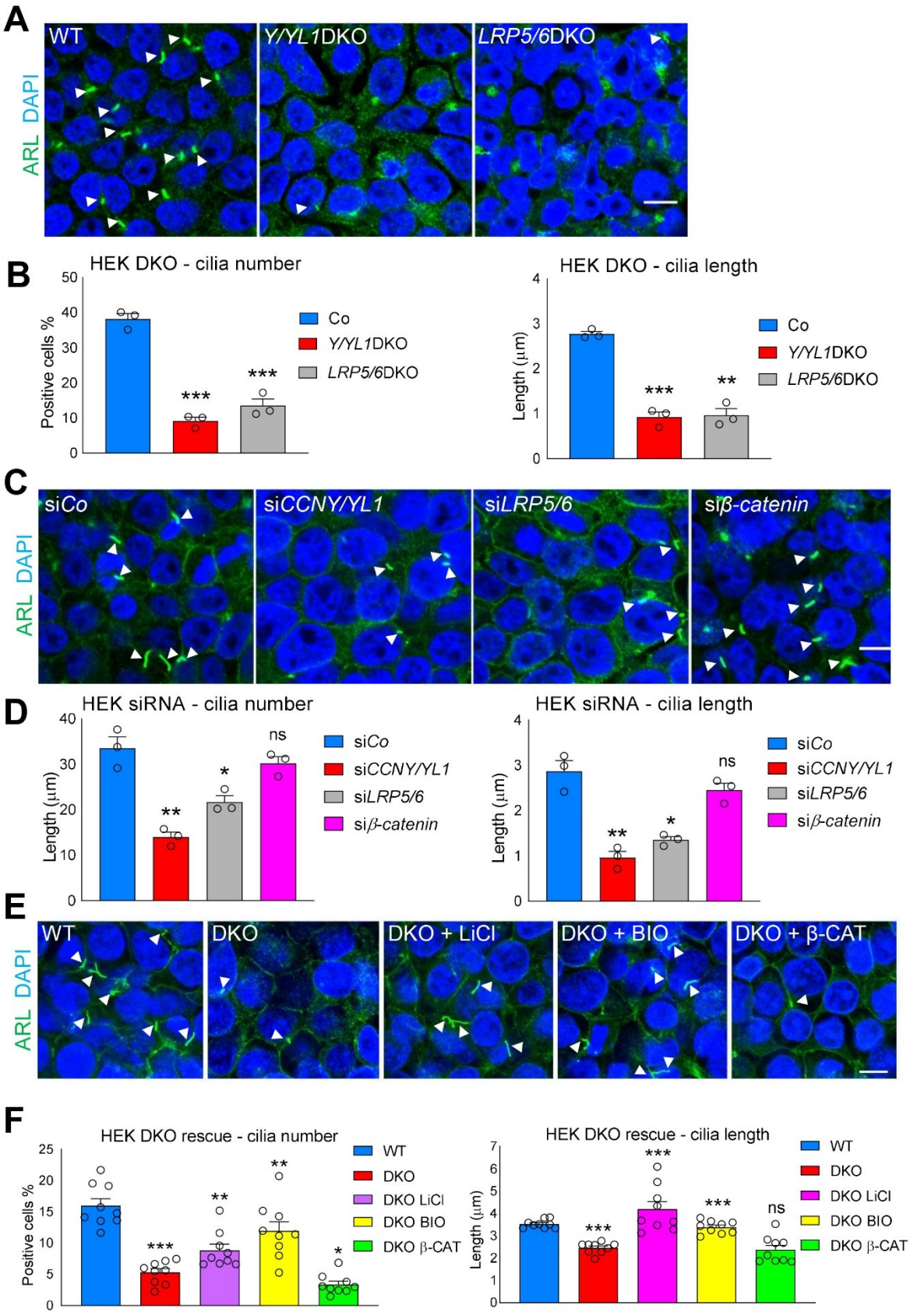
A
WT
Y/YL1DKO
LRP5/6DKO
ARL DAPI
B
HEK DKO - cilia number
Positive cells %
Co
Y/YL1DKO
LRP5/6DKO
HEK DKO - cilia length
Length (µm)
C
siCo
siCCNY/YL1
siLRP5/6
siβ-catenin
ARL DAPI
D
HEK siRNA - cilia number
HEK siRNA - cilia length
Length (µm)
ns
E
WT
DKO
DKO + LiCl
DKO + BIO
DKO + β-CAT
ARL DAPI
F
HEK DKO rescue - cilia number
HEK DKO rescue - cilia length
Positive cells %
Length (µm)
DKO LiCl
DKO BIO
DKO β-CAT

Figure 3.2 CCNY and CCNYL1 promote cilia formation through post-transcriptional WNT signaling.

A) ARL13B IF in serum-starved wildtype (WT), CCNY/CCNYL1 (Y/YL1) DKO and LRP5/LRP6 (LRP5/6) DKO HEK293T (293T) cells.
B) Quantification of the number and length of cilia in WT and DKO cell lines. Columns are means ± SEM (experiment performed 3 times in triplicates, representative experiment shown).
C) Acute siRNA knockdown of CCNY/YL1, LRP5/6 and β-catenin followed by ARL13B IF to analyze primary cilia (white arrowheads).
D) Quantification of cilia number and length for (C). Columns are means ± SEM (experiment performed three times in triplicates, representative experiment shown).
E) Twenty four-hour pharmacological treatments with the Glycogen synthase kinase 3 (GSK3) inhibitors Lithium Chloride (LiCl) (10mM) or BIO (1μM) and transfection of 10 ng/ml Xenopus β-catenin plasmid (xtβ-cat) in wildtype and Y/YL1 DKO cells followed by ARL13B IF to identify primary cilia (white arrowheads).
F) Quantification of cilia number and length for (E). Quantification of Y/YL1 DKO cells compared to wildtype and treatments/transfection compared to Y/YL1 DKO cells. Columns are means ± SEM (experiment performed 3 times in triplicates, all samples included in analysis). All scale bars 5 μm. Unpaired two-tailed t-test for all statistical analyses: ns, not significant; * $p < 0.05$, ** $p < 0.01$, *** $p < 0.001$.glomeruli (white arrowhead, inset). Unpaired two-tailed t-test for all statistical analyses: ns, not significant; * $p < 0.05$, *** $p < 0.001$. Figure **E-F** are provided by Dr.*Fabio da Silva.*

6.2.3 WNT signaling components localize to primary cilia and cilia are WNT-responsive organelles

Cilia are physically distinguished from the rest of the cell body by a selective barrier, the transition zone, which controls the entry and exit of ciliary proteins(Goncalves and Pelletier, 2017). As a result, cilia harbor a distinct protein composition and their membranes are able to concentrate receptors of several signaling pathways(Rohatgi et al., 2007). Given the conserved role of WNT/GSK3 signaling in promoting ciliogenesis, we next explored if cilia harbor WNT/GSK3 components.

In serum-starved 293T cells, IF revealed highly specific localization of endogenous CCNY to the ciliary membrane in 95% of cilia (n=35) (Figure 3.3A). CCNYL1 was also detected within the ciliary membrane (Figure 3.3B), although at a lower frequency (50%, n=30). These staining patterns were abolished in *Y/L1* DKO cells, indicating the specificity of the antibodies (Figure 3.6A-B). In addition, we confirmed GSK3β localization in primary cilia (Figure 3.3C), as previously published(Thoma et al., 2007). Dishevelled 3 (DVL3) was also detected in cilia (Figure 3.3D), consistent with previous work(Veland et al., 2013), although at low levels. In addition, overexpressed FZD5 could be detected in primary cilia as well (Figure 3.3E).

We then explored the localization of the WNT co-receptor LRP6. Due to the low endogenous level of LRP6 in 293T cells, we overexpressed LRP6-EGFP and, interestingly, we found that the WNT co-receptor localized to the axoneme (Figure 3.3F). To exclude the possibility that this effect was due to EGFP, we used non-tagged LRP6 and observed the same staining pattern. (Figure 3.6C)

To confirm cilia localization of endogenous LRP6 we analyzed serum starved mouse embryonic fibroblasts (MEFs), which express higher levels of *Lrp6*. Consistently, 30% (n=100) of MEF cilia showed specific LRP6 localization, confirming that endogenous LRP6 indeed localizes to the ciliary membrane (Figure 3.3G). LRP6 staining was absent in LRP5/6 DKO MEFs, validating the IF staining (Figure 3.6D). *In vivo*, IF for CCNY and ARL13B in the neocortex and kidney glomeruli showed prominent co-localization (Figure 3.3H-I). CCNY/L1 also localized to motile cilia from mouse ependymal epithelium lining the post-natal neocortex (Figure 3.6E-F). In summary, key components of WNT/GSK3 cascade localize to cilia in human and mouse.

Given the conserved role of WNT/GSK3 signaling in promoting ciliogenesis, could cilia themselves be WNT-responsive organelles? Active, ligand-triggered WNT signaling can be monitored with LRP6 antibodies specific for the cyclin Y/CDK14 priming phosphorylation site Sp1490 (‘active LRP6)(Davidson et al., 2005; Zeng et al., 2005). This LRP6 phospho-site is critical for further sequestration and inhibition of GSK3(Piao et al., 2008). Following overexpression of non-tagged LRP6 in 293T cells, Sp1490-LRP6 was detected in cilia (Figure 3.3J). A 30 min Wnt3a treatment led to a further increase in Sp1490-LRP6 cilia staining (Figure 3.3J).

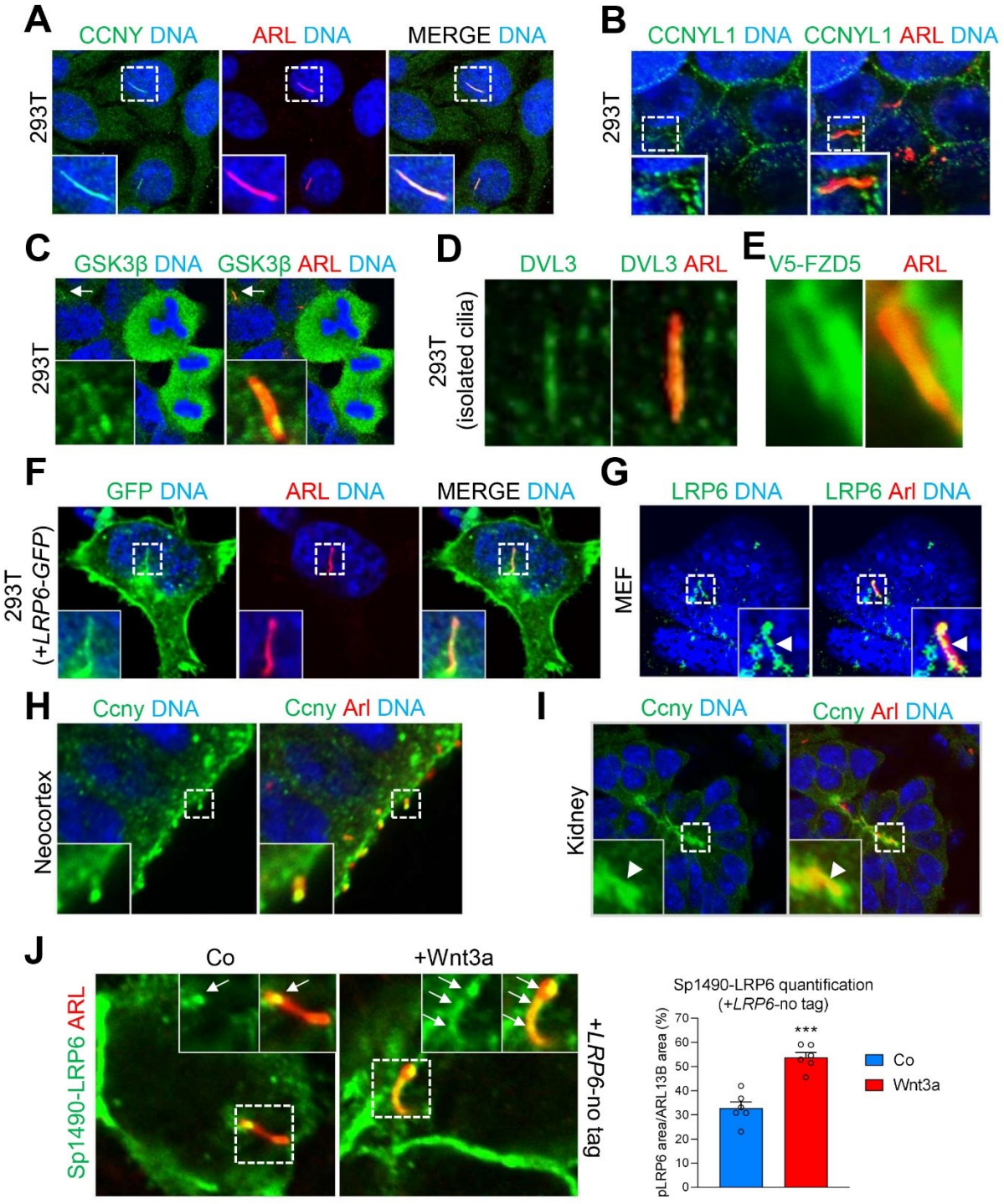
A
CCNY DNA
ARL DNA
MERGE DNA
293T
B
CCNYL1 DNA
CCNYL1 ARL DNA
293T
C
GSK3β DNA
GSK3β ARL DNA
293T
D
DVL3
DVL3 ARL
293T
(isolated cilia)
E
V5-FZD5
ARL
F
GFP DNA
ARL DNA
MERGE DNA
293T
(+LRP6-GFP)
G
LRP6 DNA
LRP6 Arl DNA
MEF
H
Ccny DNA
Ccny Arl DNA
Neocortex
I
Ccny DNA
Ccny Arl DNA
Kidney
J
Co
+Wnt3a
Sp1490-LRP6 ARL
+LRP6-no tag
Sp1490-LRP6 quantification
(+LRP6-no tag)
pLRP6 area/ARL13B area (%)
70
60
50
40
30
20
10
0
***
Co
Wnt3a

Figure 3.3 WNT signaling components localize to primary cilia and cilia are WNT-responsive organelle.

A) Co-IF for CCNY and ARL13B in 293T cells.
B) CCNYL1 and ARL13B co-IF in 293T cells.
C) Co-IF for GSK3β and ARL13B in 293T cells.
D) Co-IF for DVL3 and ARL13B in isolated cilia from 293T cells.
E) Co-IF for V5 tag and ARL13B in 293T cells transfected with V5-FZD5 plasmid.
F) Co-IF for GFP and ARL13B in 293T cells transfected with EGFP-LRP6 plasmid.
G) Co-IF for LRP6 and ARL13B in MEF cells.
H) Co-IF for CCNY and ARL13B in embryonic neocortex.
I) Co-IF for CCNY and ARL13B in embryonic kidney.
J) Images and quantification of p-LRP6 level in primary cilia in 293T cells transfected with LRP6 plasmid upon Wnt3a conditioned medium treatment for 30 min. Cells were serum starved for 48 hours. Figure A-D and H-J are provided by Dr.*Fabio da Silva.*

6.2.4 A WNT ⊣ PP1 signaling axis promotes ciliogenesis in HEK293T cells

A possible molecular target regulating ciliogenesis downstream of WNT/GSK3 is serine/threonine protein phosphatase 1 (PP1). PP1 is a well-established regulator of flagellar motility in *Paramecium*, *Chlamydomonas*, and mammalian sperm(Habermacher and Sale, 1996; Klumpp et al., 1990) (Vijayaraghavan et al., 1996; Yang et al., 2004). Mechanistically, PP1 regulates the phosphorylation and function of the intraflagellar transport motor KIF3B in *Chlamydomonas*(Liang et al., 2018). PP1 also binds to the ciliary ion channel polycystin-1 (PC1) and shortens the length of primary cilia in mammalian cells(Luo et al., 2019). PP1 is regulated by a large family of regulatory subunits, some of which are inhibitory and maintain the enzyme in an inactive state(Casamayor and Arino, 2020). Among the inhibitory subunits, PPP1R2 is inactivated by GSK3-dependent phosphorylation at Thr72 (Tp72). GSK3 can thereby

activate PP1(Cohen and Cohen, 1989). We previously showed that during mouse sperm maturation, WNT signaling inhibits PP1 via the GSK3β ⊣ PPP1R ⊣ PP1 axis, leading to a global increase in protein phosphorylation, and the unlocking of flagellar motility(Koch et al., 2015). Given the similarity between flagella and cilia, we hypothesized that WNT/GSK3 signaling may connect to ciliogenesis via PPP1R2-PP1 (Figure 3.4A).

To test this hypothesis, we serum-starved CCNY/L1 and LRP5/6 DKO 293T cells and performed IF with an antibody against the GSK3-specific Tp72 phosphorylation site of PPP1R2. Tp72-PPP1R2 localized to cilia, and both the number and the intensity of Tp72-PPP1R2^{+} cells was significantly increased in DKO cells (Figure 3.4B-C). This increase was not due to more PPP1R2 protein in cilia since IF for total PPP1R2 revealed similar staining frequency in DKO and control cilia (Figure 3.6G). Immunoblot analysis of cell lysates confirmed increased Tp72-PPP1R2 levels in CCNY/L1 and LRP5/6 DKO cells, indicating WNT-receptor engagement in regulation of PPP1R2 phosphorylation (Figure 3.4D). Moreover, BIO treatment drastically reduced PPP1R2 phosphorylation by immunoblot, confirming PPP1R2 as a GSK3 substrate in ciliated 293T cells (Figure 3.4E).

Our model predict that ciliogenic WNT signaling functions to repress PP1 activity and that the ciliogenesis defects in CCNY/L1 DKO cells are due to elevated PP1 activity. To corroborate this model, we carried out rescue experiments in CCNY/L1 DKO cells using the general phosphatase inhibitors Okadaic acid (OA) and Calyculin A (CalyA) (Figure). OA and CalyA treatment led to respective 4.6 and 2.6 fold inductions in cilia number in DKO cells (Figure 3.4F-I). To confirm a functional role for PPP1R2 in cilia formation in 293T cells, we performed siRNA knockdown of PPP1R2, which strongly decreased cilia number and length (Figure 3.4J-L). Taken together, these results support a WNT⊣ PP1 axis in promoting ciliogenesis in HEK293T cells.

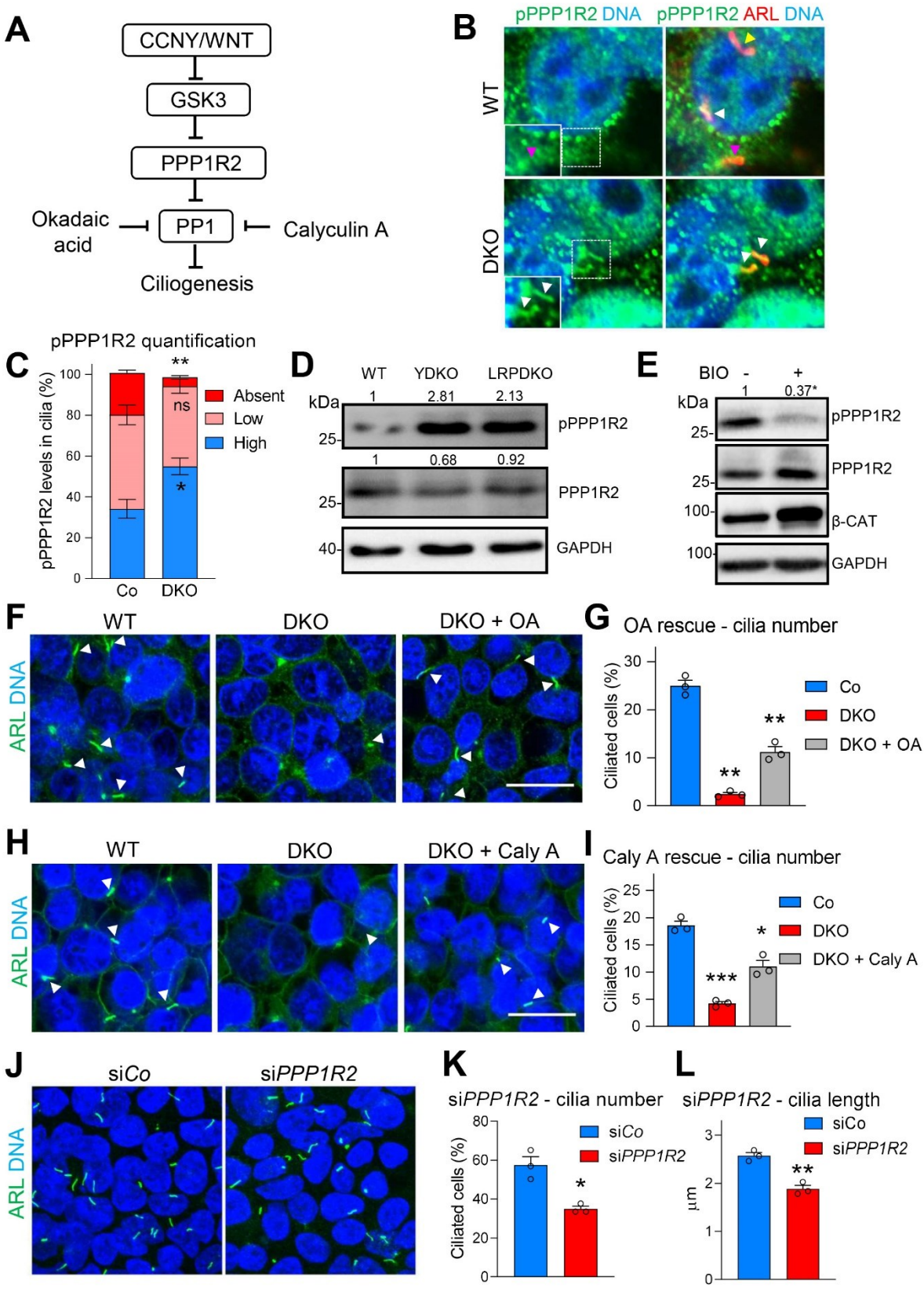
A
CCNY/WNT
GSK3
PPP1R2
Okadaic acid
PP1
Calyculin A
Ciliogenesis
B
pPPP1R2 DNA
pPPP1R2 ARL DNA
WT
DKO
C
pPPP1R2 quantification
pPPP1R2 levels in cilia (%)
Absent
Low
High
ns
Co
DKO
D
WT
YDKO
LRPDKO
kDa
pPPP1R2
PPP1R2
GAPDH
E
BIO
0.37*
β-CAT
F
WT
DKO
DKO + OA
ARL DNA
G
OA rescue - cilia number
Ciliated cells (%)
Co
DKO
DKO + OA
H
DKO + Caly A
I
Caly A rescue - cilia number
DKO + Caly A
J
siCo
siPPP1R2
K
siPPP1R2 - cilia number
L
siPPP1R2 - cilia length
µm

Figure 3.4 A WNT ⊣ PP1 signaling axis promotes ciliogenesis in HEK293T cells.

A) Schematic demonstrating the role of post-transcriptional WNT signalling in Protein phosphatase 1 Regulatory Inhibitor Subunit 2 (PPP1R2) regulation and primary cilia formation. CCNY/WNT reduces GSK3-mediated PPP1R2 phosphorylation, which leads to Protein phosphatase 1 (PP1) inhibition and increased microtubule acetylation/ciliogenesis. Treatment with Okadaic acid (OA) and Calyculin A (Caly A) inhibits PP1 activity and rescues the effects of GSK3-mediated PPP1R2 inhibition.
B-C) Co-IF for Phospho-PPP1R2 (T72) (pPPP1R2) and ARL13B in WT and Y/YL1 DKO cells. Percentage of cilia with high (white arrowhead), low (purple arrowhead) or absent (yellow arrowhead) pPPP1R2 staining quantified for WT and DKO cells. Columns are means ± SEM (Experiment performed twice in duplicates, all samples quantified). Scale bar 2.5 µm.
D) Western blots for p-PPP1R2 and total PPP1R2 in CCNY/L1 and LRP5/6 DKO cells.
E) Western for for p-PPP1R2 and total PPP1R2 in 293T cells upon 1 hour BIO treatment
F-G) ARL13B immunostaining on WT and DKO cells treated with 0.1 µM OA for 4 hours prior to serum starvation and quantification of cilia number. Cilia number in DKO cells compared to WT and OA treatment to DKO cells. Columns are means ± SEM (experiment performed three times in triplicates, representative experiment shown). Scale bar 10 µm.
H-I) ARL13B immunostaining on WT and DKO cells treated with 0.5 nM Caly A for 24 hours and quantification of cilia number. Cilia number in DKO cells compared to wildtype and Caly A treatment to DKO cells. Columns are means ± SEM (experiment performed 3 times in triplicates, representative experiment shown). Scale bar 10 µm.
J-L) ARL13B immunostaining on siCon and siPPP1R2 cells with the quantification of the cilia number and cilia length. Panels **B-C** are provided by Dr *Fabio da Silva.*

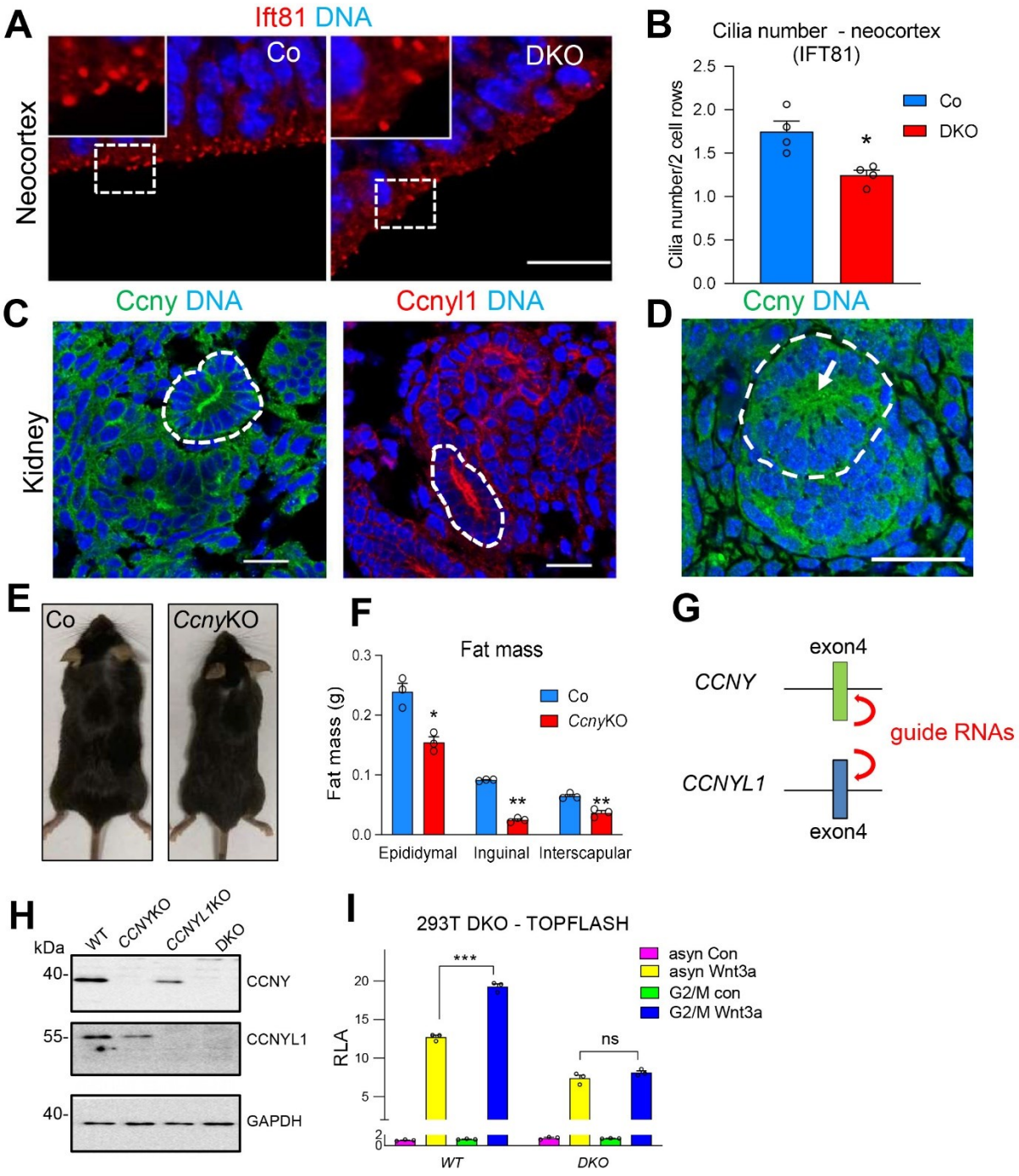
A
Ift81 DNA
Co
DKO
Neocortex
B
Cilia number - neocortex
(IFT81)
Cilia number/2 cell rows
Co
DKO
C
Ccny DNA
Ccnyl1 DNA
Kidney
D
Ccny DNA
E
Co
CcnyKO
F
Fat mass
Fat mass (g)
Co
CcnyKO
Epididymal
Inguinal
Interscapular
G
exon4
CCNY
guide RNAs
CCNYL1
exon4
H
kDa
WT
CCNYKO
CCNYL1KO
DKO
40-
CCNY
55-
CCNYL1
40-
GAPDH
I
293T DKO - TOPFLASH
RLA
asyn Con
asyn Wnt3a
G2/M con
G2/M Wnt3a
***
ns
WT
DKO

Figure 3.5 WNT/STOP signaling is required for ciliogenesis and adipogenesis.

A-B) Quantification of cilia number in DKO forebrains by IF against the ciliary axoneme protein IFT81 (Intraflagellar Transport protein 81). Columns are means ± SEM (n=4 embryos, 3 litters). Scale bar 10 μm. Unpaired two-tailed t-test for statistical anaylsis: * $p < 0.05$.
C-D) CCNY and CCNYL1 localize to developing glomeruli (white dotted lines) in E13.5 kidneys. Scale bar 20 μm.
E-F) Images of Con and Ccny KO 16-weeks-old adult and the weight measurments of each part of fat tissue from Con and Ccny KO mice. Columns are means ± SEM (n=4 mice). Unpaired two-tailed t-test for statistical anaylsis.
G) Schematic demonstrating the strategy used to generate CCNY and CCNYL1 individual knockout and CCNY/CCNYL1 double knockout (DKO) 293T cells using CRISPR/Cas9 technology. For both genes, guide RNAs targeting exon 4 were used to generate insertion/deletion mutants.
H) Immunoblot with CCNY and CCNYL1-specific antibodies demonstrating the absence of CCNY/YL1 in individual and DKO cell lines.
I) β-catenin reporter (SuperTOPFLASH) assay of individual KO and DKO cells treated with 100 ng/ml nocodazole to arrest cells in G2/M and Wnt3a-conditioned media to activate canonical WNT signalling. Both treatments performed foe 16 hours. Data are represented as relative luciferase activity (RLA) fold change vs controls and columns are means ± SEM (n=3). Panels **A-D** are provided by Dr. *Fabio da Silva.*

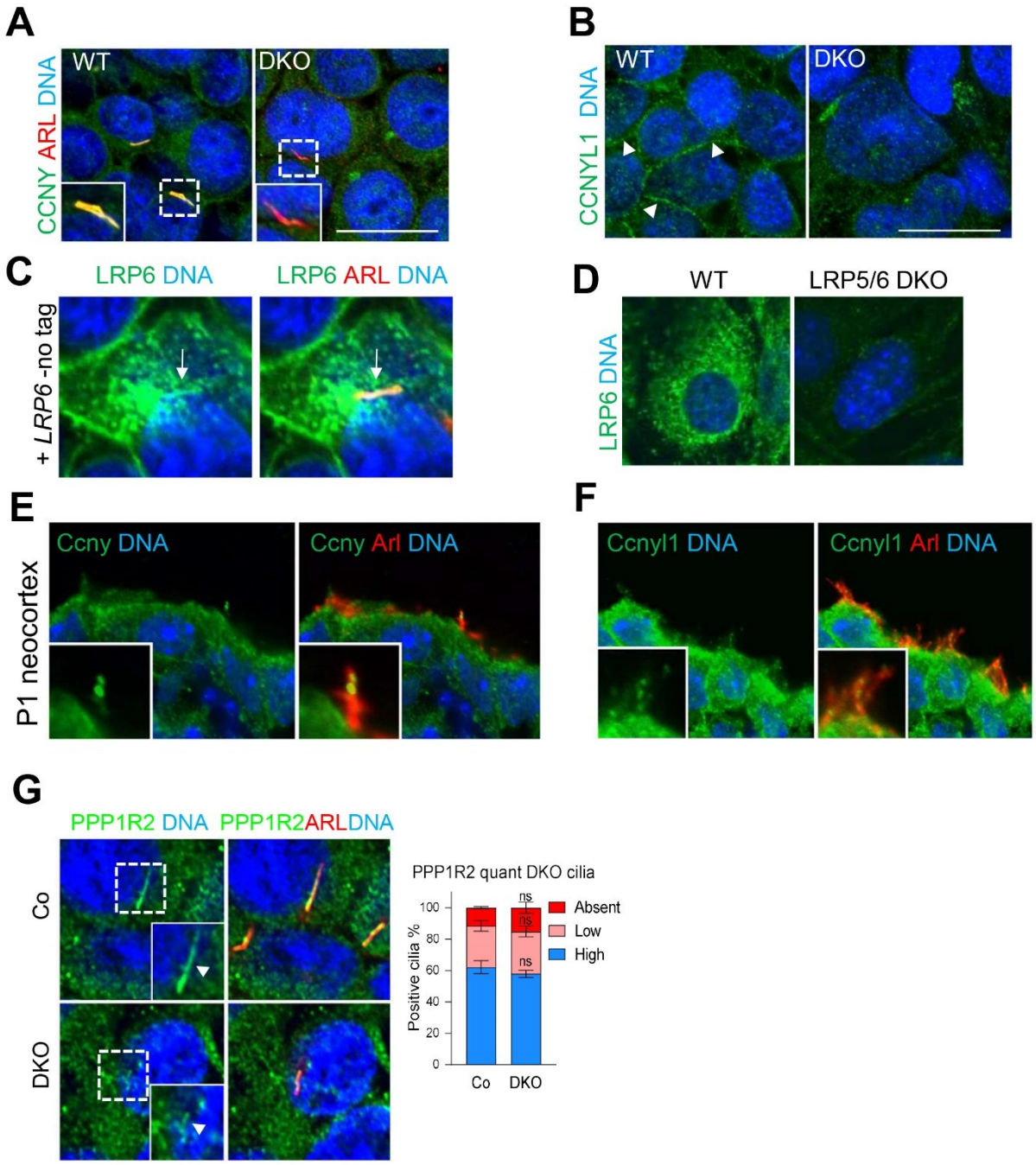

Figure 3.6 A WNT ┤ PP1 signaling axis promotes ciliogenesis in HEK293T cells.

A-B) Validation of CCNY localization to primary cilia by co-IF for CCNY and ARL13B. No CCNY staining is detected in the cilia of Y/YL1DKO (DKO) 293T cells. Scale bar 10 μm.

C) IF with LRP6 antibody in 293T cells transfected with non-tagged LRP6. Scale bar 5 μm.

D) Validation of LRP6 IF in WT and LRP5/6 DKO MEF cells. Staining is absent in DKO cells..

E-F) Co-IF for CCNY and AcTUB in motile cilia of the postnatal neocortex. CCNY detected as distinct punctae in cilia. Scale bar 5 μm.

G) Co-IF and quantification for PPP1R2 and ARL13B on serum starved 293T cells. PPP1R2 levels classified as high, low or absent based on pixel intensity. Columns are means ± SEM (n=3). Panel **C-G** are provided by Dr. *Fabio da Silva.*

6.3 Discussion

Despite a large body of work relating WNT signalling and cilia, key questions have remained elusive: Are cilia WNT signalling organelles? If so, what may be the role of such intra-ciliary WNT signalling? and, Is there is a physiological connection *in vivo*? To answer these questions, we took advantage of the specificity of CCNY/L1 for β-catenin-independent WNT/GSK3 signalling to explore the pathway's function in cilia. By characterizing CCNY/L1 deficiency both *in vitro* and *in vivo*, including mouse embryos, adult mice, and human cell lines. we uncover a WNT ┤ PP1 signalling axis in cilia, wherein deficiency of WNT/GSK3 axis phenocopies well-known ciliopathies. We also discover that cilia are WNT signalling organelles. Collectively, the results indicate an evolutionary conserved WNT ┤ PP1 signalling axis as a common regulator of ciliogenesis in primary cilia.

6.3.1 A WNT ┤ PP1 axis promotes ciliogenesis

The most important finding of this study is the discovery of a WNT ┤ PP1 signalling axis as the underlying mechanism whereby WNT promotes primary ciliogenesis. Yet, not all ciliated cells, such as RPE1 and HEK293 cells, require WNT signalling for ciliogenesis(Bernatik et al., 2021). These observations suggest that WNT signalling is not universally required for ciliogenesis, and they also indicate cell type specificity of unknown origin. Even in cells that do engage ciliary WNT/GSK3 signalling, the requirement is not absolute since in e.g. *LRP5/6DKO* 293T cells ciliogenesis was reduced but not abolished. Altogether, these data indicate a modulatory role of ciliary WNT/GSK3 signalling.

At the heart of the ciliogenic WNT cascade is GSK3 inhibition. Consistent with this effect, this ubiquitous kinase localizes to cilia and is a well-known negative regulator of ciliogenesis that is evolutionary conserved: In *Chlamydomonas*, zebrafish embryos, and mammalian cells, GSK3 inhibition results in cilium elongation(Nakakura et al., 2015; Ou et al., 2012; Wilson and Lefebvre, 2004). Yet, GSK3β can also promote ciliogenesis e.g. by regulating the ciliary effectors Dzip1 and pVHL(Thoma et al., 2007; Zhang et al., 2015). The difference may be due to context- or dose dependence since e.g. in *Chlamydomonas* pharmacological inhibition of GSK3 for one hour induces long

cilia while longer treatment induces an aflagellate phenotype(Wilson and Lefebvre, 2004). It is thought that GSK3 can reside in different pools(Thoma et al., 2007), possibly biomolecular condensates(Schaefer and Peifer, 2019), which may also have distinct roles during ciliogenesis. Moreover, GSK3β activity can also be inhibited by Insulin and Insulin-like growth factor signalling, both of which can trigger IGFR/AKT signalling in cilia(Christensen et al., 2017). This suggests that the ciliary GSK3 ┤ PPP1R ┤ PP1 axis may also be regulated by other growth factors.

We identify the PP1 inhibitor PPP1R2 as a key target of the WNT/GSK3 module in primary cilia. PPP1R2 is concentrated in cilia and PPP1R2 is a known effector of primary cilium- and flagellum morphogenesis upstream of PP1(Cohen and Cohen, 1989; Wang and Brautigan, 2008). Mechanistically, PP1 binds polycystin-1 (PC1) and shortens the length of primary cilia in mammalian cells(Luo et al., 2019). Furthermore, PP1 regulates the intraflagellar transport (IFT) system via phosphorylation of the kinesin motor protein FLA8/KIF3B in *Chlamydomonas*(Liang et al., 2018). Since WNT signalling induces a dramatic increase in serine phosphorylation in motile cilia and flagella(Koch et al., 2015), there likely exist many other ciliary PP1 targets besides PC1 and FLA8/KIF3B. Moreover, there will likely be additional GSK3 targets besides PPP1R2/PP1 that are regulated by WNT signalling in the cilium. For example, in mouse spermatozoa, GSK3-mediated phosphorylation of septin4 is WNT-inhibited to establish a membrane barrier at the flagellar annulus(Koch et al., 2015) and septins also function in the biogenesis of primary cilia(Palander et al., 2017).

6.3.2 The WNT ┤ PP1 axis and ciliopathy models

The second important finding of this study is that interfering with ciliary WNT signalling recapitulates primary ciliopathies: Ccny/l1 deficiency causes exencephaly (this study), lipodystrophy (this study), as well as male infertility in mice(Koch et al., 2015). Reduced LRP6 phosphorylation, as well as results from the inhibition of LRP6, corroborate that these ciliary defects are due to impaired WNT signalling. Amelioration of the ciliary defects by inhibition of GSK3 and PP1 but not β-catenin support the involvement of WNT/GSK3 rather than WNT/β-catenin signalling. On the other hand, transcriptional

WNT/β-catenin signalling as well as WNT/PCP (planar cell polarity) signalling are also prominent regulators of ciliogenesis in multiple other systems,(Corkins et al., 2019) so we cannot fully exclude these pathways from our DKO cilia phenotypes.

If ciliary WNT signalling plays a widespread role, then *LRP5/6* deficiency should recapitulate ciliopathies *in vivo*. Consistently, exencephaly and cystic kidneys are seen in *Lrp6* null mutant mice(Pinson et al., 2000) and *Lrp6* heterozygosity exacerbates pathology in a cystic kidney mouse model(Lancaster et al., 2009). LRP6 variants are associated with *spina bifida* in patients(Allache et al., 2014; Lei et al., 2015; Shi et al., 2018) and LRP5 variants may contribute to autosomal dominant polycystic kidney disease(Cnossen et al., 2016). In addition, mice mutant for the LRP6 kinase *Cdk16* show male infertility with sperm flagellar defects(Mikolcevic et al., 2012). Thus, we expect that the discovery of ciliary WNT ⊣ PP1 signalling will aid in the understanding of the etiology of ciliopathies in the future.

6.4 Working model

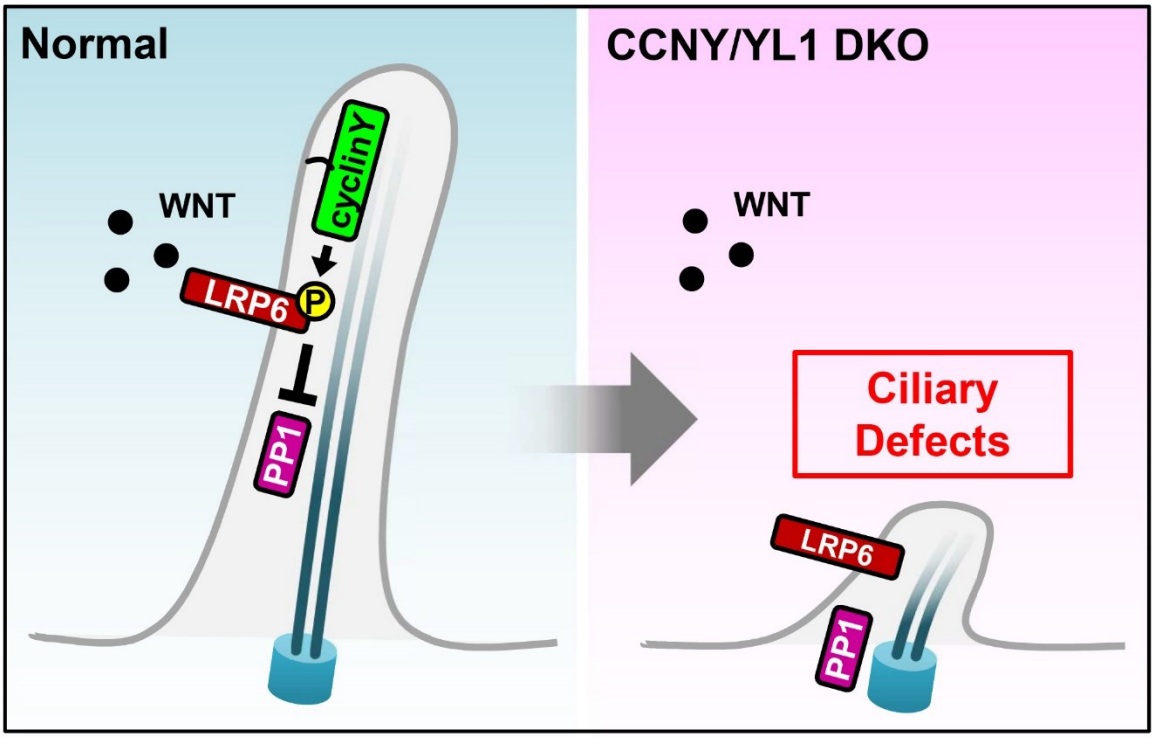

Figure 3.7 A WNT ┤ PP1 signaling axis promotes ciliogenesis.

Schematic description of WNT ┤ PP1 signaling axis regulation of ciliogenesis. In normal ciliated cells, WNT/GSK3 components CCNY and LRP6 are locating in cilia and responding to WNT stimulation. However, CCNY/L1 DKO cells display ciliogenesis defects via disrupted WNT┤ PP1 signaling axis.

7. CONCLUSION AND OUTLOOK

In this PhD thesis, the physiological relevance of WNT/STOP signaling has been extended and two new *in vivo* roles for the pathway were discovered. First, mitotic WNT governs embryonic neurogenesis via two neurogenic transcription factors, Sox4 and Sox11, specifically during mitosis(Da Silva et al., 2021). In addition, WNT/GSK3 signaling regulates primary cilia formation via a WNT-PP1 axis in a post-transcriptional manner.

The WNT & neurogenesis sheds new light on the function of post-transcriptional WNT signalling in the neuroscience field. GSK3 phosphorylates numerous target proteins, including, possibly, certain proteins responsible for neural disease. Of note, tau, a Parkinson's disease (AD) related protein, was found to be hyperphosphorylated in AD patients. Moreover, the enzymatic activity of GSK3 was also found to be hyperactivated in AD patients, suggesting tau may be regulated by GSK3 in this context(Toral-Rios et al., 2020). More interestingly, Lrp6 loss of function exacerbates amyloid pathology in an AD mouse model(Liu et al., 2014) further suggesting a potential connection between WNT/STOP, tau, and AD. Finally, the WNT/STOP regulators Ccny and co-receptor Lrp6 are localized at the axon of neurons and are required for synaptic integrity, suggesting another possible function of WNT/STOP in synaptic plasticity and cognition(Cho et al., 2015; Liu et al., 2014)

In regards to the WNT & cilia, we discovered a new WNT/GSK3/ PP1 axis that regulates ciliogenesis. Specifically, this axis promotes cilia formation via regulating the phosphorylation rather than protein levels of PPP1R2, a well-known GSK3 target. Hence, while this axis represents a non-transcriptional GSK3 dependent WNT signaling, it does not classify as WNT/STOP (stabilization of proteins) in the narrow sense. Indeed, not every GSK3-phosphorylated protein is destined for proteasomal degradation. Rather, GSK3 phosphorylation can also change the subcellular localization and/or translocation of proteins, both of which can alter their biological functions(Dusi et al., 1993). Therefore, it is bold but reasonable to suggest that, for future investigations, it would be valuable to explore the effects of WNT/STOP on the subcellular translocation of target proteins(Lidke et al., 2010).

We initially struggled to find novel *in vivo* roles of WNT/STOP due to the interference from transcriptional WNT signaling activity in nearly all organs analyzed. However, it is reported that some specific biological events display no transcriptional WNT activity (i.e. no changes in target gene expression), despite WNT reporter activity. For example, mouse intestinal stem cells have been reported to show no β-Catenin-regulated metabolic gene transcription due to restricted chromatin accessibility. In this context, it is therefore worthwhile to investigate WNT/STOP signaling, which functions post-transcriptionally(Sun et al., 2021; Sun et al., 2020). Furthermore, it will be interesting to find additional biological situations in which there is no or low transcriptional WNT activity due to epigenetic modifications, as these could serve as new model systems to study WNT/STOP signaling *in vivo*.

8. MATERIALS AND METHODS

8.1 Equipments and reagents

8.1.1 Equipments

Instruments	Company
Agarose gel chambers	Biozym
Balances	Sartorius, Kern
Trans-Blot SD Semi-Dry Transfer cell	Biorad
Centrifuges	Heraeus
Chromatography Columns	BioRad
Electroporator	BioRad
Fluorescent microscope	Nikon
Incubators	Labotect, Heraeus
Inverted contrasting microscope DM IL	Leica
Laminar flow hoods	Lobotect
LAS-3000 Imaging System	Fujifilm
Luminometer	Luminoscan Ascent, Labsystems
Magnetic stirrer	CAT
Microcentrifuges	Heraeus
Microfluidizer	
Microwave oven	Sharp
Multi-channel pipettes	Transferpette
Nanodrop 2000 Spectrophotometer	Thermo Fisher
PAGE minigel chambers	Biorad
PCR thermocyclers	MJ Research
pH meter	Sartorius
Pipetboy	Integra Bioscience
Pipette (P2, P10, P100, P200, P1000)	Gilson, Eppendorf
Power supplies	Biorad
Refrigerator	Liebherr,
Rotators	CAT, Kisker
Scintillation counter Packard Tri-Carb 2100 TR	Perkin Elmer

Shakers	Thermo, EB
Spectrophotometer	WPA
Thermoshaker	Eppendorf
Uptrapure water purification system	Sartorius
Vortexer	Scientific industries
Electrode (3mm)	BTX genetronics Inc.
Waterbaths	Julabo, GFL

8.1.2 Chemicals

Chemical	Company	Chemical	Company
Acrylamide	Carl Roth	LB agar	Fluka
Agarose	Biozym	methanol	Sigma-Aldrich
Ampicillin	Sigma-Aldrich	$MgCl_2$	Merk
APS	Serva	$MgSO_4$	Merk
Bacto-Tryptone	Sigma-Aldrich	MG132	Sigma
Bacto Yeast Extract	Carl Roth	NaOH	Fluka
Bromophenol blue	Serva	NaCl	Sigma-Aldrich
BSA grade V	Roche	NaF	Sigma-Aldrich
Chloroform	Carl Roth	NaOAc	Merk
Complete EDTA-free protease inhibitor cocktail	Roche	Non-fat dry milk	Serva
β-mercaptoethanol	Sigma-Aldrich	Nonidet NP-40	Sigma-Aldrich
DMSO	Sigma-Aldrich	H_3PO_4	Sigma-Aldrich
dNTPs	Thermo Fisher	PBS	Lonza
DTT	Sigma-Aldrich	Pyrophosphate	Sigma-Aldrich
EDTA	Gerbu	PMSF	Sigma-Aldrich
EGTA	Sigma-Aldrich	RNAse DNAse-free H2O	Qiagen
Ethanol	Sigma-Aldrich	Sodium citrate	Santa cruz
Ethidium bromide	Carl Roth	Sodium orthovanadate	Sigma-Aldrich
Fast green	Sigma-Aldrich	Sodium deoxycholate	Sigma-Aldrich
Glucose	Merk	SDS	Sigma-Aldrich

Glycerol	Carl Roth
Glycine	Gerbu
HCl	Sigma-Aldrich
HEPES	Gerbu
Isoflurane	Baxter
Isopropanol	Sigma-Aldrich
KCl	Sigma-Aldrich

TEMED	Serva
TCA	Sigma-Aldrich
Triton X-100	Gerbu
Tris Base	Sigma-Aldrich
Trypan blue	VWR
Tween-20	Gerbu

8.1.3 Enzymes, reagents and kits

Chemical	Company
Clarity Western ECL substrate	Bio-Rad
DNase I	Qiagen
DNA orange loading dye 6x	Thermo
Dual-Luciferase reporter assay system	Promega
Dye reagent concentrate	Bio-Rad
Gene Ruler DNA ladder 1kb and 100bp	Thermo
Light cycler 480 probe master	Roche
Nucleaospin gel and pcr clean-up	Macherey-Nagel

Chemical	Company
QIAquick PCR purification Kit	Qiagen
Riboblock RNase inhibitor	Thermo
RiboRuler High/low range RNA ladder	Thermo
RNA loading dye2x	Thermo
RNase A	Thermo
RNase-free DNase set	Qiagen
SuperScript II reverse transcriptase	Invitrogen
Supersignal West Pico plus chemiluminescent substrate	Thermo

8.1.4 Cell culture reagents and cell lines

Cell culture	Company
DMEM	Gibco
DMEM/F12	Invitrogen
FBS	Capricorn
L-glutamine	Sigma-Aldrich
B27	LIFE
Hepes	Sigma
Progesterone	Sigma
Putrescine	Sigma
Heparin	Sigma
Insulin-transferrin-sodium selenite supplements	Roche
Sodium bicarbonate	Sigma
EGF	Sigma
Opti-MEM® I reduced serum medium	Gibco
Penicillin/Streptomycin (Pen/Strep)	Lonza
Accutase	Capricorn
Trypsin-EDTA solution	Gibco
XtremeGENE 9 DNA transfection reagent	Roche
Poly-D-lysine	Sigma
Poly-L-lysine	Sigma

8.1.5 Antibodies

Antibodies	Manufacturer	Identifier
Mouse monoclonal anti -active β-catenin	Millipore	Cat#05-665
Mouse monoclonal anti-β-catenin	BD Bioscience	Cat#610154
Mouse monoclonal anti-BrdU	BD Bioscience	Cat#555627
Rabbit polyclonal anti-active caspase 3	R&D	Cat#AF835
Rabbit polyclonal anti-CCNY	Homemade	Davidson et al., 2009-
Rabbit polyclonal anti-CCNYL1	Homemade	Koch et al., 2015
Guinea pig polyclonal anti-SOX4	Homemade	Hoser et al., 2008
Guinea pig polyclonal anti-SOX4	Homemade	Hoser et al., 2008
Rabbit polyclonal anti-SOX4	Diagenode	Cat#C15310129
Rat monoclonal anti-CTIP2	Abcam	Cat#Ab18465
Rabbit polyclonal anti-CDK14	Abnova	Cat#PAB2949
Mouse monoclonal anti-FLAG M2	Sigma Aldrich	Cat#F3165
Goat polyclonal anti-GFP	genomics	Cat#ABIN100085
Rat monoclonal anti-TBR2	Invitrogen	Cat#14-4875-80
Rabbit polyclonal anti-TBR2	Abcam	Cat# ab23345
Mouse monoclonal anti-GSK3β	BD bioscience	Cat#610201
Mouse monoclonal anti-tubulin	Sigma Aldrich	Cat#T5168
Rat monoclonal anti-Ki67	ebioscience	Cat#14-5698-82
Rat monoclonal anti-IdU	Abcam	Cat#ab187742
Rabbit monoclonal anti-LRP6	CST	Cat#2560S

Rabbit polyclonal anti-Phospho-LRP6 (S1490)	CST	Cat#2568S
Rabbit polyclonal anti-Phospho-LRP6 (T1479)	Homemad	Davidson et al., 2005
Rabbit polyclonal anti-PAX6	Biolegend	Cat#901301
Mouse monoclonal anti-nestin	EMD Millipore	Cat#MAB353
Mouse monoclonal anti-pan-cadherin	Santa Cruz	Cat#sc-59876
Mouse monoclonal anti-phospho-Histone H3	CST	Cat#9706S
Rat monoclonal anti-HA	Roche	Cat# ROAHAHA
Goat anti-mouse IgG (H+L) HRP	Jackson ImmunoResearch	Cat#115-035-146
Goat anti-rabbit igG (H+L) HRP	Jackson ImmunoResearch	Cat#111-035-144
Goat anti-Guinea pig (H+L) HRP	Jackson ImmunoResearch	Cat#106-035-003
Goat anti-Rat IgG Light chain specific HRP	Jackson ImmunoResearch	Cat#112-035-175
Donkey polyclonal Anti-Mouse IgG CTMy3	Jackson ImmunoResearch	Cat#715-165-150
Donkey polyclonal Anti-Mouse IgG, Alexa Fluor 647	Jackson ImmunoResearch	Cat#715-605-151
Donkey polyclonal Anti-Mouse IgG, Alexa Fluor 488	Jackson ImmunoResearch	Cat#715-545-150
Donkey polyclonal Anti-Rabbit IgG CTMy3	Jackson ImmunoResearch	Cat#711-165-152
Donkey polyclonal Anti-Rabbit IgG, Alexa Fluor 647	Jackson ImmunoResearch	Cat#711-605-152
Goat polyclonal Anti-Rabbit IgG, Alexa Fluor 488	Invitrogen	Cat#A11008
Goat polyclonal Anti-Guinea Pig IgG, Alexa Fluor 546	Invitrogen	Cat#A11074
Donkey polyclonal Anti-Rat IgG, Alexa Fluor 647	Jackson ImmunoResearch	Cat#712-605-153
Rabbit polyclonal Anti-ARL13B	Proteintech	Cat#17711-1-AP
Mouse monoclonal Anti-ARL13B	NeuroMab	Cat#N295B/66
Rabbit polyclonal Anti-PPP1R2	Sigma	Cat#SAB4502285

Rabbit polyclonal Anti-Protein phosphatase 1 inhibitor subunit 2 (phosphor T72)	Abcam	Cat#ab27850
Rabbit polyclonal Anti-IFT81	Proteintech	Cat#117441-1-AP

8.1.6 Plasmids

General plasmids including TopFlash, Renilla, pCS2+ are described previously(Cruciat et al., 2010).Plasmids encoding shCon, shCcny and shCcnyl1 are mentioned previsouly(Zeng et al., 2016).For the electroporation plasmids, shCon, shCcny and shCcnyl1 sequences were cloned into pSuper plasmid. For Sox4/11 cloning and mutagenesis, full length cDNA sequences of Sox4/11 are cloned into pCS2+ plasmid BamHI and XhoI sites together with N-terminal Flag tag sequence. Mutagenesis of the Sox4/11 GSK3 phospho-motifs was performed by amplifying full length Flag-tagged plasmids with primers designed to mutate selected serines into alanines.

8.1.7 Buffers and solutions

10X Lämmli Running buffer: 250 mM Tris-base pH, 1,92 M glycine, 1% SDS, in 1 L ddH_2O, pH 8.3

10X TBE for Agarose gel-electrophoresis: 275 g Boric Acid, 200 mL of 0.5 M EDTA, 540 g Tris Base, up to a total of 5 L with ddH_2O, pH adjusted to 8.0

10X TBE for SDS-PAGE transfer: 55 g Boric Acid, 40 mL of 0.5 M EDTA, 108 g Tris Base, up to a total of 1 L with ddH_2O, pH adjusted to 8.3

10X TBS-T: 200 mM Tris-base pH 8.0, 1,5 M NaCl, Tween-20, (0,5 % w/v)

Blocking Buffer for Western Blot: 5% milk powder or BSA prepared in TBST with 0.2% Tween 20

Lämmli loading buffer (4x): 200 mM Tris-HCl, pH 6.8, 20% β-Mercaptoethanol, 8% SDS, 0.4% bromophenol blue, 40% glycerol

SDS-PAGE Solution B: 0.4% SDS, 1.5 M Tris in ddH2O, pH 8.8.

***SDS-PAGE Solution C*:** 0.4% SDS, 0.5 M Tris in dd H_2O, pH 6.8.

Tirton lysis buffer: 20mM Tris-HCl (pH7.4), 150mM NaCl, 1% Triton, 1mM EDTA, 1mM EGTA, 1mM b-Glycerophosphate, 2.5mM sodium pyrophosphate. 1xComplete EDTA-free protease inhibitor cocktail and 10mM Na_3VO_4 were added freshly.

RIPA lysis buffer: 20mM Tris-HCl, 120mM NaCl, 5mM EDTA, 1% Triton X-100, 0.25% Na-deoxycholate. 0.05% SDS, 1x proteinase inhibitor, 1mM β-glycerophosphate, 2.5mM Na-pyophosphate, 2mM Na_3VO_4

Blocking buffer for IF: 5% donkey serum, 0.05 Triton X-100 in PBS

10xAntigen retrieval buffer (Cryo-section): 10mM soudium citrate, 0.05% Tween 20, pH6.0 in ddH_2O

10xAntigen retrieval buffer (Paraffin-section):

***Cyto-skeletal buffer*:** 100mM NaCl, 300mM sucrose, 3mM $MgCl_2$, 10mM PIPES, pH6.9 in ddH_2O

DEPC-H_2O: DEPC/ddH_2O, mixed for 12h at room temperature and autoclaved

dNTP mix (5mM): 5mM dATP, dCTP, dGTP, dUTP in ddH_2O.

Phosphate-buffered saline(PBS 10x): 1.37M NaCl, 27M KCl, 18mM KH_2PO_4, 100mM Na_2HPO_4 in ddH_2O, pH7.4, autoclaved.

8.2 Molecular biology

General molecular biology method like competent cells preparation, DNA transformation into the bacteria, DNA amplification and quantification, PCR amplification and restriction enzyme digestion were basically performed as described(Green et al., 2012). Isolation of DNA from bacterial, gel purification and RNA isolation were performed with Qiagen or Macherey-Nagel Kits.

8.2.1 RNA isolation and cDNA synthesis

RNA from mouse tissue or cultured cells was isolated with the RNeasy mini kit (Qiagen) or RNA isolation kit (Macherey-Nagel) following the manufactorer's instruction. cDNA was synthesized from total RNA using Superscript II or homemade reverse transcriptase. For reverse transcription, up to 1µg of total RNA was mixed with 1 µl of the random primer (0.5 µg/µl) and 2 µl dNTP(5nM) in a total volume of 12µl. Samples were heated at 65 degree for 5 mins and then cooled down to 4 degree, followed by addition of 4 µl of 5x First-strand buffer, 2µl of DTT(0.1M), and 1µl of RNase inhibitor. After incubation at 25 degree for 10mins, 1µl of Superscript II enzyme was applied. The reaction was performed at 42 degree for 90 mins and stopped by heat-inactivation at 70 degree for 15 mins. The synthesized cDNA was then diluted 1:5 with nuclease-free H_2O and used for real-time PCR.

8.2.2 Quantitative Real-time PCR (qRT-PCR)

The gene expression was measured with universal probe-library (UPL) mono-color hydrolysis probes. UPL probes and sequences of primers used in this thesis were listed in following table

Species	Gene	Primer sequence	UPL probe
Mouse	*Axin2*	FW:CCATGACGGACAGTAGCGTA RV: GCCATTGGCCTTCACACT	50
Mouse	*N-myc*	FW:CCTCCGGAGAGGATACCTTG RV:TCTCTACGGTGACCACATCG	12
Mouse	*Gapdh*	FW:AGCTTGTCATCAACGGGAAG RV: TTTGATGTTAGTGGGTCTCG	9
Mouse	*βIII-tubulin*	FW:GCGCATCAGCGTATACTACAA RV:TTCCAAGTCCACCAGAATGG	104
Mouse	*Doublecortin*	FW:AGCTGACTCAGGTAACGACCA RV:GCTTTGACTTAGGTGTTGAGAGC	18
Mouse	*Sox2*	FW:GGCAGAGAAGAGAGTGTTTGC RV: TCTTCTTTCTCCCAGCCCTA	67
Mouse	*Sox4*	FW:ACAGCGACAAGATTCCGTTC RV: GTCAGCCATGTGCTTGAGG	79
Mouse	*Sox11*	FW:GAGCTGAGCGAGATGATCG RV: GAACACCAGGTCGGAGAAGT	20

8.3 Cell culture

8.3.1 Cell culture condition

HEK293T cells, mouse embryonic fibroblasts (MEF) and 3T3-L1 cells were cultured in DMEM supplemented with 10% v/v fetal bovine serum (calf bovine serum for 3T3-L1), 2mM glutamine and 1% v/v penicillin/streptomycin. Cells were grown at 37°C and 5% CO_2 (10% CO_2 for 293T) in a humidified chamber. The plasmids were transfected using XtremeGENE 9 DNA Transfection reagent (Roche) according to the manufacturer's instructions. Scrambled and targeted siRNA SMARTpools were obtained from Horizon and transfections were performed using Dharmafect 1 (Horizon). Where indicated, cells were treated with nocodazole, Lithium Chloride (LiCl), 6-Bromoindirubin-3'-oxime (BIO), Okadaic acid (OA) and Calyculin A (Caly A) (length and dose of treatments indicated in figure legends). Wnt3a and control conditioned media (CM) were prepared from stably transfected L cells (ATCC) as per the supplier's guidelines and used at 1:10 dilution. For cilia analysis, cells were grown to 70-90% confluency and then serum starved for 24 hours by replacing the media with DMEM containing no serum. For 3T3-L1 cells cilia were analyzed after culturing cells at full confluency with 1% FCS for 24 hours. The *LRP5/LRP6* DKO HEK293T and MEF cell lines have been described prviously(Kirsch et al., 2017).

8.3.2 Lentivirus preparation

The Ccny and Ccnyl1 shRNA plasmids were obtained from the lab of Arial Zeng and are described previously(Zeng et al., 2016). For the Sox4 and Sox11 overexpression plasmids, full length Flag-Sox4/11 were excised from respective pCS2+ plasmids and ligated into the pLenti-CAG-ires-EGFP plasmid using BamHI and BsrGI restriction sites. EGFP was removed with this cloning strategy. All lentiviruses were packaged in 293T cells(Lois et al., 2002).

8.3.3 NPCs isolation and culturing

NPCs were obtained by incrossing Ccny+/- Ccnyl1+/- animals and collecting embryos at E13.5. The forebrain cerebral cortex was dissected from individual embryos, dissociated into a single cell suspension by repetitive pipetting, and then filtered through a 70 μm cell strainer. The resulting neurospheres were cultured in NPC media (DMEM/F12 (Invitrogen, p5780), B27 (LIFE, 1074547), glucose (Sigma Aldrich, s5761) hepes, progesterone (Sigma Aldrich, 12587010) putrescine (Sigma Aldrich, p7556), heparin (Sigma Aldrich, E4127) penicillin/streptomycin, insulin-transferrin-sodium selenite supplements (Roche, H3149), sodium bicarbonate (Sigma Aldrich, p5780) and 20 ng/ml EGF (Sigma Aldrich, 11243217001) for 5-7 days before being passaged. For passaging, cells were treated with accutase (Capricorn, ACC-1B) and then pipetted repetitively to obtain a single-cell suspension. Cells were passaged at least two times before performing experiments. Where indicated, NPCs were treated with BIO or nocodazole. Doses and duration of treatments are indicated in the figure legends. For NPC differentiation assays, 2x105 cells/ were plated on poly-D-lysine-coated 24 well plates for 48 hours and then media was switched to NPC differentiation media (DMEM/F12, B27, glucose, hepes, progesterone, putrescine, heparin, penicillin/streptomycin, insulin-transferrin-sodium selenite supplements, sodium bicarbonate). Cells were grown for 7-9 days to a confluency ~ 80% before being harvested for RNA, protein or IF analysis. Knockdown of Ccny and overexpression of Sox4/11 were performed by transducing shCcny and Flag-Sox4/11 lentiviruses respectively, plus 4 ug/ml polybrene (Sigma Aldrich TR1003) into NPCs 24 hours prior to differentiation assays.

8.3.4 TOPFLASH assay

HEK293T cells were transfected with 30ng Super TOPflash (Firefly), 3ng Renilla, 117 ng empty PCS2+ vector and, where indicated, 0.4ng xtβ-catenin. 16 hours after transfection cells were serum starved and treated with LiCl or BIO for 24 hours. For testing TOPflash activation in CCNYL1 single and double knockout cell lines, cells were first synchronized with nocodazole treatment according to standard procedures and then treated with Wnt3a conditioned media for 16 hours. In all experiments buffer alone was used as a control. Cells were resuspended in passive lysis buffer and

luminescence was recorded on a Fluoroskan Ascent FL luminometer (Thermo Scientific), using the Dual-Luciferase Reporter Assay system (Promega).

8.4 Animals

All animal work was conducted according to national and international guidelines and was approved by the state review board of Baden-Württemberg (protocol no. G-123/18). Sperm from mice carrying a flanked by loxP (floxed) allele of cyclin Y (Ccnytm1(flox)Smoc) was obtained from the lab of Arial Zeng (Shanghai, China) and used for in vitro fertilization of wild-type C57BL/6N oocytes. Heterozygous Ccny-flox mice were bred with transgenic animals expressing Cre recombinase under the control of the CMV promoter to achieve organism-wide gene knockout (CcnyKO). Generation of cyclin Y-like 1-deficient (Ccnyl1tm1a(EUCOMM)Wtsi/H; Ccnyl1KO) mice has been described previously(Koch et al., 2015). Ccny and Ccnyl1 double knockout embryos (DKO) were generated by incrossing Ccny- /-Ccnyl1+/- males with Ccny+/-Ccnyl1-/- females. Embryos with wildtype or heterozygous Ccny and Ccnyl1 alleles were used as controls. Embryos were analyzed at various time-points (E11.5, E12.5 and E13.5) and gender was not taken into consideration. For proliferation assays BrdU (Sigma-Aldrich, B5002) and IdU (Sigma-Aldrich, I0050000) were dissolved in 0.9% NaCl and administered to pregnant dams via intraperitoneal (IP) injection at a dose of 50 mg/kg. Injection strategies are indicated in the figure legends. Adult mice were sacrificed by cervical dislocation. For in utero electroporation experiments, C57BL/6J mice were bred at the Biomedical Services Facility of the MPI-CBG under standardized hygienic conditions and all procedures were conducted in agreement with the German Animal Welfare Legislation after approval by the Landesdirektion Sachsen (licenses: mouse TVV 5/2015 and TVV 20/2020).

8.4.1 Immunofluorescence

Paraffin - Tissues were fixed overnight in 4% paraformaldehyde at 4°C, progressively dehydrated and embedded in paraffin. 7 µm thick sections were rehydrated, boiled in a pressure cooker for 2 min with citrate/EDTA buffer (10 mM sodium citrate, 5 mM TrisHCL, 2 mM EDTA, pH 8.0) and blocked in blocking buffer (PBS solution

containing 10% normal donkey serum, 1% BSA and 0.1% Triton X-100) for 30 min at room temperature. All primary antibodies were diluted in blocking buffer and applied overnight at 4°C. Secondary antibodies were diluted 1:500 in blocking buffer containing Hoechst 33258 dye (1:1000)(Sigma Aldrich, 861405) to stain DNA and applied at room temperature for 1 h. For histological analysis 7 µm thick sections were stained with haematoxylin and eosin according to standard procedures.
Frozen sections – Tissues were fixed for 2 hours in 4% paraformaldehyde at 4°C, incubated in 30% sucrose overnight, embedded in Tissue-Tek (OCT, Sakura, 4583) and frozen at -20°C. Sections of 8 µm thickness were washed briefly in PBS and then heated in a microwave for 5 minutes in sodium citrate buffer (10mM sodium citrate, 0.05% Tween pH 6.0). Blocking and antibody applications were performed as described above. 34 Cell culture – Cells were cultured on coverslips coated with poly D-lysine and fixed with 4% PFA at room temperature for 10 min. Following fixation cells were washed twice in PBS and then blocked and stained with indicated antibodies.
Cell culture - Cells were cultured on coverslips coated with poly D-Lysine and fixed with ice-cold methanol on ice for 10 min or 4% PFA at room temperature for 10 min. Following fixation cells were washed twice in PBS and then blocked and stained with indicated antibodies as described above. For anti-Acetylated Tubulin and GSK3β staining on 293T cells as well as LRP6 staining in MEF cells a brief wash with cytoskeletal buffer (CB) (100mM NaCl, 300mM Sucrose, 3mM MgCl2, 10mM PIPES and 5mM EGTA) was performed prior to fixation. Cells were then fixed in 4% PFA diluted in CB buffer at room temperature. Subsequent blocking and antibody applications were carried out as described above.
For Neurosphere monolayer immunofluorescence, cells were fixed in 4% PFA at 4°C for 2 hours. Following fixation, cells were washed in PBS with 0.1% Triton and blocked in blocking buffer (5% donkey serum, 3%BSA, 0.1% Tween20 in PBS) for 30 mins. Subsequent antibody applications were carried out as described above.

8.4.2 TUNEL staining

TUNEL staining was performed with the Click-IT Plus TUNEL assay (Thermofisher, C10617) according to the manufacturer’s instructions.

8.5 Biochemical methods

8.5.1 Immunoblotting

Cells were adjusted to equal numbers, washed with PBS, resuspended in triton lysis buffer (20 mM Tris HCl, 150 M NaCl, 1% Triton X-100, 1 mM EDTA, 1 mM EGTA, 1 mM b-glycerolphosphate, 2.5 mM sodium pyrophosphate and 1 mM sodium orthovanadate), incubated for 30min on ice and then spun down at full speed for 7 minutes to clear lysates. For brain tissue samples, forebrains were dissected, resuspended in triton lysis buffer and sonicated in a water bath for 15 minutes before being processing as described above. Lysates were heated at 70°C in NuPage LDS buffer (Thermofisher, NP0007) with 50 mM DTT. Samples were separated on 7.5% polyacrylamide gels, transferred to nitrocellulose and blocked with 5% skim milk powder or 5% BSA in Tris-buffered saline with 0.05% Tween-20 (TBST) for 1 hour at room temperature. Primary antibodies were diluted in blocking buffer and incubated overnight at 4°C. After 3 washes in TBST, membranes were incubated with peroxidase-linked secondary antibodies for 1h at RT. Following an additional 3 washes, membranes were treated with 31 Supersignal West Pico solution (Thermo Scientific, 34579). Images were acquired on an LAS3000 system (Fuji Film).

8.5.2 Lambda-Phosphatase treatment

Cells were lysed in modified RIPA lysis buffer (50 mM HEPES pH 8.0, 300 mM NaCl, 1% Triton X-100, 0.2% sodium deoxycholate, 0.05% SDS, 5 mM MgCl2 supplemented with EDTA-free protease inhibitor tablet (Pierce, A32965) for 30 min on ice, spun down full speed at 4°C for 5 min and supernatants collected. Lysates were incubated with lambda phosphatase (NEB, P0753S) for 30 or 60 min (indicated in figure legends) at 30°C according to the manufacturer’s instructions.

8.5.3 Ubiquitination assays

HA-tagged ubiquitin plasmid was co-transfected with Flag-tagged Sox4/Sox11 or PCS2+ empty vector into 293T cells in 6 cm dishes for 48 hours. Cells were treated for 4 hours with 20 μM MG132 (Sigma Aldrich) before being harvested in triton lysis

buffer. A total of 200 µg protein was incubated with 20 µl FLAG beads (Sigma Aldrich, A2220) overnight at 4°C with rotation. Beads were washed 4x with triton lysis buffer, resuspended in 20 mM TrisHCl pH 7.5 buffer containing 0.1% SDS and heated for 5 minutes at 95°C to dissociate Sox binding partners. Cells were spun down, resuspended in triton lysis buffer and incubated a second time with 20 µl FLAG beads overnight at 4°C with rotation. Following 4 additional washes, NuPage LDS buffer supplemented with 50mM DTT was added to beads and samples were boiled at 70°C for 10 minutes.

8.6 Image and data analysis

Data were analyzed with an unpaired Student's t-test or Chi square test as indicated in the figure legends, using Graphpad software. Results are displayed as arithmetic mean ± standard error of mean (SEM). Statistically significant data are indicated as follows: * $p<0.05$, ** $p<0.01$ and *** $p<0.001$. Non-significant data is indicated as ns. Statistical outliers were calculated using the Grubb's test with Graphpad software and were excluded from analyzes.

8.6.1 Neocortex thickness and length

Average cortical wall thickness was measured on HE stained sections of the cortical forebrain in 5 different areas per section. Neocortex length was measured from the junction between the lateral ganglionic eminence and lateral neocortex to the most medial point of the neocortex. At least 6 matched (similar regions of the neocortex) sections were measured per embryo for both analyses.

8.6.2 Measurement of VZ, SVZ and IZ+CP

Thickness VZ, SVZ and IZ+CP thickness was measured using Fiji. VZ vs. SVZ vs. IZ+CP were defined based on the orientation and density of the cell nuclei as revealed by DNA staining and the immunofluorescence pattern of the basal progenitor marker Tbr2. At least 7 sections were measured per embryo.

8.6.3 Quantification of specific cell types in developing neocortex

IF using anti-Pax6 + Tbr2, Tbr2 only, and Tbr1 antibodies was performed to quantify the number of APs, BPs and post-mitotic neurons, respectively. Data were expressed as percentages of Pax6 +Tbr2 – (APs), Tbr2 + (BPs), or Tbr1 + (neurons) nuclei per total nuclei (DNA+) in at least 5 matched sections per embryo for each analysis.

8.6.4 Analysis of BrdU-labeled NPCs

Co-IF using anti-BrdU plus either anti-Pax6 + Tbr2 or anti-Tbr2 only antibodies was performed to quantify the number of APs and BPs in S-phase, respectively. Data were expressed as percentages of BrdU+Pax6 +Tbr2 – or BrdU+Tbr2 + cells per the total number of Pax6 +Tbr2 – or Tbr2 + cells, respectively. Two pictures from at least 6 matched sections were counted per embryo.

8.6.5 Calculation of the length of S-phase, total cell cycle, and mitosis

E13.5 neocortex sections were triple-stained for IdU, BrdU and Tbr2, and the numbers of IdU+ /BrdU– cells (i.e. cells having left S-phase) and IdU+ /BrdU+ cells (i.e. cells remaining in S-phase) were counted for APs (Tbr2 –) and BPs (Tbr2 +) on at least 10 images from matched sections of control and DKO embryos. For each of the four NPC population, the numbers obtained were expressed as percentages of the total number of IdU+ cells. S-phase length was calculated by dividing 1.5 hours (the interval between IdU and BrdU injection) by the percentage of cells having left S-phase after this time period (IdU+ /BrdU– cells) and multiplying the resulting value times 100. Total cell cycle length was calculated by dividing the S-phase length value by the percentage of cells in S-phase (as determined after a 1-hour BrdU pulse) and multiplying the resulting value times 100. Different sections from the same embryos were stained for pHH3, Ki67 and Tbr2, and the percentage of cells in mitosis was determined for APs (pHH3 +Ki67+Tbr2 – /Ki67+Tbr2 –) and BPs (pHH3 +Ki67+Tbr2 + /Ki67+Tbr2 +) on at least 10 matched sections per embryo. The length of mitosis was calculated by multiplying the total cell cycle length value times the percentage of cells in mitosis.

8.6.6 Apoptosis analysis

Quantification of apoptotic cells was performed by IF with an anti-active caspase3 antibody or by fluorescent TUNEL staining. Results were obtained after scoring the percentage of active caspase 3 or TUNEL cells/5000 cells on at least 5 matched sections per embryo.

8.6.7 Asymmetric vs. symmetric AP division

Asymmetric vs. symmetric AP division was determined as described previously (Kosodo et al. 2004). Briefly, to identify asymmetrically vs. symmetrically dividing APs at the ventricular surface of the neocortex, sections were immunostained with an anti-pan-cadherin antibody to visualize the apical-most lateral plasma membrane and to thereby identify the apical plasma membrane (pan-cadherin-negative region, referred to as "cadherin hole"). Anaphase and early telophase APs were identified by DNA staining using Hoechst 33258 dye. The orientation of the cleavage plane was deduced from the position of the Hoechst-stained sister chromatids. APs whose cleavage plane was predicted to result in an unequal (bypassing the cadherin hole) or equal (bisecting the cadherin hole) distribution of apical membrane were considered as asymmetrically and symmetrically dividing cells, respectively. At least 25 mitotic APs were analyzed per embryo.

8.6.8 Astral microtubule quantification

IF for α-tubulin was performed on sections of E13.5 control and DKO embryos containing neocortex. Z-stacks (8-10 μm thick) were acquired at 1-μm intervals and the number of apical, basal and central astral microtubules was counted for at least 10 metaphase cells per embryo, as described previously (Mora-Bermúdez et al. 2014) using the Cell Counter plugin in Fiji.

8.6.9 IUE quantification

For all analyses, indicated co-immunostaining quantified on at least 3 bins per embryo for each treatment.

8.6.10 Sox4/Sox11 *in vivo* quantification

IF for Sox4/Sox11 plus Tbr2 and pHH3 was performed on sections of E13.5 control and DKO embryos. At least 30 mitotic BPs were analyzed per embryo. Cells were scored as high or low based on fluorescence intensity compared to non-mitotic cells. Ratio of high vs. low intensity cells was plotted as the final result. For quantification of Sox11 in BPs, the number of Tbr2 + /Sox11+ cells divided by the total number of Tbr2 + cells was counted on at least 6 matched sections per embryo (2 pictures per section).

9. ABBREVIATIONS

STOP	Stablisation of proteins
GSK3	Glycogen synthase kinase 3
APC	Adenomatous Polyposis Coli
LRP6	Low-density lipoprotein receptor-related protein 6
DVL	Dishevelled
FZD	Frizzled
CDK14	Cyclin dependent kinase 14
CDK16	Cyclin dependent kinase 16
CK1	Casein kinase 1
B-Trcp	β-Transducin Repeat Containing Protein
PCP	Planer cell polarity
ROCK	Rho-associated protein kinase
JNK	c-Jun N-terminal kinase
PLC	Phospholipase C
DAG	Diacylglycerin
PKC	Protein kinase C
IP3	Inositol trisphosphate or inositol 1,4,5-trisphosphate
NFAT	Nuclear factor of activated T cells
CaMK	Ca2+/calmodulin-dependent protein kinase
FBW7	F-box and WD repeat domain-containing 7
NSC	Neural stem cell
NEC	Neural epithelial cell
RG	Radial glia
IP	Intermediate progenitor
BP	Basal progenitor
AP	Apical progenitor
VZ	Ventricular zone
SVZ	Subventricular zone
CP	Cortical plate
PAX6	Paired Box 6
TBR2	T-box brain protein 2
NGN2	Neurogenin-2
CUX	Cut Like Homeobox 2
BMP	Bone morphogenetic protein
TUJ1	Neuron-specific class III beta-tubulin
MAP2	Microtubule Associated Protein 2
GPCR	G protein coupled receptor

PDGF	Platelet-derived growth factor
cAMP	Cyclic adenosine monophosphate
TMEM	Transmembrane
MCC	Multiciliated cell
BB	Basal body
IFT	Intraflagellar transport
WAT	White adipose tissue
αMT	Alpha microtubule
PP1	Protein phosphatse 1
PPP1R2	Protein Phosphatase 1 Regulatory Inhibitor Subunit 2
H&E	Hematoxylin and eosin
IF	Immunofluorescence
IUE	*In utero* electrophoresis
BrdU	5-bromo-2'-deoxyuridine
IdU	5-iodo-2′-deoxyuridine
SEM	Scanning electron microscope
CRISPR	Clustered Regularly Interspaced Short Palindromic Repeats
OA	Okadaic acid
CalyA	Calyculin A
HEK293T	Human embryonic kidney 293T
GFP	Green fluorescent protein
kDa	Kilodalton
RNA	Ribonucleic acid
RNAse A	Ribonuclease A
PAGE	Polyacrylamide Gel Electrophoresis
PBS	Phosphate Buffered Saline
DMEM	Dulbecco’s modified eagle’s medium
DMSO	Dimethyl sulfoxide
DTT	Dithiothreitol
EDTA	Ethylene diamine tetraacetate
EGTA	Ethylene glycol tetraacetate
FACs	Fluorescence activated cell sorting
PCR	Polymerase chain reaction
Rec-A	Recombinase A
RNA	Ribonucleic Acid
RNP	Ribonucleoprotein
rpm	Revolutions per minute
SD	Standard Deviation
SDS	Sodium dodecyl sulfate
SEM	Standard Error of the Mean

siRNA	Small interfering RNA
sgRNA	Single guide RNA
TEMED	Tetramethyl ethylene diamine
WT	Wild Type

10. PUBLICATION

Da Silva F, Zhang K, Pinson A, Fatti E, Wilsch-Bräuninger M, Herbst J, Vidal V, Schedl A, Huttner W.B, Niehrs C (2021). Mitotic WNT signaling orchestrates neurogenesis in the developing neocortex. ***EMBO J*** e108041

.

11. REFERENCES

(1970). Embryonic vertebrate central nervous system: revised terminology. The Boulder Committee. Anat Rec *166*, 257-261.
Aberle, H., Bauer, A., Stappert, J., Kispert, A., and Kemler, R. (1997). beta-catenin is a target for the ubiquitin-proteasome pathway. EMBO J *16*, 3797-3804.
Acebron, S.P., Karaulanov, E., Berger, B.S., Huang, Y.L., and Niehrs, C. (2014). Mitotic wnt signaling promotes protein stabilization and regulates cell size. Mol Cell *54*, 663-674.
Acebron, S.P., and Niehrs, C. (2016). beta-Catenin-Independent Roles of Wnt/LRP6 Signaling. Trends Cell Biol *26*, 956-967.
Agirman, G., Broix, L., and Nguyen, L. (2017). Cerebral cortex development: an outside-in perspective. FEBS Lett *591*, 3978-3992.
Allache, R., Lachance, S., Guyot, M.C., De Marco, P., Merello, E., Justice, M.J., Capra, V., and Kibar, Z. (2014). Novel mutations in Lrp6 orthologs in mouse and human neural tube defects affect a highly dosage-sensitive Wnt non-canonical planar cell polarity pathway. Hum Mol Genet *23*, 1687-1699.
An, W., Zhang, Z., Zeng, L., Yang, Y., Zhu, X., and Wu, J. (2015). Cyclin Y Is Involved in the Regulation of Adipogenesis and Lipid Production. PLoS One *10*, e0132721.
Anvarian, Z., Mykytyn, K., Mukhopadhyay, S., Pedersen, L.B., and Christensen, S.T. (2019). Cellular signalling by primary cilia in development, organ function and disease. Nat Rev Nephrol *15*, 199-219.
Arai, Y., and Taverna, E. (2017). Neural Progenitor Cell Polarity and Cortical Development. Front Cell Neurosci *11*, 384.
Arner, P., Andersson, D.P., Thorne, A., Wiren, M., Hoffstedt, J., Naslund, E., Thorell, A., and Ryden, M. (2013). Variations in the size of the major omentum are primarily determined by fat cell number. J Clin Endocrinol Metab *98*, E897-901.
Asami, M., Pilz, G.A., Ninkovic, J., Godinho, L., Schroeder, T., Huttner, W.B., and Gotz, M. (2011). The role of Pax6 in regulating the orientation and mode of cell division of progenitors in the mouse cerebral cortex. Development *138*, 5067-5078.
Backman, M., Machon, O., Mygland, L., van den Bout, C.J., Zhong, W., Taketo, M.M., and Krauss, S. (2005). Effects of canonical Wnt signaling on dorso-ventral specification of the mouse telencephalon. Dev Biol *279*, 155-168.
Balta, E.A., Wittmann, M.T., Jung, M., Sock, E., Haeberle, B.M., Heim, B., von Zweydorf, F., Heppt, J., von Wittgenstein, J., Gloeckner, C.J.*, et al.* (2018). Phosphorylation Modulates the Subcellular Localization of SOX11. Front Mol Neurosci *11*, 211.
Bayatti, N., Sarma, S., Shaw, C., Eyre, J.A., Vouyiouklis, D.A., Lindsay, S., and Clowry, G.J. (2008). Progressive loss of PAX6, TBR2, NEUROD and TBR1 mRNA gradients correlates with translocation of EMX2 to the cortical plate during human cortical development. Eur J Neurosci *28*, 1449-1456.
Bengoa-Vergniory, N., and Kypta, R.M. (2015). Canonical and noncanonical Wnt signaling in neural stem/progenitor cells. Cell Mol Life Sci *72*, 4157-4172.
Berg, J.M., Tymoczko, J.L., and Stryer, L. (2012). Biochemistry, 7th edn (New York: W.H. Freeman).
Bergsland, M., Ramskold, D., Zaouter, C., Klum, S., Sandberg, R., and Muhr, J. (2011). Sequentially acting Sox transcription factors in neural lineage development. Genes Dev *25*, 2453-2464.

Bernatik, O., Paclikova, P., Kotrbova, A., Bryja, V., and Cajanek, L. (2021). Primary Cilia Formation Does Not Rely on WNT/beta-Catenin Signaling. Front Cell Dev Biol *9*, 623753.
Berry, R., and Rodeheffer, M.S. (2013). Characterization of the adipocyte cellular lineage in vivo. Nat Cell Biol *15*, 302-308.
Beurel, E., Grieco, S.F., and Jope, R.S. (2015). Glycogen synthase kinase-3 (GSK3): regulation, actions, and diseases. Pharmacol Ther *148*, 114-131.
Bhattaram, P., Penzo-Mendez, A., Kato, K., Bandyopadhyay, K., Gadi, A., Taketo, M.M., and Lefebvre, V. (2014). SOXC proteins amplify canonical WNT signaling to secure nonchondrocytic fates in skeletogenesis. J Cell Biol *207*, 657-671.
Bilic, J., Huang, Y.L., Davidson, G., Zimmermann, T., Cruciat, C.M., Bienz, M., and Niehrs, C. (2007). Wnt induces LRP6 signalosomes and promotes dishevelled-dependent LRP6 phosphorylation. Science *316*, 1619-1622.
Blom, N., Gammeltoft, S., and Brunak, S. (1999). Sequence and structure-based prediction of eukaryotic protein phosphorylation sites. J Mol Biol *294*, 1351-1362.
Bollen, M., Peti, W., Ragusa, M.J., and Beullens, M. (2010). The extended PP1 toolkit: designed to create specificity. Trends Biochem Sci *35*, 450-458.
Borrell, V., and Calegari, F. (2014). Mechanisms of brain evolution: regulation of neural progenitor cell diversity and cell cycle length. Neurosci Res *86*, 14-24.
Bowles, J., Schepers, G., and Koopman, P. (2000). Phylogeny of the SOX family of developmental transcription factors based on sequence and structural indicators. Dev Biol *227*, 239-255.
Britanova, O., Alifragis, P., Junek, S., Jones, K., Gruss, P., and Tarabykin, V. (2006). A novel mode of tangential migration of cortical projection neurons. Dev Biol *298*, 299-311.
Buck, L., and Axel, R. (1991). A novel multigene family may encode odorant receptors: a molecular basis for odor recognition. Cell *65*, 175-187.
Caron, A., Xu, X., and Lin, X. (2012). Wnt/beta-catenin signaling directly regulates Foxj1 expression and ciliogenesis in zebrafish Kupffer's vesicle. Development *139*, 514-524.
Caronia-Brown, G., Yoshida, M., Gulden, F., Assimacopoulos, S., and Grove, E.A. (2014). The cortical hem regulates the size and patterning of neocortex. Development *141*, 2855-2865.
Casamayor, A., and Arino, J. (2020). Controlling Ser/Thr protein phosphatase PP1 activity and function through interaction with regulatory subunits. Adv Protein Chem Struct Biol *122*, 231-288.
Ceulemans, H., and Bollen, M. (2004). Functional diversity of protein phosphatase-1, a cellular economizer and reset button. Physiol Rev *84*, 1-39.
Chen, C., Lee, G.A., Pourmorady, A., Sock, E., and Donoghue, M.J. (2015). Orchestration of Neuronal Differentiation and Progenitor Pool Expansion in the Developing Cortex by SoxC Genes. J Neurosci *35*, 10629-10642.
Chenn, A. (2008). Wnt/beta-catenin signaling in cerebral cortical development. Organogenesis *4*, 76-80.
Chenn, A., and Walsh, C.A. (2002). Regulation of cerebral cortical size by control of cell cycle exit in neural precursors. Science *297*, 365-369.
Chiang, S.Y., Wu, H.C., Lin, S.Y., Chen, H.Y., Wang, C.F., Yeh, N.H., Shih, J.H., Huang, Y.S., Kuo, H.C., Chou, S.J., *et al.* (2021). Usp11 controls cortical neurogenesis and neuronal migration through Sox11 stabilization. Sci Adv *7*.

Cho, E., Kim, D.H., Hur, Y.N., Whitcomb, D.J., Regan, P., Hong, J.H., Kim, H., Ho Suh, Y., Cho, K., and Park, M. (2015). Cyclin Y inhibits plasticity-induced AMPA receptor exocytosis and LTP. Sci Rep *5*, 12624.
Christensen, S.T., Morthorst, S.K., Mogensen, J.B., and Pedersen, L.B. (2017). Primary Cilia and Coordination of Receptor Tyrosine Kinase (RTK) and Transforming Growth Factor beta (TGF-beta) Signaling. Cold Spring Harb Perspect Biol *9*.
Clevers, H. (2006). Wnt/beta-catenin signaling in development and disease. Cell *127*, 469-480.
Cnossen, W.R., te Morsche, R.H., Hoischen, A., Gilissen, C., Venselaar, H., Mehdi, S., Bergmann, C., Losekoot, M., Breuning, M.H., Peters, D.J.*, et al.* (2016). LRP5 variants may contribute to ADPKD. Eur J Hum Genet *24*, 237-242.
Cohen, P., and Cohen, P.T. (1989). Protein phosphatases come of age. J Biol Chem *264*, 21435-21438.
Cole, D.G., Chinn, S.W., Wedaman, K.P., Hall, K., Vuong, T., and Scholey, J.M. (1993). Novel heterotrimeric kinesin-related protein purified from sea urchin eggs. Nature *366*, 268-270.
Cole, D.G., Diener, D.R., Himelblau, A.L., Beech, P.L., Fuster, J.C., and Rosenbaum, J.L. (1998). Chlamydomonas kinesin-II-dependent intraflagellar transport (IFT): IFT particles contain proteins required for ciliary assembly in Caenorhabditis elegans sensory neurons. J Cell Biol *141*, 993-1008.
Corbit, K.C., Shyer, A.E., Dowdle, W.E., Gaulden, J., Singla, V., Chen, M.H., Chuang, P.T., and Reiter, J.F. (2008). Kif3a constrains beta-catenin-dependent Wnt signalling through dual ciliary and non-ciliary mechanisms. Nat Cell Biol *10*, 70-76.
Corkins, M.E., Krneta-Stankic, V., Kloc, M., McCrea, P.D., Gladden, A.B., and Miller, R.K. (2019). Divergent roles of the Wnt/PCP Formin Daam1 in renal ciliogenesis. PLoS One *14*, e0221698.
Cruciat, C.M., Ohkawara, B., Acebron, S.P., Karaulanov, E., Reinhard, C., Ingelfinger, D., Boutros, M., and Niehrs, C. (2010). Requirement of prorenin receptor and vacuolar H+-ATPase-mediated acidification for Wnt signaling. Science *327*, 459-463.
Da Silva, F., Zhang, K., Pinson, A., Fatti, E., Wilsch-Brauninger, M., Herbst, J., Vidal, V., Schedl, A., Huttner, W.B., and Niehrs, C. (2021). Mitotic WNT signalling orchestrates neurogenesis in the developing neocortex. EMBO J, e108041.
Davidson, G., and Niehrs, C. (2010). Emerging links between CDK cell cycle regulators and Wnt signaling. Trends Cell Biol *20*, 453-460.
Davidson, G., Shen, J., Huang, Y.L., Su, Y., Karaulanov, E., Bartscherer, K., Hassler, C., Stannek, P., Boutros, M., and Niehrs, C. (2009). Cell cycle control of wnt receptor activation. Dev Cell *17*, 788-799.
Davidson, G., Wu, W., Shen, J., Bilic, J., Fenger, U., Stannek, P., Glinka, A., and Niehrs, C. (2005). Casein kinase 1 gamma couples Wnt receptor activation to cytoplasmic signal transduction. Nature *438*, 867-872.
Dehay, C., and Kennedy, H. (2007). Cell-cycle control and cortical development. Nat Rev Neurosci *8*, 438-450.
Delaunay, D., Kawaguchi, A., Dehay, C., and Matsuzaki, F. (2017). Division modes and physical asymmetry in cerebral cortex progenitors. Curr Opin Neurobiol *42*, 75-83.
DePaoli-Roach, A.A. (1984). Synergistic phosphorylation and activation of ATP-Mg-dependent phosphoprotein phosphatase by F A/GSK-3 and casein kinase II (PC0.7). J Biol Chem *259*, 12144-12152.

Draganova, K., Zemke, M., Zurkirchen, L., Valenta, T., Cantu, C., Okoniewski, M., Schmid, M.T., Hoffmans, R., Gotz, M., Basler, K.*, et al.* (2015). Wnt/beta-catenin signaling regulates sequential fate decisions of murine cortical precursor cells. Stem Cells *33*, 170-182.
Dusi, S., Della Bianca, V., Grzeskowiak, M., and Rossi, F. (1993). Relationship between phosphorylation and translocation to the plasma membrane of p47phox and p67phox and activation of the NADPH oxidase in normal and Ca(2+)-depleted human neutrophils. Biochem J *290 (Pt 1)*, 173-178.
Dy, P., Penzo-Mendez, A., Wang, H., Pedraza, C.E., Macklin, W.B., and Lefebvre, V. (2008). The three SoxC proteins--Sox4, Sox11 and Sox12--exhibit overlapping expression patterns and molecular properties. Nucleic Acids Res *36*, 3101-3117.
Elias, R.V., Sezate, S.S., Cao, W., and McGinnis, J.F. (2004). Temporal kinetics of the light/dark translocation and compartmentation of arrestin and alpha-transducin in mouse photoreceptor cells. Mol Vis *10*, 672-681.
Eto, M. (2009). Regulation of cellular protein phosphatase-1 (PP1) by phosphorylation of the CPI-17 family, C-kinase-activated PP1 inhibitors. J Biol Chem *284*, 35273-35277.
Fardilha, M., Esteves, S.L., Korrodi-Gregorio, L., Pelech, S., da Cruz, E.S.O.A., and da Cruz, E.S.E. (2011). Protein phosphatase 1 complexes modulate sperm motility and present novel targets for male infertility. Mol Hum Reprod *17*, 466-477.
Fernandez, V., Llinares-Benadero, C., and Borrell, V. (2016). Cerebral cortex expansion and folding: what have we learned? EMBO J *35*, 1021-1044.
Forcioli-Conti, N., Lacas-Gervais, S., Dani, C., and Peraldi, P. (2015). The primary cilium undergoes dynamic size modifications during adipocyte differentiation of human adipose stem cells. Biochem Biophys Res Commun *458*, 117-122.
Gaertig, J., and Wloga, D. (2008). Ciliary tubulin and its post-translational modifications. Curr Top Dev Biol *85*, 83-113.
Garcia-Gonzalo, F.R., Corbit, K.C., Sirerol-Piquer, M.S., Ramaswami, G., Otto, E.A., Noriega, T.R., Seol, A.D., Robinson, J.F., Bennett, C.L., Josifova, D.J.*, et al.* (2011). A transition zone complex regulates mammalian ciliogenesis and ciliary membrane composition. Nat Genet *43*, 776-784.
Gerdes, J.M., Liu, Y., Zaghloul, N.A., Leitch, C.C., Lawson, S.S., Kato, M., Beachy, P.A., Beales, P.L., DeMartino, G.N., Fisher, S.*, et al.* (2007). Disruption of the basal body compromises proteasomal function and perturbs intracellular Wnt response. Nat Genet *39*, 1350-1360.
Ghossoub, R., Molla-Herman, A., Bastin, P., and Benmerah, A. (2011). The ciliary pocket: a once-forgotten membrane domain at the base of cilia. Biol Cell *103*, 131-144.
Goetz, S.C., and Anderson, K.V. (2010). The primary cilium: a signalling centre during vertebrate development. Nat Rev Genet *11*, 331-344.
Gomez-Orte, E., Saenz-Narciso, B., Moreno, S., and Cabello, J. (2013). Multiple functions of the noncanonical Wnt pathway. Trends Genet *29*, 545-553.
Goncalves, J., and Pelletier, L. (2017). The Ciliary Transition Zone: Finding the Pieces and Assembling the Gate. Mol Cells *40*, 243-253.
Gotz, M., and Barde, Y.A. (2005). Radial glial cells defined and major intermediates between embryonic stem cells and CNS neurons. Neuron *46*, 369-372.
Grasby, K.L., Jahanshad, N., Painter, J.N., Colodro-Conde, L., Bralten, J., Hibar, D.P., Lind, P.A., Pizzagalli, F., Ching, C.R.K., McMahon, M.A.B.*, et al.* (2020). The genetic architecture of the human cerebral cortex. Science *367*.

Green, M.R., Sambrook, J., and Sambrook, J. (2012). Molecular cloning : a laboratory manual, 4th edn (Cold Spring Harbor, N.Y.: Cold Spring Harbor Laboratory Press).
Grove, E.A., Tole, S., Limon, J., Yip, L., and Ragsdale, C.W. (1998). The hem of the embryonic cerebral cortex is defined by the expression of multiple Wnt genes and is compromised in Gli3-deficient mice. Development *125*, 2315-2325.
Gunhaga, L., Marklund, M., Sjodal, M., Hsieh, J.C., Jessell, T.M., and Edlund, T. (2003). Specification of dorsal telencephalic character by sequential Wnt and FGF signaling. Nat Neurosci *6*, 701-707.
Habermacher, G., and Sale, W.S. (1996). Regulation of flagellar dynein by an axonemal type-1 phosphatase in Chlamydomonas. J Cell Sci *109 (Pt 7)*, 1899-1907.
Haczeyni, F., Bell-Anderson, K.S., and Farrell, G.C. (2018). Causes and mechanisms of adipocyte enlargement and adipose expansion. Obes Rev *19*, 406-420.
Han, W., Shi, J., Cao, J., Dong, B., and Guan, W. (2020). Current advances of long non-coding RNAs mediated by wnt signaling in glioma. Pathol Res Pract *216*, 153008.
Harrison-Uy, S.J., and Pleasure, S.J. (2012). Wnt signaling and forebrain development. Cold Spring Harb Perspect Biol *4*, a008094.
Hashimoto-Torii, K., Torii, M., Sarkisian, M.R., Bartley, C.M., Shen, J., Radtke, F., Gridley, T., Sestan, N., and Rakic, P. (2008). Interaction between Reelin and Notch signaling regulates neuronal migration in the cerebral cortex. Neuron *60*, 273-284.
Haubensak, W., Attardo, A., Denk, W., and Huttner, W.B. (2004). Neurons arise in the basal neuroepithelium of the early mammalian telencephalon: a major site of neurogenesis. Proc Natl Acad Sci U S A *101*, 3196-3201.
Hemmings, B.A., Resink, T.J., and Cohen, P. (1982). Reconstitution of a Mg-ATP-dependent protein phosphatase and its activation through a phosphorylation mechanism. FEBS Lett *150*, 319-324.
Hilgendorf, K.I., Johnson, C.T., Mezger, A., Rice, S.L., Norris, A.M., Demeter, J., Greenleaf, W.J., Reiter, J.F., Kopinke, D., and Jackson, P.K. (2019). Omega-3 Fatty Acids Activate Ciliary FFAR4 to Control Adipogenesis. Cell *179*, 1289-+.
Hinze, L., Pfirrmann, M., Karim, S., Degar, J., McGuckin, C., Vinjamur, D., Sacher, J., Stevenson, K.E., Neuberg, D.S., Orellana, E.*, et al.* (2019). Synthetic Lethality of Wnt Pathway Activation and Asparaginase in Drug-Resistant Acute Leukemias. Cancer Cell *35*, 664-676 e667.
Hirabayashi, Y., Itoh, Y., Tabata, H., Nakajima, K., Akiyama, T., Masuyama, N., and Gotoh, Y. (2004). The Wnt/beta-catenin pathway directs neuronal differentiation of cortical neural precursor cells. Development *131*, 2791-2801.
Hornbeck, P.V., Kornhauser, J.M., Tkachev, S., Zhang, B., Skrzypek, E., Murray, B., Latham, V., and Sullivan, M. (2012). PhosphoSitePlus: a comprehensive resource for investigating the structure and function of experimentally determined post-translational modifications in man and mouse. Nucleic Acids Res *40*, D261-270.
Hoshiba, Y., Toda, T., Ebisu, H., Wakimoto, M., Yanagi, S., and Kawasaki, H. (2016). Sox11 Balances Dendritic Morphogenesis with Neuronal Migration in the Developing Cerebral Cortex. J Neurosci *36*, 5775-5784.
Huang, P., and Schier, A.F. (2009). Dampened Hedgehog signaling but normal Wnt signaling in zebrafish without cilia. Development *136*, 3089-3098.
Huang, Y.L., Anvarian, Z., Doderlein, G., Acebron, S.P., and Niehrs, C. (2015). Maternal Wnt/STOP signaling promotes cell division during early Xenopus embryogenesis. Proc Natl Acad Sci U S A *112*, 5732-5737.

Huangfu, D., Liu, A., Rakeman, A.S., Murcia, N.S., Niswander, L., and Anderson, K.V. (2003). Hedgehog signalling in the mouse requires intraflagellar transport proteins. Nature *426*, 83-87.
Ikeda, S., Kishida, S., Yamamoto, H., Murai, H., Koyama, S., and Kikuchi, A. (1998). Axin, a negative regulator of the Wnt signaling pathway, forms a complex with GSK-3beta and beta-catenin and promotes GSK-3beta-dependent phosphorylation of beta-catenin. EMBO J *17*, 1371-1384.
Ishikawa, H., and Marshall, W.F. (2011). Ciliogenesis: building the cell's antenna. Nat Rev Mol Cell Biol *12*, 222-234.
Iwata, T., and Hevner, R.F. (2009). Fibroblast growth factor signaling in development of the cerebral cortex. Dev Growth Differ *51*, 299-323.
Jeffery, E., Church, C.D., Holtrup, B., Colman, L., and Rodeheffer, M.S. (2015). Rapid depot-specific activation of adipocyte precursor cells at the onset of obesity. Nat Cell Biol *17*, 376-385.
Kaas, J.H. (2013). The evolution of brains from early mammals to humans. Wiley Interdiscip Rev Cogn Sci *4*, 33-45.
Karastergiou, K., and Fried, S.K. (2017). Cellular Mechanisms Driving Sex Differences in Adipose Tissue Biology and Body Shape in Humans and Mouse Models. Adv Exp Med Biol *1043*, 29-51.
Kathem, S.H., Mohieldin, A.M., and Nauli, S.M. (2014). The Roles of Primary cilia in Polycystic Kidney Disease. AIMS Mol Sci *1*, 27-46.
Kikuchi, A., Yamamoto, H., and Sato, A. (2009). Selective activation mechanisms of Wnt signaling pathways. Trends Cell Biol *19*, 119-129.
Kim, W.Y., Wang, X., Wu, Y., Doble, B.W., Patel, S., Woodgett, J.R., and Snider, W.D. (2009). GSK-3 is a master regulator of neural progenitor homeostasis. Nat Neurosci *12*, 1390-1397.
Kirsch, N., Chang, L.S., Koch, S., Glinka, A., Dolde, C., Colozza, G., Benitez, M.D.J., De Robertis, E.M., and Niehrs, C. (2017). Angiopoietin-like 4 Is a Wnt Signaling Antagonist that Promotes LRP6 Turnover. Dev Cell *43*, 71-82 e76.
Klumpp, S., Cohen, P., and Schultz, J.E. (1990). Okadaic acid, an inhibitor of protein phosphatase 1 in Paramecium, causes sustained Ca2(+)-dependent backward swimming in response to depolarizing stimuli. EMBO J *9*, 685-689.
Koch, S., Acebron, S.P., Herbst, J., Hatiboglu, G., and Niehrs, C. (2015). Post-transcriptional Wnt Signaling Governs Epididymal Sperm Maturation. Cell *163*, 1225-1236.
Konno, D., Shioi, G., Shitamukai, A., Mori, A., Kiyonari, H., Miyata, T., and Matsuzaki, F. (2008). Neuroepithelial progenitors undergo LGN-dependent planar divisions to maintain self-renewability during mammalian neurogenesis. Nat Cell Biol *10*, 93-101.
Kosodo, Y., Roper, K., Haubensak, W., Marzesco, A.M., Corbeil, D., and Huttner, W.B. (2004). Asymmetric distribution of the apical plasma membrane during neurogenic divisions of mammalian neuroepithelial cells. EMBO J *23*, 2314-2324.
Kubo, T., Yanagisawa, H.A., Yagi, T., Hirono, M., and Kamiya, R. (2010). Tubulin polyglutamylation regulates axonemal motility by modulating activities of inner-arm dyneins. Curr Biol *20*, 441-445.
Kuwahara, A., Hirabayashi, Y., Knoepfler, P.S., Taketo, M.M., Sakai, J., Kodama, T., and Gotoh, Y. (2010). Wnt signaling and its downstream target N-myc regulate basal progenitors in the developing neocortex. Development *137*, 1035-1044.
Kyun, M.L., Kim, S.O., Lee, H.G., Hwang, J.A., Hwang, J., Soung, N.K., Cha-Molstad, H., Lee, S., Kwon, Y.T., Kim, B.Y.*, et al.* (2020). Wnt3a Stimulation

Promotes Primary Ciliogenesis through beta-Catenin Phosphorylation-Induced Reorganization of Centriolar Satellites. Cell Rep *30*, 1447-1462 e1445.
LaMonica, B.E., Lui, J.H., Hansen, D.V., and Kriegstein, A.R. (2013). Mitotic spindle orientation predicts outer radial glial cell generation in human neocortex. Nat Commun *4*, 1665.
Lancaster, M.A., Louie, C.M., Silhavy, J.L., Sintasath, L., Decambre, M., Nigam, S.K., Willert, K., and Gleeson, J.G. (2009). Impaired Wnt-beta-catenin signaling disrupts adult renal homeostasis and leads to cystic kidney ciliopathy. Nat Med *15*, 1046-1054.
Lancaster, M.A., Schroth, J., and Gleeson, J.G. (2011). Subcellular spatial regulation of canonical Wnt signalling at the primary cilium. Nat Cell Biol *13*, 700-707.
Lee, K.H., Johmura, Y., Yu, L.R., Park, J.E., Gao, Y., Bang, J.K., Zhou, M., Veenstra, T.D., Yeon Kim, B., and Lee, K.S. (2012). Identification of a novel Wnt5a-CK1varepsilon-Dvl2-Plk1-mediated primary cilia disassembly pathway. EMBO J *31*, 3104-3117.
Lefebvre, V., Dumitriu, B., Penzo-Mendez, A., Han, Y., and Pallavi, B. (2007). Control of cell fate and differentiation by Sry-related high-mobility-group box (Sox) transcription factors. Int J Biochem Cell Biol *39*, 2195-2214.
Lei, Y., Fathe, K., McCartney, D., Zhu, H., Yang, W., Ross, M.E., Shaw, G.M., and Finnell, R.H. (2015). Rare LRP6 variants identified in spina bifida patients. Hum Mutat *36*, 342-349.
Li, J., Li, C., Liang, D., Lv, F., Yuan, T., The, E., Ma, X., Wu, Y., Zhen, L., Xie, D.*, et al.* (2016). LRP6 acts as a scaffold protein in cardiac gap junction assembly. Nat Commun *7*, 11775.
Lian, G., Dettenhofer, M., Lu, J., Downing, M., Chenn, A., Wong, T., and Sheen, V. (2016). Filamin A- and formin 2-dependent endocytosis regulates proliferation via the canonical Wnt pathway. Development *143*, 4509-4520.
Lian, G., Wong, T., Lu, J., Hu, J., Zhang, J., and Sheen, V. (2019). Cytoskeletal Associated Filamin A and RhoA Affect Neural Progenitor Specification During Mitosis. Cereb Cortex *29*, 1280-1290.
Liang, Y., Zhu, X., Wu, Q., and Pan, J. (2018). Ciliary Length Sensing Regulates IFT Entry via Changes in FLA8/KIF3B Phosphorylation to Control Ciliary Assembly. Curr Biol *28*, 2429-2435 e2423.
Lidke, D.S., Huang, F., Post, J.N., Rieger, B., Wilsbacher, J., Thomas, J.L., Pouyssegur, J., Jovin, T.M., and Lenormand, P. (2010). ERK nuclear translocation is dimerization-independent but controlled by the rate of phosphorylation. J Biol Chem *285*, 3092-3102.
Lienkamp, S., Ganner, A., and Walz, G. (2012). Inversin, Wnt signaling and primary cilia. Differentiation *83*, S49-55.
Liu, C., Li, Y., Semenov, M., Han, C., Baeg, G.H., Tan, Y., Zhang, Z., Lin, X., and He, X. (2002). Control of beta-catenin phosphorylation/degradation by a dual-kinase mechanism. Cell *108*, 837-847.
Liu, C.C., Tsai, C.W., Deak, F., Rogers, J., Penuliar, M., Sung, Y.M., Maher, J.N., Fu, Y., Li, X., Xu, H.*, et al.* (2014). Deficiency in LRP6-mediated Wnt signaling contributes to synaptic abnormalities and amyloid pathology in Alzheimer's disease. Neuron *84*, 63-77.
Liu, P., Ramachandran, S., Ali Seyed, M., Scharer, C.D., Laycock, N., Dalton, W.B., Williams, H., Karanam, S., Datta, M.W., Jaye, D.L.*, et al.* (2006). Sex-determining region Y box 4 is a transforming oncogene in human prostate cancer cells. Cancer Res *66*, 4011-4019.

Lizarraga, S.B., Margossian, S.P., Harris, M.H., Campagna, D.R., Han, A.P., Blevins, S., Mudbhary, R., Barker, J.E., Walsh, C.A., and Fleming, M.D. (2010). Cdk5rap2 regulates centrosome function and chromosome segregation in neuronal progenitors. Development *137*, 1907-1917.
Lois, C., Hong, E.J., Pease, S., Brown, E.J., and Baltimore, D. (2002). Germline transmission and tissue-specific expression of transgenes delivered by lentiviral vectors. Science *295*, 868-872.
Luo, C., Wu, M., Su, X., Yu, F., Brautigan, D.L., Chen, J., and Zhou, J. (2019). Protein phosphatase 1alpha interacts with a novel ciliary targeting sequence of polycystin-1 and regulates polycystin-1 trafficking. FASEB J *33*, 9945-9958.
Machon, O., Backman, M., Machonova, O., Kozmik, Z., Vacik, T., Andersen, L., and Krauss, S. (2007). A dynamic gradient of Wnt signaling controls initiation of neurogenesis in the mammalian cortex and cellular specification in the hippocampus. Dev Biol *311*, 223-237.
Malicki, J.J., and Johnson, C.A. (2017). The Cilium: Cellular Antenna and Central Processing Unit. Trends Cell Biol *27*, 126-140.
Margolis, S.S., Perry, J.A., Weitzel, D.H., Freel, C.D., Yoshida, M., Haystead, T.A., and Kornbluth, S. (2006). A role for PP1 in the Cdc2/Cyclin B-mediated positive feedback activation of Cdc25. Mol Biol Cell *17*, 1779-1789.
Marion, V., Stoetzel, C., Schlicht, D., Messaddeq, N., Koch, M., Flori, E., Danse, J.M., Mandel, J.L., and Dollfus, H. (2009). Transient ciliogenesis involving Bardet-Biedl syndrome proteins is a fundamental characteristic of adipogenic differentiation. Proc Natl Acad Sci U S A *106*, 1820-1825.
Martynoga, B., Drechsel, D., and Guillemot, F. (2012). Molecular control of neurogenesis: a view from the mammalian cerebral cortex. Cold Spring Harb Perspect Biol *4*.
Matsumoto, N., Shinmyo, Y., Ichikawa, Y., and Kawasaki, H. (2017). Gyrification of the cerebral cortex requires FGF signaling in the mammalian brain. Elife *6*.
Melnik, S., Dvornikov, D., Muller-Decker, K., Depner, S., Stannek, P., Meister, M., Warth, A., Thomas, M., Muley, T., Risch, A.*, et al.* (2018). Cancer cell specific inhibition of Wnt/beta-catenin signaling by forced intracellular acidification. Cell Discov *4*, 37.
Mikolcevic, P., Sigl, R., Rauch, V., Hess, M.W., Pfaller, K., Barisic, M., Pelliniemi, L.J., Boesl, M., and Geley, S. (2012). Cyclin-dependent kinase 16/PCTAIRE kinase 1 is activated by cyclin Y and is essential for spermatogenesis. Mol Cell Biol *32*, 868-879.
Mitchison, H.M., and Valente, E.M. (2017). Motile and non-motile cilia in human pathology: from function to phenotypes. J Pathol *241*, 294-309.
Miterko, L.N., Lackey, E.P., Heck, D.H., and Sillitoe, R.V. (2018). Shaping Diversity Into the Brain's Form and Function. Front Neural Circuits *12*, 83.
Mukhtar, T., and Taylor, V. (2018). Untangling Cortical Complexity During Development. J Exp Neurosci *12*, 1179069518759332.
Munji, R.N., Choe, Y., Li, G., Siegenthaler, J.A., and Pleasure, S.J. (2011). Wnt signaling regulates neuronal differentiation of cortical intermediate progenitors. J Neurosci *31*, 1676-1687.
Mutch, C.A., Schulte, J.D., Olson, E., and Chenn, A. (2010). Beta-catenin signaling negatively regulates intermediate progenitor population numbers in the developing cortex. PLoS One *5*, e12376.

Nakagawa, N., Li, J., Yabuno-Nakagawa, K., Eom, T.Y., Cowles, M., Mapp, T., Taylor, R., and Anton, E.S. (2017). APC sets the Wnt tone necessary for cerebral cortical progenitor development. Genes Dev *31*, 1679-1692.
Nakakura, T., Asano-Hoshino, A., Suzuki, T., Arisawa, K., Tanaka, H., Sekino, Y., Kiuchi, Y., Kawai, K., and Hagiwara, H. (2015). The elongation of primary cilia via the acetylation of alpha-tubulin by the treatment with lithium chloride in human fibroblast KD cells. Med Mol Morphol *48*, 44-53.
Nekhai, S., Jerebtsova, M., Jackson, A., and Southerland, W. (2007). Regulation of HIV-1 transcription by protein phosphatase 1. Curr HIV Res *5*, 3-9.
Niehrs, C. (2012). The complex world of WNT receptor signalling. Nat Rev Mol Cell Biol *13*, 767-779.
Niehrs, C., and Shen, J. (2010). Regulation of Lrp6 phosphorylation. Cell Mol Life Sci *67*, 2551-2562.
Noctor, S.C., Martinez-Cerdeno, V., Ivic, L., and Kriegstein, A.R. (2004). Cortical neurons arise in symmetric and asymmetric division zones and migrate through specific phases. Nat Neurosci *7*, 136-144.
Ocbina, P.J., Tuson, M., and Anderson, K.V. (2009). Primary cilia are not required for normal canonical Wnt signaling in the mouse embryo. PLoS One *4*, e6839.
Ohata, S., Nakatani, J., Herranz-Perez, V., Cheng, J., Belinson, H., Inubushi, T., Snider, W.D., Garcia-Verdugo, J.M., Wynshaw-Boris, A., and Alvarez-Buylla, A. (2014). Loss of Dishevelleds disrupts planar polarity in ependymal motile cilia and results in hydrocephalus. Neuron *83*, 558-571.
Ou, Y., Zhang, Y., Cheng, M., Rattner, J.B., Dobrinski, I., and van der Hoorn, F.A. (2012). Targeting of CRMP-2 to the primary cilium is modulated by GSK-3beta. PLoS One *7*, e48773.
Palander, O., El-Zeiry, M., and Trimble, W.S. (2017). Uncovering the Roles of Septins in Cilia. Front Cell Dev Biol *5*, 36.
Palmer, A.K., and Kirkland, J.L. (2016). Aging and adipose tissue: potential interventions for diabetes and regenerative medicine. Exp Gerontol *86*, 97-105.
Palozola, K.C., Lerner, J., and Zaret, K.S. (2019). A changing paradigm of transcriptional memory propagation through mitosis. Nat Rev Mol Cell Biol *20*, 55-64.
Paridaen, J.T., Wilsch-Brauninger, M., and Huttner, W.B. (2013). Asymmetric inheritance of centrosome-associated primary cilium membrane directs ciliogenesis after cell division. Cell *155*, 333-344.
Park, I.K., Roach, P., Bondor, J., Fox, S.P., and DePaoli-Roach, A.A. (1994). Molecular mechanism of the synergistic phosphorylation of phosphatase inhibitor-2. Cloning, expression, and site-directed mutagenesis of inhibitor-2. J Biol Chem *269*, 944-954.
Park, T.J., Mitchell, B.J., Abitua, P.B., Kintner, C., and Wallingford, J.B. (2008). Dishevelled controls apical docking and planar polarization of basal bodies in ciliated epithelial cells. Nat Genet *40*, 871-879.
Pathak, N., Obara, T., Mangos, S., Liu, Y., and Drummond, I.A. (2007). The zebrafish fleer gene encodes an essential regulator of cilia tubulin polyglutamylation. Mol Biol Cell *18*, 4353-4364.
Pazour, G.J., Wilkerson, C.G., and Witman, G.B. (1998). A dynein light chain is essential for the retrograde particle movement of intraflagellar transport (IFT). J Cell Biol *141*, 979-992.
Pedersen, L.B., and Rosenbaum, J.L. (2008). Intraflagellar transport (IFT) role in ciliary assembly, resorption and signalling. Curr Top Dev Biol *85*, 23-61.

Peti, W., Nairn, A.C., and Page, R. (2013). Structural basis for protein phosphatase 1 regulation and specificity. FEBS J *280*, 596-611.
Piao, S., Lee, S.H., Kim, H., Yum, S., Stamos, J.L., Xu, Y., Lee, S.J., Lee, J., Oh, S., Han, J.K.*, et al.* (2008). Direct inhibition of GSK3beta by the phosphorylated cytoplasmic domain of LRP6 in Wnt/beta-catenin signaling. PLoS One *3*, e4046.
Pilaz, L.J., Lennox, A.L., Rouanet, J.P., and Silver, D.L. (2016). Dynamic mRNA Transport and Local Translation in Radial Glial Progenitors of the Developing Brain. Curr Biol *26*, 3383-3392.
Pinson, K.I., Brennan, J., Monkley, S., Avery, B.J., and Skarnes, W.C. (2000). An LDL-receptor-related protein mediates Wnt signalling in mice. Nature *407*, 535-538.
Piperno, G., and Mead, K. (1997). Transport of a novel complex in the cytoplasmic matrix of Chlamydomonas flagella. Proc Natl Acad Sci U S A *94*, 4457-4462.
Pramoonjago, P., Baras, A.S., and Moskaluk, C.A. (2006). Knockdown of Sox4 expression by RNAi induces apoptosis in ACC3 cells. Oncogene *25*, 5626-5639.
Pronobis, M.I., Rusan, N.M., and Peifer, M. (2015). A novel GSK3-regulated APC:Axin interaction regulates Wnt signaling by driving a catalytic cycle of efficient betacatenin destruction. Elife *4*, e08022.
Qu, Q., Sun, G., Murai, K., Ye, P., Li, W., Asuelime, G., Cheung, Y.T., and Shi, Y. (2013). Wnt7a regulates multiple steps of neurogenesis. Mol Cell Biol *33*, 2551-2559.
Reiter, J.F., Blacque, O.E., and Leroux, M.R. (2012). The base of the cilium: roles for transition fibres and the transition zone in ciliary formation, maintenance and compartmentalization. EMBO Rep *13*, 608-618.
Reiter, J.F., and Leroux, M.R. (2017). Genes and molecular pathways underpinning ciliopathies. Nat Rev Mol Cell Biol *18*, 533-547.
Rohatgi, R., Milenkovic, L., and Scott, M.P. (2007). Patched1 regulates hedgehog signaling at the primary cilium. Science *317*, 372-376.
Rosen, E.D., and Spiegelman, B.M. (2014). What we talk about when we talk about fat. Cell *156*, 20-44.
Rosen, E.D., Walkey, C.J., Puigserver, P., and Spiegelman, B.M. (2000). Transcriptional regulation of adipogenesis. Genes Dev *14*, 1293-1307.
Rosenbaum, J.L., and Witman, G.B. (2002). Intraflagellar transport. Nat Rev Mol Cell Biol *3*, 813-825.
Rosenbloom, A.B., Tarczynski, M., Lam, N., Kane, R.S., Bugaj, L.J., and Schaffer, D.V. (2020). beta-Catenin signaling dynamics regulate cell fate in differentiating neural stem cells. Proc Natl Acad Sci U S A *117*, 28828-28837.
Sakaguchi, M., Fujisaka, S., Cai, W., Winnay, J.N., Konishi, M., O'Neill, B.T., Li, M., Garcia-Martin, R., Takahashi, H., Hu, J.*, et al.* (2017). Adipocyte Dynamics and Reversible Metabolic Syndrome in Mice with an Inducible Adipocyte-Specific Deletion of the Insulin Receptor. Cell Metab *25*, 448-462.
Schaefer, K.N., and Peifer, M. (2019). Wnt/Beta-Catenin Signaling Regulation and a Role for Biomolecular Condensates. Dev Cell *48*, 429-444.
Scholey, J.M., and Anderson, K.V. (2006). Intraflagellar transport and cilium-based signaling. Cell *125*, 439-442.
Semenov, M.V., Habas, R., Macdonald, B.T., and He, X. (2007). SnapShot: Noncanonical Wnt Signaling Pathways. Cell *131*, 1378.
Shi, Z., Yang, X., Li, B.B., Chen, S., Yang, L., Cheng, L., Zhang, T., Wang, H., and Zheng, Y. (2018). Novel Mutation of LRP6 Identified in Chinese Han Population Links Canonical WNT Signaling to Neural Tube Defects. Birth Defects Res *110*, 63-71.
Simons, M., Gloy, J., Ganner, A., Bullerkotte, A., Bashkurov, M., Kronig, C., Schermer, B., Benzing, T., Cabello, O.A., Jenny, A.*, et al.* (2005). Inversin, the gene

product mutated in nephronophthisis type II, functions as a molecular switch between Wnt signaling pathways. Nat Genet *37*, 537-543.
Singla, V., and Reiter, J.F. (2006). The primary cilium as the cell's antenna: signaling at a sensory organelle. Science *313*, 629-633.
Song, L., Jia, Y., Zhu, W., Newton, I.P., Li, Z., and Li, W. (2014). N-terminal truncation mutations of adenomatous polyposis coli are associated with primary cilia defects. Int J Biochem Cell Biol *55*, 79-86.
Sorokin, S.P. (1968). Reconstructions of centriole formation and ciliogenesis in mammalian lungs. J Cell Sci *3*, 207-230.
Strissel, K.J., Lishko, P.V., Trieu, L.H., Kennedy, M.J., Hurley, J.B., and Arshavsky, V.Y. (2005). Recoverin undergoes light-dependent intracellular translocation in rod photoreceptors. J Biol Chem *280*, 29250-29255.
Sun, T., Annunziato, S., Bergling, S., Sheng, C., Orsini, V., Forcella, P., Pikiolek, M., Kancherla, V., Holwerda, S., Imanci, D.*, et al.* (2021). ZNRF3 and RNF43 cooperate to safeguard metabolic liver zonation and hepatocyte proliferation. Cell Stem Cell.
Sun, T., and Hevner, R.F. (2014). Growth and folding of the mammalian cerebral cortex: from molecules to malformations. Nat Rev Neurosci *15*, 217-232.
Sun, T., Pikiolek, M., Orsini, V., Bergling, S., Holwerda, S., Morelli, L., Hoppe, P.S., Planas-Paz, L., Yang, Y., Ruffner, H.*, et al.* (2020). AXIN2(+) Pericentral Hepatocytes Have Limited Contributions to Liver Homeostasis and Regeneration. Cell Stem Cell *26*, 97-107 e106.
Taelman, V.F., Dobrowolski, R., Plouhinec, J.L., Fuentealba, L.C., Vorwald, P.P., Gumper, I., Sabatini, D.D., and De Robertis, E.M. (2010). Wnt signaling requires sequestration of glycogen synthase kinase 3 inside multivesicular endosomes. Cell *143*, 1136-1148.
Thazhath, R., Jerka-Dziadosz, M., Duan, J., Wloga, D., Gorovsky, M.A., Frankel, J., and Gaertig, J. (2004). Cell context-specific effects of the beta-tubulin glycylation domain on assembly and size of microtubular organelles. Mol Biol Cell *15*, 4136-4147.
Thoma, C.R., Frew, I.J., Hoerner, C.R., Montani, M., Moch, H., and Krek, W. (2007). pVHL and GSK3beta are components of a primary cilium-maintenance signalling network. Nat Cell Biol *9*, 588-595.
Toral-Rios, D., Pichardo-Rojas, P.S., Alonso-Vanegas, M., and Campos-Pena, V. (2020). GSK3beta and Tau Protein in Alzheimer's Disease and Epilepsy. Front Cell Neurosci *14*, 19.
Veland, I.R., Montjean, R., Eley, L., Pedersen, L.B., Schwab, A., Goodship, J., Kristiansen, K., Pedersen, S.F., Saunier, S., and Christensen, S.T. (2013). Inversin/Nephrocystin-2 is required for fibroblast polarity and directional cell migration. PLoS One *8*, e60193.
Vijayaraghavan, S., Stephens, D.T., Trautman, K., Smith, G.D., Khatra, B., da Cruz e Silva, E.F., and Greengard, P. (1996). Sperm motility development in the epididymis is associated with decreased glycogen synthase kinase-3 and protein phosphatase 1 activity. Biol Reprod *54*, 709-718.
Virshup, D.M., and Shenolikar, S. (2009). From promiscuity to precision: protein phosphatases get a makeover. Mol Cell *33*, 537-545.
Viti, J., Gulacsi, A., and Lillien, L. (2003). Wnt regulation of progenitor maturation in the cortex depends on Shh or fibroblast growth factor 2. J Neurosci *23*, 5919-5927.
Vogel, T.W., Carter, C.S., Abode-Iyamah, K., Zhang, Q., and Robinson, S. (2012). The role of primary cilia in the pathophysiology of neural tube defects. Neurosurg Focus *33*, E2.

Vuolo, L., Stevenson, N.L., Mukhopadhyay, A.G., Roberts, A.J., and Stephens, D.J. (2020). Cytoplasmic dynein-2 at a glance. J Cell Sci *133*.
Walentek, P., Beyer, T., Thumberger, T., Schweickert, A., and Blum, M. (2012). ATP4a is required for Wnt-dependent Foxj1 expression and leftward flow in Xenopus left-right development. Cell Rep *1*, 516-527.
Walentek, P., Hagenlocher, C., Beyer, T., Muller, C., Feistel, K., Schweickert, A., Harland, R.M., and Blum, M. (2015). ATP4 and ciliation in the neuroectoderm and endoderm of Xenopus embryos and tadpoles. Data Brief *4*, 22-31.
Wang, Q.A., Tao, C., Gupta, R.K., and Scherer, P.E. (2013). Tracking adipogenesis during white adipose tissue development, expansion and regeneration. Nat Med *19*, 1338-1344.
Wang, W., and Brautigan, D.L. (2008). Phosphatase inhibitor 2 promotes acetylation of tubulin in the primary cilium of human retinal epithelial cells. BMC Cell Biol *9*, 62.
Wei, Q., Zhang, Y., Li, Y., Zhang, Q., Ling, K., and Hu, J. (2012). The BBSome controls IFT assembly and turnaround in cilia. Nat Cell Biol *14*, 950-957.
Weigle, B., Ebner, R., Temme, A., Schwind, S., Schmitz, M., Kiessling, A., Rieger, M.A., Schackert, G., Schackert, H.K., and Rieber, E.P. (2005). Highly specific overexpression of the transcription factor SOX11 in human malignant gliomas. Oncol Rep *13*, 139-144.
Wheway, G., Nazlamova, L., and Hancock, J.T. (2018). Signaling through the Primary Cilium. Front Cell Dev Biol *6*, 8.
Wilson, N.F., and Lefebvre, P.A. (2004). Regulation of flagellar assembly by glycogen synthase kinase 3 in Chlamydomonas reinhardtii. Eukaryot Cell *3*, 1307-1319.
Woodhead, G.J., Mutch, C.A., Olson, E.C., and Chenn, A. (2006). Cell-autonomous beta-catenin signaling regulates cortical precursor proliferation. J Neurosci *26*, 12620-12630.
Yang, J., Hurley, T.D., and DePaoli-Roach, A.A. (2000). Interaction of inhibitor-2 with the catalytic subunit of type 1 protein phosphatase. Identification of a sequence analogous to the consensus type 1 protein phosphatase-binding motif. J Biol Chem *275*, 22635-22644.
Yang, Y., He, Q., Cheng, P., Wrage, P., Yarden, O., and Liu, Y. (2004). Distinct roles for PP1 and PP2A in the Neurospora circadian clock. Genes Dev *18*, 255-260.
Zeng, L., Cai, C., Li, S., Wang, W., Li, Y., Chen, J., Zhu, X., and Zeng, Y.A. (2016). Essential Roles of Cyclin Y-Like 1 and Cyclin Y in Dividing Wnt-Responsive Mammary Stem/Progenitor Cells. PLoS Genet *12*, e1006055.
Zeng, X., Tamai, K., Doble, B., Li, S., Huang, H., Habas, R., Okamura, H., Woodgett, J., and He, X. (2005). A dual-kinase mechanism for Wnt co-receptor phosphorylation and activation. Nature *438*, 873-877.
Zhang, B., Zhang, T., Wang, G., Wang, G., Chi, W., Jiang, Q., and Zhang, C. (2015). GSK3beta-Dzip1-Rab8 cascade regulates ciliogenesis after mitosis. PLoS Biol *13*, e1002129.
Zhang, J., Chandrasekaran, G., Li, W., Kim, D.Y., Jeong, I.Y., Lee, S.H., Liang, T., Bae, J.Y., Choi, I., Kang, H.*, et al.* (2020). Wnt-PLC-IP3-Connexin-Ca(2+) axis maintains ependymal motile cilia in zebrafish spinal cord. Nat Commun *11*, 1860.
Zhou, C.J., Borello, U., Rubenstein, J.L., and Pleasure, S.J. (2006). Neuronal production and precursor proliferation defects in the neocortex of mice with loss of function in the canonical Wnt signaling pathway. Neuroscience *142*, 1119-1131.

Zhu, D., Shi, S., Wang, H., and Liao, K. (2009). Growth arrest induces primary-cilium formation and sensitizes IGF-1-receptor signaling during differentiation induction of 3T3-L1 preadipocytes. J Cell Sci *122*, 2760-2768.

12. ACKNOWLEDGEMENTS

Finally I am here of my PhD journey. Six years can be short can also be long. But to me every day of this experience deeply rooted in my life. All through this I would like to thank the people who supported me and helped me out and of course, without you, I may not make it finished today.

First, I would like to thank ***Prof. Dr. Christof Niehrs*** *for giving me the opportunity to work on these two exciting projects and the scientific thinking and skills training. In addition, many thanks go to his enthusiasim towards science which encouraged me all the way during my PhD.*

I want to thank my thesis advisor committee members, ***Prof. Dr. Ana Martin-Villalba, Prof. Dr. Thomas Holstein*** *and* ***Dr. Haikun Liu*** *for their valuable scientific advice.*

A special thanks to ***Prof.Dr.Wieland Huttner*** *for all the help and support provided during the collaboration together with his lab member* ***Dr. Wilsch-Bräuninger, Michaela*** *and* ***Dr. Pinson, Anneline.***

Thanks to all the present and former Niehrs lab members for their valuable discussions and comments and their friendly support.

I want to thank ***Dr. Stefan Koch*** *for his amazing supervision and for motivating me at the beginning of my PhD.*

A special thanks goes to the team ***Dr. Fabio da Silva****,* ***Jessica Herbst*** *and* ***Carina Seidl*** *all the help provided for neurogenesis& cilia project.*

I would like to thank my coffee team and best friends ***Dr. Minseong Kim*** *and* ***Dr. Hyeyoon Lee*** *for being always there when I needed coffee (help) and all the best moments we shared in life.*

I want to thank my teammate again ***Dr. Fabio Da Silva*** *for critically reading my thesis providing helpful suggestions.*

Finally, a special thanks goes to my family who constantly supported me through every moment of my life to make of me the person I am today. Thanks for my basketball teammates as well, without basketball I am sure I cannot get it healthily.